archive

STABILITY AND MIXING OF A VERTICAL
ROUND BUOYANT JET IN SHALLOW WATER

by

Joseph H. Lee, Gerhard H. Jirka,
and Donald R. F. Harleman

Energy Laboratory
Report No. MIT-EL 74-014

November 1974

STABILITY AND MIXING OF A VERTICAL ROUND BUOYANT JET IN SHALLOW WATER

by

Joseph H. Lee

Gerhard H. Jirka

and

Donald R. F. Harleman

ENERGY LABORATORY

in association with

RALPH M. PARSONS LABORATORY
FOR
WATER RESOURCES AND HYDRODYNAMICS,
Department of Civil Engineering

MASSACHUSETTS INSTITUTE OF TECHNOLOGY

Sponsored by

New England Electric System and Northeast Utilities Service Company

under the

M.I.T. Energy Laboratory

Electric Power Program

Energy Laboratory Report No. MIT-EL 74-014 November 1974
R. M. Parsons Technical Report No. 195

ABSTRACT

Discharging heated water through submerged vertical round ports located at the bottom of a receiving water body is a currently used method of waste heat disposal. The prediction of the temperature reduction in the near field of the buoyant jet is a problem of environmental concern.

The mechanics of a vertical axisymmetric buoyant jet in shallow water is theoretically and experimentally investigated. Four flow regimes with distinct hydrodynamic properties are discerned in the vicinity of the jet: the buoyant jet region, the surface impingement region, the internal hydraulic jump, and the stratified counterflow region. An analytical framework is formulated for each region. The coupling of the solutions of the four regions yields a prediction of the near field stability as well as the temperature reduction of the buoyant discharge.

It is found that the near field of the buoyant jet is stable only for a range of jet densimetric Froude numbers and submergences. A theoretical solution is given for the stability criterion and the dilution of an unstable buoyant jet.

A series of experiments were conducted to verify the theory. The experimental results are compared to the theoretical predictions. Good agreement is obtained.

TABLE OF CONTENTS

		Page
ABSTRACT		2
ACKNOWLEDGEMENTS		5
I.	INTRODUCTION AND BACKGROUND	6
II.	THEORETICAL FRAMEWORK	12
	2.1 The Buoyant Jet Region	14
	2.1.2 Statement of the problem	14
	2.1.2 General characteristics of the axisymmetric jet	16
	2.1.3 General analytical treatment	17
	2.1.4 Governing equations	19
	2.1.5 The entrainment principle	21
	2.1.6 Mathematical formulation	25
	2.1.7 Mathematical solution	26
	2.2 The Surface Impingement Region	29
	2.2.1 Analysis of the control volume	31
	2.2.2 Limiting cases	33
	2.3 Radial Stratified Flow	35
	2.4 The Radial Internal Hydraulic Jump	40
	2.5 Stratified Counterflow Region	52
	2.5.1 The momentum equation for axisymmetric stratified flow	52
	2.5.2 Behavior of the counterflow system	55
	2.5.3 Critical flow in a two-layered system	60
	2.5.4 Behavior of flow at large distances	65
	2.6 Summary of Theoretical Framework	67
	2.6.1 Definition of the near field dilution	67

TABLE OF CONTENTS (Continued)

	Page
2.6.2 Stable near field dilution	67
2.6.3 Unstable near field dilution	70
2.6.4 Equal counterflow	70
2.6.5 Nonequal counterflow	72
III. EXPERIMENTAL INVESTIGATION	74
3.1 The Experimental Setup	74
3.2 Experimental Procedure	81
3.3 Experimental Program	85
3.4 Experimental Observation	85
IV. COMPARISON OF THEORY AND EXPERIMENTAL RESULTS	98
4.1 Near Field Stability	98
4.2 Near Field Dilution	98
V. CONCLUSION	105
REFERENCES	107
LIST OF FIGURES AND TABLES	108
LIST OF SYMBOLS	110
APPENDIX	113

ACKNOWLEDGEMENTS

Funds for the publication of this study were made available from the Waste Heat Management Research Program of the M.I.T. Energy Laboratory.

The material in this study was submitted by Joseph H. Lee, Research Assistant, to the Department of Civil Engineering in partial fulfillment of the requirements for the degree of Master of Science. Technical and administrative supervision was provided for by Professor Donald R.F. Harleman, Professor of Civil Engineering and Director of the R.M. Parsons Laboratory for Water Resources and Hydrodynamics, M.I.T., and Dr. Gerhard H. Jirka, Research Engineer, Energy Laboratory, M.I.T.

Several discussions with Professor Ole S. Madsen have been very helpful. Mr. Roy C. Milley, machinist, and Mr. Harry Garabedian, graduate student, assisted in the construction of the experimental setup. The manuscript was typed by Ms. Susan Wiseman.

Computational work was carried out at the Civil Engineering - Mechanical Engineering Joint Computer Facility at M.I.T.

I. Introduction and Background

With the increasing demand in electric power in the U.S., waste heat disposal has become a problem of important environmental concern. Steam electric power plants, both fossil-fueled and nuclear-fueled, require a continuous cooling water flow to remove the waste heat from the steam condenser. Two modes of cooling water operation are possible: In a once-through system, the cooling water is circulated through the power plant only once and then discharged as heated water into an adjacent receiving waterbody. In closed-loop systems, the cooling water is continuously recirculated, the heat being rejected directly to the atmosphere before the water returns to the plant.

Due to the low efficiencies of existing power plants (determined by the thermodynamics of the steam cycle), enormous quantities of waste heat are discharged. In a nuclear fueled power plant, for every kilowatt of electrical energy produced, an equivalent of two kilowatts of energy is rejected to the environment in the form of heat.

The artificial heat addition into a natural water body has a definite impact on the local ecological balance. Consequently decision makers as well as ecologists are very concerned with the thermal effects in the natural waterway induced by various methods of condenser cooling water discharges.

Common methods of waste-heat disposal for present once-through cooling water systems can be classified into two categories:

a) Surface Discharge schemes: The condenser cooling water is discharged through a canal or a number of pipes located at the water surface into the neighboring waterway. This method of discharge usually results in a larger surface area with elevated water temperatures, but has the advantage that the heated water forms a stably stratified surface layer and the effect on the bottom of the receiving water is reduced. Pilgrim Nuclear Power Station in Plymouth, Mass. is one such example.

b) Submerged discharge schemes: Either single port or multiport submerged discharges are in common application. Single port discharges involve a single (or dual) outlet located at the bottom of the receiving water and discharging either vertically or horizontally. Two examples of large existing vertical single port outfalls on the Pacific coast are:

1. San Onofore nuclear plant. The cooling water flow from approximately 450 MW generation is 3.2×10^6 ft^3/hr. discharged through a 14-ft. diameter pipe 2600 ft. offshore, about 15 ft. below sea surface.

2. Redondo beach fossil fueled plant with 1612 MW capacity. One of the two offshore outfall systems consists of a single 14-ft. diameter pipe discharge 300 ft. offshore, about 16 ft. below water surface.

Recent innovations propose the use of multiport diffusers as an efficient way of heat disposal. This consists of a long pipe with the condenser flow discharged through many openings spaced along the pipe. The high velocity jet discharges induce intense turbulent mixing with the ambient water, thus achieving rapid temperature reduction of the heated discharge within a relatively small area.

The ultimate heat sink is the earth's atmosphere. The entire temperature distribution in the nearby waterway induced by the flow and heat input of the condenser cooling water is governed by the interaction of a variety of complicated physical processes and boundary conditions: turbulent mixing of the discharge with the ambient water, the hydrodynamic conditions in the receiving water, conduction, convection, evaporation and radiation to the atmosphere. For once-through cooling water systems the receiving water can be broadly classified into two regions with respect to the thermal effects of waste heat input: Far from the discharge the temperature pattern is dependent on ambient processes and consequently is not under the direct control of the engineer: the wind speed, the prevailing direction and magnitude of the currents, the ambient temperature, humidity and other meteorological conditions that govern the heat transfer between the water surface and the atmosphere. Near the discharge the temperature distribution is sensitive to the mode of discharge (surface discharge or submerged discharge) as well as the design characteristics (orientation, spacing, and number of discharge ports, diameter of port opening, size and geometry of channel). The task facing the engineer is to produce the best design with respect to specified thermal discharge criteria. The quantity of interest is often an average dilution defined by the ratio of the temperature rise across the condenser to the temperature rise above ambient near the discharge. This serves as a general indicator of the effectiveness of temperature reduction achieved by the discharge design. Other considerations include the time of travel of organisms entrained in the discharge, whether the near field is stratified or fully mixed, the area of a certain surface isotherm.

The discharge of heated water through a vertical round port located at the bottom of the receiving water is a currently used method of waste heat disposal. The temperature distribution induced by such a method of discharge entails an understanding of the hydrodynamics of the physical situation. The heated discharge entrains surrounding water by virtue of its momentum and its buoyant acceleration as it rises to the water surface, with a corresponding dilution of the discharge flow. The mechanics of a round buoyant jet in an infinite ambient field has been investigated by many investigators. However, in many practical situations, these vertical outfalls are situated in shallow water (a physical parameter that measures the 'degree of shallowness' is the ratio of the water depth to the port diameter). Near field dilution is usually computed by extending the buoyant jet solution in an infinite field in some arbitrary way. An attempt at a more refined treatment has been Trent and Welty's (1973) work on numerical modelling of turbulent jet flows. These studies, however, have neglected the important question of hydrodynamic stability of the near field. The boundary conditions chosen always dictate a stable near field, i.e., the heated water always form a stratified flow away and the jet discharge is always entraining ambient cooling water.

The stability of the near field for a two dimensional slot, buoyant jet was investigated by Jirka and Harleman. It has been found that the densimetric Froude number, the submergence and the angle of discharge of the jet are the governing parameters that determine the stability of the near field. In an unstable near field, it is not possible to distinguish an upper layer in the flow away zone, and there is continuous heat reentrainment into the jet. The dilution is hence decreased considerably as compared to that obtained in a stable near field (fig. 1-1).

The objective of this thesis is to extend the physical and analytical notions of the two dimensional case to the simplest three dimensional case - an axisymmetric vertical buoyant (round) jet in stagnant shallow water. With the exception of two experimentally determined coefficients, a theoretical solution is derived to determine the near field dilution and establish the criterion of the stability of the near field. If a stable near field exists, the near field dilution is dependent solely on the near field parameters (jet densimetric Froude numbers, submergence). In the case of an unstable near field, the dilution is dependent on both the near field parameters as well as the far field boundary condition.

A series of experiments were conducted to verify the theory.

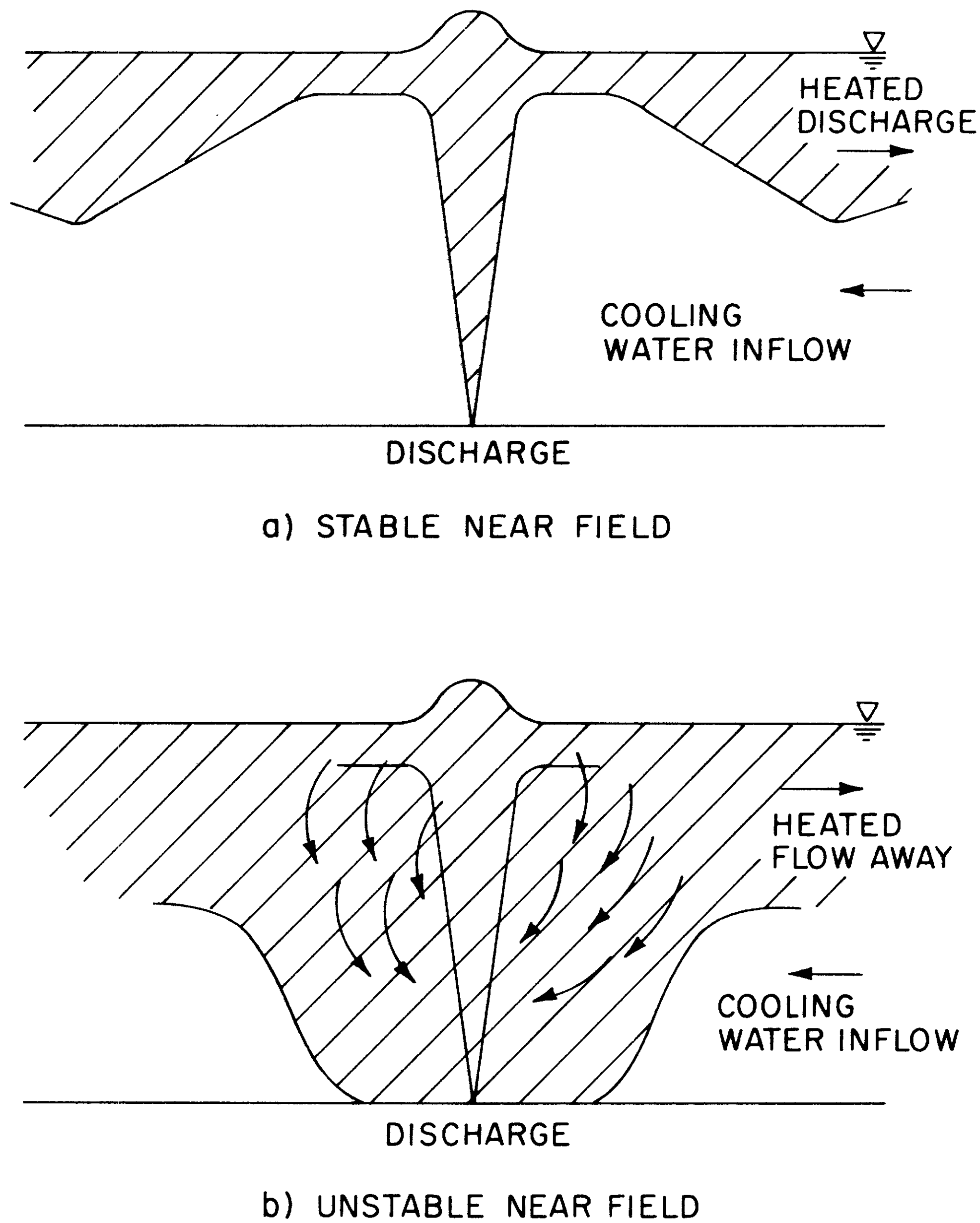

FIGURE (1-1) ILLUSTRATION OF NEAR FIELD STABILITY

II. Theoretical Framework

Both the experiments done for a two-dimensional buoyant jet (Jirka and Harleman, 1973) and the experiments carried out in this study for an axisymmetric vertical buoyant jet in shallow water (ch. 3) suggest strongly the classification of the near field into several distinct flow regimes; (Fig. 2-1) A) Buoyant Jet Region: Before the bouyant jet rises to the surface of the water, its behavior is postulated to be the same as that of a buoyant jet in an infinite field. B) Surface Impingement Region: this refers to the surface hump formed by the jet impingement on the free surface, followed by horizontal spreading of the jet discharge. C) The Internal Hydraulic Jump: An abrupt transition from the high velocity flow in the surface impingement region to a lower velocity flow away occurs some distance away from the jet axis, with a thickening and a corresponding decrease of velocity of the upper layer. D) Stratified Counter-Flow Region: the flow that occurs after the internal jump is described by a stratified two-layered slowly varying flow.

Fig. 2-1 illustrated the flow details for the case of a stable near field condition. In the case of an unstable near field continuous reentrainment of already mixed water into the jet region occurs. Hence a large vertical eddy (of toroidal shape in the axisymmetric case) comprises the near field region. Outside this region exists a stratified counterflow system as in the stable case.

The classification of the problem into distinct flow regimes with appropriate assumptions renders the description of the flow field amenable to analysis. In the following sections the properties of the flow and temperature for each region will be analysed. The coupling of the

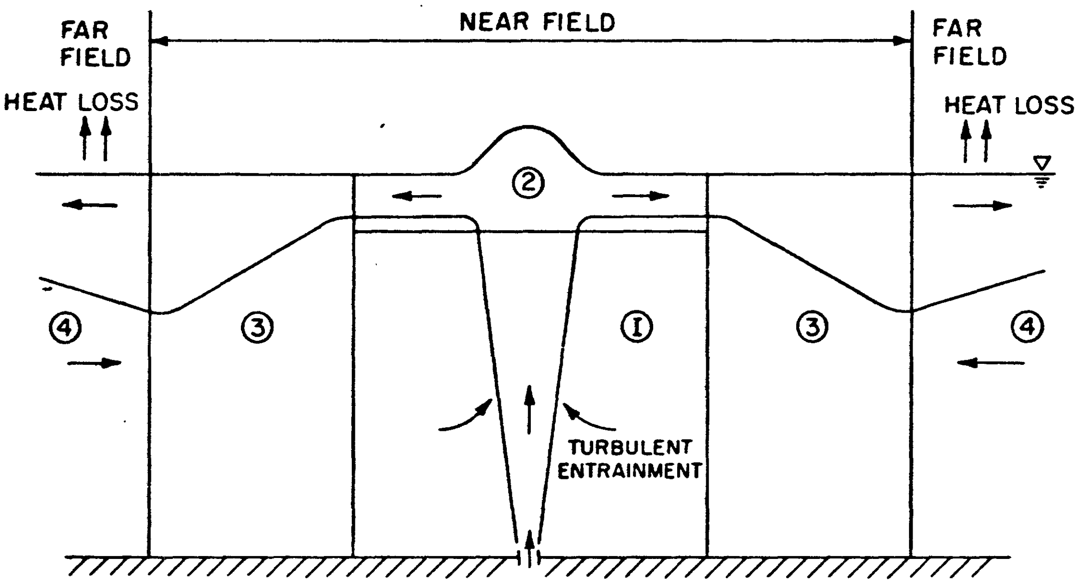

I BUOYANT JET REGION
2 SURFACE IMPINGEMENT REGION
3 INTERNAL JUMP REGION
4 STRATIFIED COUNTER FLOW REGION

FIGURE (2-1) FLOW STRUCTURE IN THE PLANE OF SYMMETRY OF A VERTICAL AXI-SYMMETRIC JET IN SHALLOW WATER analyses of the four regions yields the prediction of the near field dilution.

Since the near field is of small areal extent, the heat loss from the surface is excluded from the subsequent analysis. A scaling argument demonstrates this assumption is well-justified under typical thermal discharge conditions (Appendix F).

The flow is assumed turbulent for all the analytical treatment in the following sections. No generality is lost by considering the specific case of a hydrothermal jet. The words 'water' and 'density deficiency' can be replaced by 'fluid' and 'concentration' without altering the method of analysis.

2.1 The Buoyant Jet Region

2.1.1 Statement of the problem

Fig. 2-2 shows an axi-symmetric buoyant jet of fluid issuing from a source of finite diameter vertically upwards into a denser homogeneous ambient fluid (of infinite lateral extent) at rest. The physical variables of interest are the velocity and density of the jet at any particular position (z,r) in a cylindrical co-ordinate system.

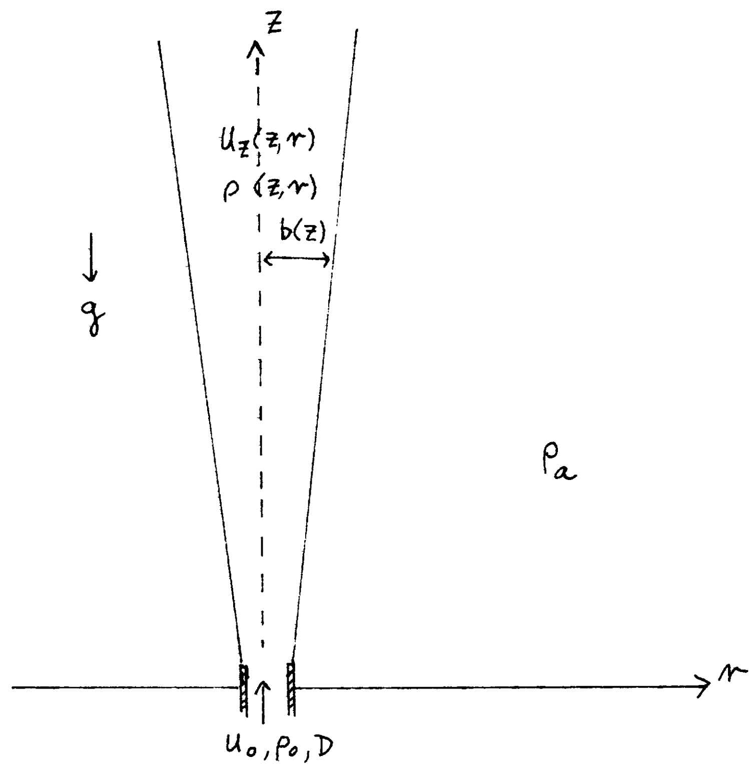

Fig. 2-2. An axi-symmetric jet discharging vertically

$u_z(z,r)$	:	vertical velocity at (z,r)
$\rho(z,r)$	:	density of fluid at (z,r)
$b(z)$	:	width of jet
g	:	acceleration due to gravity, acting in direction -z
u_o	:	exit jet velocity
ρ_o	:	initial jet fluid density
D	:	nozzle diameter
ρ_a	:	density of ambient fluid

2.1.2 General Characteristics of the Axi-symmetric jet

The general characteristics of the buoyant jet (or forced plume) in a fluid of unlimited vertical extent are well established by extensive research. In any given physical situation (convection induced by fires, plumes rising from smoke stacks, sewage disposal from a submerged outfall), the fundamental physical variable is the density of the issuing fluid (be it due to a temperature difference or embodied pollutant), and the characteristic dimensionless parameter that governs the mechanics of the buoyant jet is the exit densimetric Froude number as defined by $F_o = \dfrac{u_o}{\sqrt{g\dfrac{\Delta\rho_o}{\rho}D}}$, where $\Delta\rho_o = \rho_a - \rho_o$: initial density difference between jet and ambient fluid. This parameter describes the ratio of the sum of all forces per unit mass, $\dfrac{u_o^2}{D}$, to the buoyancy force per unit mass $g\dfrac{\Delta\rho_o}{\rho}$ of the fluid. When $F_o \to \infty$, inertia dominates, and the buoyant jet behaves like a pure momentum jet. Conversely, when F_o is small, buoyancy dominates, and a plume-like convective motion arises. In the intermediate case when F_o has a finite value, both inertia and buoyancy effects are important. Near the source the initial momentum dominates and the discharge behaves like a pure jet. Far from the source buoyancy predominates and all buoyant jets behave like plumes.

Near the source of a pure momentum jet, the sharp discontinuity in velocity between the jet and the ambient fluid creates a region of high shear. Such a region is highly unstable; eddies accompanied by turbulent mixing result, with the effect that ambient fluid is entrained into the jet, increasing the mass flux of the jet. The width of the jet, and hence the dilution of the fluid increases in the direction of the discharge. The momentum flux is conserved.

For a pure plume, the discharge with no initial momentum is continuously accelerated by the buoyancy force. A certain distance away from the source, the plume will have acquired enough momentum to entrain the ambient fluid; the basic turbulent mixing process that ensues after this point is then similar to the momentum jet. The buoyancy flux is preserved in this case, whereas the mass flux and the momentum flux increases in the direction of the discharge.

2.1.3 General Analytical Treatment

The structure of a submerged buoyant and non-buoyant jet has been determined from a number of experimental investigations(e.g., Albertson, Rouse and Yih, Morton):

1. Near the source, where turbulent diffusion of the momentum has not penetrated to the center of the jet, the velocity profile consists of a top hat portion, and a bell-shaped tail approximating the drop in velocity due to the entrainment of the ambient fluid (Fig. 2-3).
2. A certain distance away from the discharge, where the central core of constant exit velocity ceases to exist, the velocity profiles are of bell-shaped form.

Gaussian profiles can usually be well-fitted to the experimental results.

It can also be observed in experiments that the profiles of density deficiency, defined as $\Delta\rho(z,r) = \rho_a - \rho(z,r)$, are of bell-shaped form as well. The rate of spreading, however, is larger, indicating that heat or concentration of a pollutant diffuses faster than momentum.

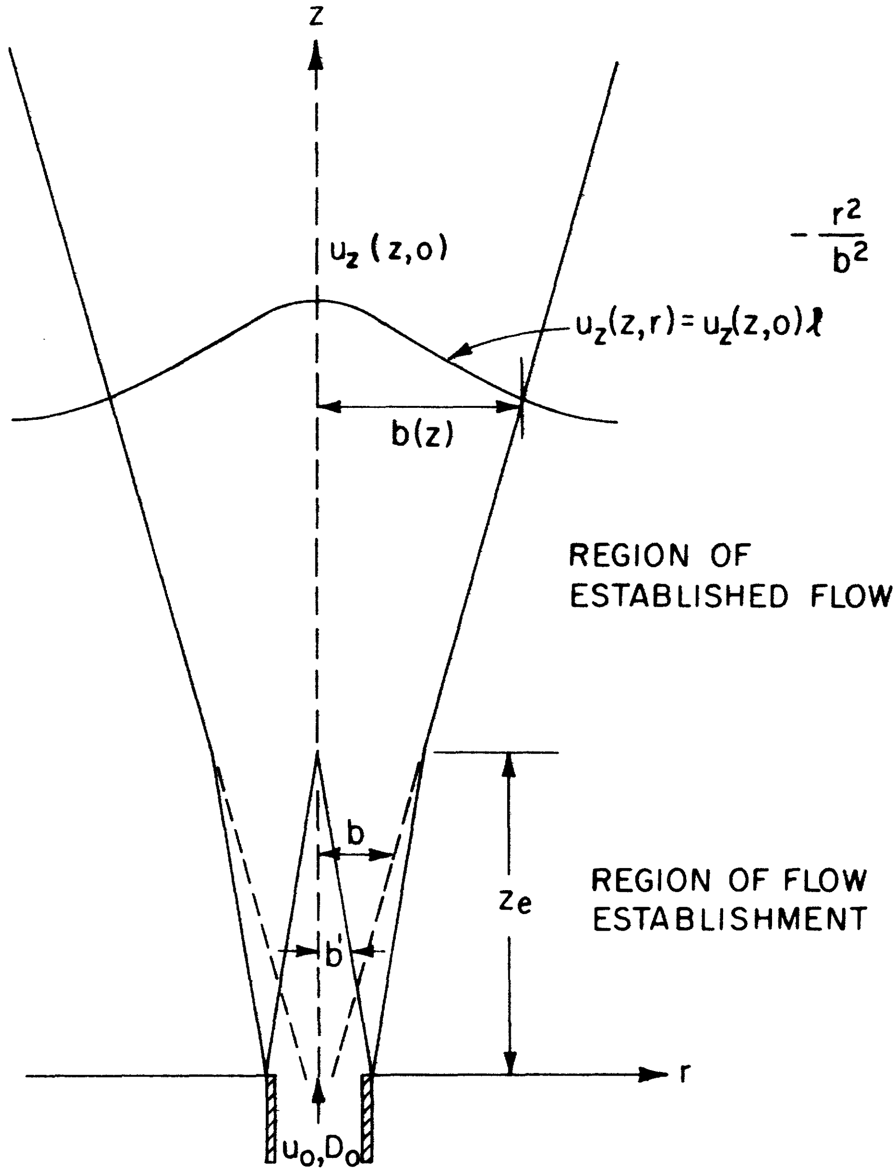

FIGURE(2-3) SCHEMATIZED STRUCTURE OF AN AXISYMMETRIC BUOYANT JET

2.1.4. Governing equations:

A steady state formulation of the problem is presented in this section:

Continuity: Invoking Boussinesq's(constant mass but variable weight);

$$\frac{1}{r}\frac{\partial}{\partial r}[\, r\, u_z(z,r)] + \frac{\partial}{\partial z} u_z(z,r) = 0$$

Integrating across the jet, we have:

$$\frac{d}{dz}\int_0^\infty u_z(z,r)2\pi r dr \;=\; -\,2\pi r u_r(z,r)\Big|_0^\infty$$

$$= Q_e \tag{2.1.1}$$

where Q_e = entrainment flux

The change in the volume flux of the jet is due to the entrainment of ambient water.

Newton's 2nd Law of Motion:

Navier Stokes equation in the z-direction:

$$\rho r[u_r \frac{\partial u_z}{\partial r} + u_z \frac{\partial u_z}{\partial z}] = -\, r\frac{\partial p}{\partial z} - \rho g r + r\,[\frac{\partial \tau_{rz}}{\partial r} + \frac{\partial \tau_{zz}}{\partial z}]$$

where τ_{rz}, τ_{zz} are turbulent shear terms.

Assuming $\frac{\partial \tau_{zz}}{\partial z} << \frac{\partial \tau_{rz}}{\partial r}$, i.e., lateral variation of the turbulent shear is much greater than the longitudinal variation and integrating across the jet (invoking the Boussinesq assumption), we have

$$\rho_a\,[u_r u_z r\Big|_0^\infty - \int_0^\infty u_z \frac{\partial(u_r r)}{\partial r} dr + \frac{1}{2}\frac{\partial}{\partial z}\int_0^\infty u_z^2\, r dr]$$

$$= -\frac{\partial}{\partial z}[\int_0^\infty rp\; dr] - \int_0^\infty \rho g r dr \;+\; \tau_{rz}\, r\Big|_0^\infty - \int_0^\infty \tau_{rz}\, dr$$

The boundary conditions are:

$$u_z(z,\infty) = 0$$

$$\int_o^\infty \tau_{rz}\, dr = 0 \quad ; \quad \Sigma F_{internal} = 0$$

$\tau_{rz}(z,\infty) = 0$ as no work is done at zero velocity gradient.

Assuming hydrostatic pressure distribution, we obtain

$$\frac{d}{dz} \int_o^\infty u_z^2\, 2\pi r\, dr = \int_o^\infty \frac{(\rho_a - \rho)}{\rho_a}\, g 2\pi r\, dr \tag{2.1.2}$$

The change in the momentum flux of the jet is due to that added by buoyancy.

Heat Conservation:

$$\frac{\partial}{\partial r} [r\rho u_r T] + \frac{\partial}{\partial z} [r\rho u_z T] = 0$$

Noting that $T(z,\infty) = T_a$, it can be shown that

$$\frac{d}{dz} \left[\int_o^\infty \rho u_z (T - T_a)\, 2\pi r\, dr \right] = 0$$

where $T(r,z)$: temperature at (z,r)

T_a : ambient temperature

Alternatively the above heat conservation equation can be formulated as an equation of conservation of density deficiency by noting that $\rho \simeq \rho_a$ and using the equation of state in linearized form

$$T - T_a = \beta(\rho - \rho_a) \quad \text{for small } \Delta T \quad ; \quad \beta \text{ constant}$$

$$\frac{d}{dz} \left[\int_o^\infty (\rho_a - \rho)\, u_z\, 2\pi r\, dr \right] = 0 \tag{2.1.3}$$

2.1.5. The Entrainment Principle

Experiments have shown that the bell-shaped distributions for both velocity and density deficiency can be approximated by Gaussian functions:

Letting
$$u_z(z,r) = u_c(z,o)\ e^{-r^2/b^2}$$

and
$$\rho_a - \rho(z,r) = [\rho_a - \rho(z,o)]\ e^{-r^2/\lambda^2 b^2}$$

where λ^2 is the turbulent Schmidt number, a measure for the relative diffusifities of momentum and heat (or mass).

Morton, Taylor et al (1956) assumed that the entrainment flux is related to the centerline velocity u_c and 'width' b of the jet via a proportional constant:

$$Q_e = 2\pi\alpha bu$$

$$\alpha = \text{entrainment coefficient.}$$

Substituting the special forms of the velocity and density deficiency profiles into eq. 2.1.1 - 2.1.3 and carrying out the integrations, the following set of equations is obtained for the region of established flow:

$$\frac{d}{dz}(u_c b^2) = 2\alpha\, bu_c \qquad (2.1.4)$$

$$\frac{d}{dz}\left(\frac{u_c^2 b^2}{2}\right) = g\lambda^2 b^2 \frac{\Delta\rho}{\rho} \qquad (2.1.5)$$

$$\frac{d}{dz}(u_c b^2 \Delta\rho) = 0 \qquad (2.1.6)$$

The problem can be solved numerically, taking care to transfer the conditions at the source to the beginning of the region of established flow. Nevertheless, there are two principal drawbacks. As will be shown in a later section, the entrainment coefficient α is some function of the local densimetric Froude number of the jet. This is indicated by experimental data: For an axisymmetric jet it varies from 0.085 for a plume to 0.057 for a pure jet. Thus the assumption that α is a constant is not a good one. In the mathematical solution employed in this study, a better assumption is used to replace eq. 2.1.4.

For buoyant jets in deep water, the region of interest (water depth) is large compared with the length of the zone of flow establishment z_e. Neglecting buoyancy in the region of flow establishment, the constancy of momentum flux yields the relationship between conditions at the source and those at the end of the region of flow establishment. However, in many practical cases of interest (e.g., continental shelf), the submergence H/D is less than 50. The length of the region of flow establishment can constitute a significant portion of the total water depth, and cannot be conveniently left out in the analysis. In the theoretical solution of the study, z_e is derived as a function of the exit densimetric Froude number.

<u>Special Cases</u>:

Valuable information can be derived from eq. 2.1.4 - 2.1.6 by considering the limiting cases of a pure momentum jet and a plume -

a) Momentum jet: $F_o \to \infty$

Setting $\Delta\rho = 0$ in eq. 2.1.4 - 2.1.6

it can be shown that

$$\frac{db}{dz} = 2\alpha \qquad (2.1.7)$$

$$\left(\frac{u}{u_o}\right)^2 = \left(\frac{D}{2\alpha z}\right)^2 \qquad (2.1.8)$$

Hence in a momentum jet the width increases linearly with z, and the jet angle is related to the entrainment coefficient. Consequently the Reynolds number defined with respect to the centerline velocity and the width of the jet is a constant.

b) Pure plume: $F \simeq 0$

In this sub-section it will be proved that at large distances from the source, the local densimetric Froude number of all plumes approaches an asymptotic constant value. The approach employed here is similar to that by Jirka and Harleman (1973) for the two-dimensional plume.

The local densimetric Froude number is defined as

$$F = \frac{u_c}{\sqrt{g \frac{\Delta\rho}{\rho} b}}$$

The change in the densimetric Froude number can be written as

$$\frac{dF}{dz} = \frac{F^2}{u^2} \left\{ \frac{u}{F} \frac{du}{dz} - \frac{Fg}{2\rho} \frac{d}{dz} (\Delta\rho b) \right\} \tag{2.1.9}$$

It can be derived from eq. 2.1.4 - 2.1.6 that

$$u\frac{du}{dz} = \frac{g\lambda^2 b^2 \frac{\Delta\rho}{\rho} - u^2 b\frac{db}{dz}}{b^2} \tag{2.1.10}$$

and

$$b^2 u\frac{du}{dz} + 2u^2 b\frac{db}{dz} = 2\alpha b u^2 \tag{2.1.11}$$

Subtracting eq. 2.11 from eq. 2.10 and back substituting, we have

$$\frac{db}{dz} = 2\alpha - \lambda^2/F^2 \tag{2.1.13}$$

$$u\frac{du}{dz} = \frac{g\lambda^2 b^2 \frac{\Delta\rho}{\rho} - u^2 b(2\alpha - \lambda^2/F^2)}{b^2} \tag{2.1.14}$$

Substituting the expression for $u\frac{du}{dz}$ and $\frac{d}{dz}(\Delta\rho b)$ into eq. (2.1.9), we obtain

$$\frac{dF}{dz} = \frac{2\alpha}{bF}\left(\frac{5\lambda^2}{4\alpha} - F^2\right)$$

Thus if $F_o^2 < \frac{5\lambda^2}{4\alpha}$ the plume will be initially accelerated to increase the local densimetric Froude number; conversely, if $F_o^2 > \frac{5\lambda^2}{4\alpha}$, the plume will be decelerated: in both cases an asymptotic densimetric Froude number of $F = \sqrt{\frac{5\lambda^2}{4\alpha}} = 4.30$ is approached at large distances from the source of buoyancy.

In the region where the asymptotic densimetric Froude number is approached:

$$\frac{db}{dz} = \frac{6}{5}\alpha \qquad (2.1.15)$$

$$\Delta\rho = \text{const} \times z^{-5/3} \qquad (2.1.16)$$

$$u = \text{const} \times z^{-2/3}$$

That the jet angle is approximately constant (or more correctly, varies slowly with F) is easily shown by substituting the values of α, for the plume and the jet in eq. 2.1.7 and 2.1.15

Jet: $\alpha = 0.057$ $\quad \frac{db}{dz} = 0.114$

Plume: $\alpha = 0.085$ $\quad \frac{db}{dz} = 0.104$

It can be seen there is only a difference of less than 10% between the jet angle for the two limiting cases.

In the mathematical formulation of the Buoyant Jet Region Solution presented in the following section, a constant jet angle assumption is used to replace eq. 2.1.4. Besides being a more accurate description of the physical situation, this has the further advantage that an analytical solution is rendered possible.

2.1.6. Mathematical Formulation

In this section the assumptions employed to solve the problem of the bouyant jet region in shallow water will be stated:

a) $\frac{db}{dz} = \varepsilon =$ constant independent of the local densimetric Froude number i.e., the spread of the standard deviation of the cross-sectional profiles is linear with z. In the region of established flow this assumption is equivalent to that of a linear jet.

b) In the region of flow establishment, a linear spread is assumed for the development of the central core region (Fig. 2-3).

$$
\begin{aligned}
u_z(z,r) &= u_o && r < b' \\
&= u_o e^{-(r-b')^2/b^2} && r \geq b' \\
\Delta\rho(z,r) &= \Delta\rho_o && r < b' \\
&= \Delta\rho_o e^{-(r-b')^2/\lambda^2 b^2} && r \geq b'
\end{aligned}
$$

λ = spreading coefficient

The assumptions in the region of flow establishment are good only when the exit densimetric Froude number is greater than the asymptotic value of the plume. In laboratory practice laminar effects will come into play near the nozzle for extremely low densimetric Froude numbers, and jets with small F_o may possess a different turbulent structure (Ungate, 1974). In such cases the above stated assumptions will break down and there is no accurate analysis possible to determine the length of the region of flow establishment.

2.1.7 Mathematical Solution

An analytical solution is given in this section for the region of established flow and the region of flow establishment. The basic assumptions are the same as used by Abraham (1963). The analytical treatment, however, is different in two respects:

1. The assumptions that lead to the evaluation of the length of the zone of flow establishment is explicitly stated. In his evaluation of z_e, Abraham evaluated the buoyancy flux using Albertson's result that assumes a constant momentum flux. The buoyancy flux is correctly evaluated in present solution.
2. Two boundary conditions are invoked to couple the solution of the region of established flow with that of the region of flow establishment: The resulting differential equations are then explicitly solved subject to the boundary conditions rather than using an integral approach as employed by Abraham.

Region of established flow

In the region of established flow assumption (a) can be used along with eq. 2.1.5 - 2.1.6 to yield an analytical solution.

By employing a change of variables $m^{\frac{1}{3}} = u_c$ and solving the transformed equations, the following solution can be obtained:

$$u_c(z) = \frac{1}{z} \{u_e^3 z_e^3 + \frac{3g\lambda^2 u_e \Delta\rho_e z_e^2}{2\rho_a} (z^2 - z_e^2) \}^{1/3} \qquad (2.1.17)$$

$$\Delta\rho(z) = \frac{u_e \Delta\rho_e z_e^2}{z} \{u_e^3 z_e^3 + \frac{3g\lambda^2 u_e \Delta\rho_e z_e^2}{2\rho_a} (z^2 - z_e^2)\}^{-1/3} \qquad (2.1.18)$$

where $u_e = u_c(z = z_e)$

$\Delta\rho_e = \Delta\rho_o$ by definition

Hence u_c, $\Delta\rho$ in the region of established flow are reduced to a function of z and z_e. It is evident that eq. 2.1.17 and eq. 2.1.18 exhibit the expected behavior of a buoyant jet. For z sufficiently large, $u_c \sim z^{-\frac{1}{3}}$ and $\Delta\rho \sim z^{-\frac{5}{3}}$; this agrees with the behavior of a plume. For $z \sim z_e$, $u_c \sim z^{-1}$, resembling the motion of a momentum jet.

Assuming that the velocity profile is Gaussian at $z = z_e$ (density deficiency), heat conservation gives

Heat flux at $z = z_e$(density) $= \int_0^\infty \Delta\rho u 2\pi r dr = \Delta\rho_o \frac{\pi D^2 u_o}{4}$

this gives $$u_e z_e^2 = \frac{D^2 u_o (1+\lambda^2)}{4\lambda^2 \varepsilon^2} \qquad (2.1.17a)$$

Also, it can be shown that

$$\frac{u_e z_e}{u_o D} = [(\frac{M_e}{M_o}) \frac{1}{2\varepsilon^2}]^{\frac{1}{2}} \qquad (2.1.18a)$$

where M_e : momentum flux at $z = z_e$(density)

M_o : initial momentum flux

Substituting eq. 2.1.17a and eq.2.1.18a into eq. 2.1.17 - 2.1.18 yields

$$\frac{u}{u_o} = \frac{D}{z}\left[\left(\frac{1}{2\varepsilon^2}\frac{M_e}{M_o} \right)^{3/2} + \frac{3(1+\lambda^2)}{8\varepsilon^2 F_o^2} \left\{ \left(\frac{z}{D}\right)^2 - \left(\frac{z_e}{D}\right)^2 \right\} \right]^{1/3} \quad (2.1.19)$$

$$\frac{\Delta\rho}{\Delta\rho_o} = \frac{(1+\lambda^2)}{4\lambda^2\varepsilon^2}\frac{D}{z}\left[\left(\frac{1}{2\varepsilon^2}\frac{M_e}{M_o} \right)^{3/2} + \frac{3(1+\lambda^2)}{8\varepsilon^2 F_o^2} \left\{ \left(\frac{z}{D}\right)^2 - \left(\frac{z_e}{D}\right)^2 \right\} \right]^{-1/3} \quad (2.1.20)$$

Determination of the Length of Flow Establishment

Referring to Fig. 2-3 for the region of flow establishment:

By similarity $\quad b' = \frac{D}{z}(1 - z/z_e)$

The momentum flux at $z = z_e$

$$M_e = M_o + \int_o^{z_e} \int_o^{\infty} (\rho_a - \rho) g 2\pi r dr\, dz$$

By invoking assumption (b) the bouyancy contribution to M_e can be evaluated as

$$\int_o^{z_e} \int_o^{\infty} \Delta\rho g\, 2\pi r dr = g\pi\Delta\rho_o \left\{ \left(\frac{D}{2}\right)^2 \frac{z_e}{3} + \frac{\lambda^2\varepsilon^2 z_e^3}{3} + \sqrt{\pi}\,\lambda\varepsilon \frac{D}{2}\frac{z_e^2}{6} \right\}$$

Hence M_e/M_o can be expressed as

$$\frac{M_e}{M_o} = 1 + \frac{4}{F_o^2}\left[\frac{c}{12} + \frac{\sqrt{\pi}\,\lambda\varepsilon}{12} c^2 + \frac{\lambda^2\varepsilon^2}{3} c^3 \right] \quad (2.1.21)$$

where $c = z_e$ (density)/D

At $z = z_e \qquad \frac{\Delta\rho}{\Delta\rho_o} = 1$

eq. 2.1.20 then gives

$$\left(\frac{1}{2\varepsilon^2} \frac{M_e}{M_o} \right)^{\frac{1}{2}} = \frac{1+\lambda^2}{\lambda^2} \frac{1}{4\varepsilon^2} \frac{1}{c} \tag{2.1.22}$$

Equating the expressions for M_e/M_o derived from eq. 2.1.21 and eq. 2.1.22 we have

$$1 + \frac{4}{F_o^2} \left\{ \frac{c}{12} + \frac{\sqrt{\pi}\,\lambda\varepsilon}{12} c^2 + \frac{\lambda^2\varepsilon^2}{3} c^3 \right\} = \left(\frac{1+\lambda^2}{4\lambda^2\varepsilon^2}\right)^2 \frac{2\varepsilon^2}{c^2} \tag{2.1.23}$$

Eq. 2.1.23 describes c as a function of the exit densimetric Froude number. In the limiting case of a momentum jet $F_o \to \infty$ $c = \frac{1+\lambda^2}{2\lambda^2}\left(\frac{1}{\sqrt{2\varepsilon}}\right)$. This value is similar to that given by Albertson et al (1950).

Given F_o (ε and λ are approximately constants) equation 2.1.23 can be solved numerically. Fig. (2-4) shows the value of c as a function of F_o for $\lambda = 1.14$ and $\varepsilon = 0.109$ (these are respectively intermediate values for the jet-plume range: $\lambda_{plume} = 1.12$, $\lambda_{jet} = 1.16$, $\varepsilon_{jet} = 0.114$, $\varepsilon_{plume} = 0.104$). It can be seen c increases rapidly from zero for $F_o = 0.0$ to an asymptotic value of 5.74 for F_o beyond 25.0. The region of interest for buoyant jet applications is $4.3 < F_o < \infty$ where 4.3 is the asymptotic value for the densimetric Froude number of the pure plume.

2.2 The Surface Impingement Region

When the buoyant jet impinges on the free surface, the surface pressure, documented as a surface hump, causes horizontal spreading of the heated discharge. Intense turbulent mixing occurs in this region

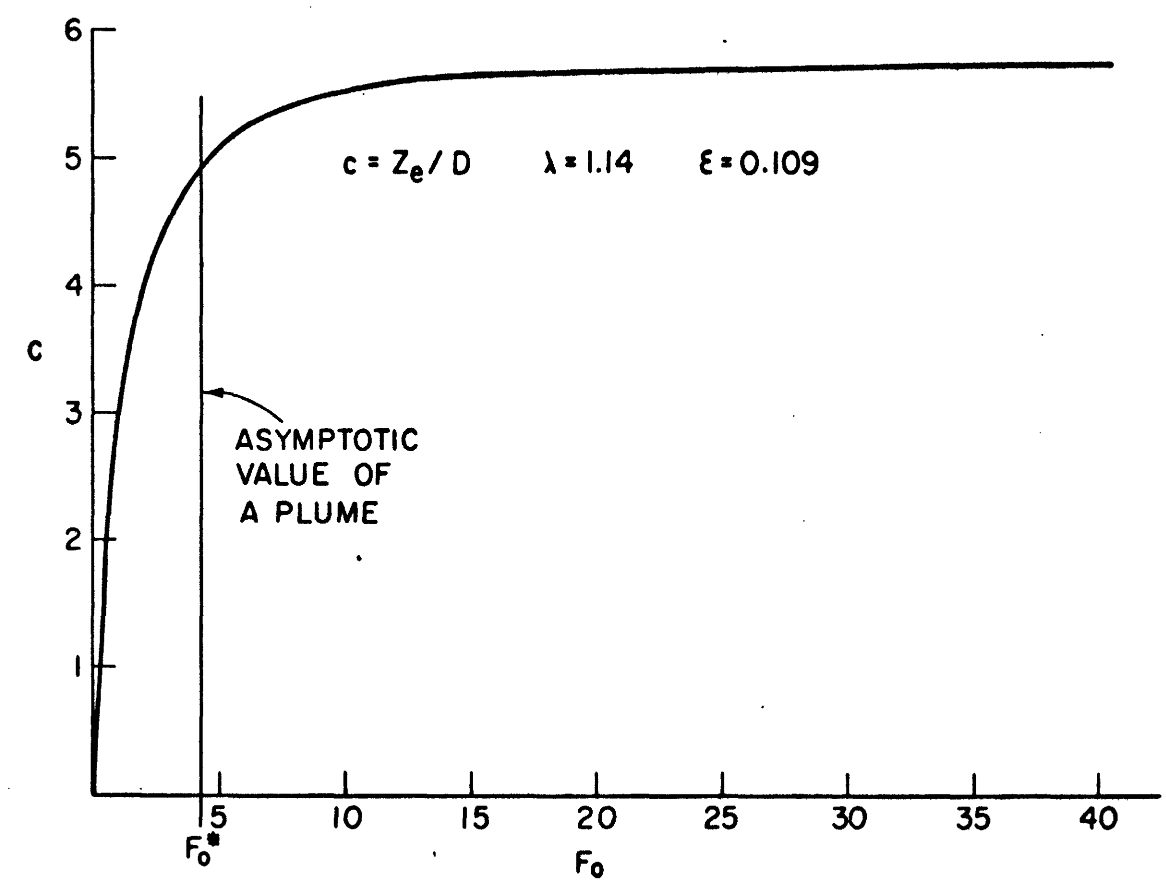

FIGURE (2-4) LENGTH OF ZONE OF FLOW ESTABLISHMENT AS A FUNCTION OF THE EXIT DENSIMETRIC FROUDE NUMBER and a detailed analysis of the exact flow and temperature distribution within this region is deemed impractical. Instead a control volume approach is taken to couple the flow conditions just before and after impingement.

A definition sketch is given in fig. 2-5. The heated flow enters as a jet through section i and leaves the control volume at section I. Flow is assumed to be fully established in section i. Let R_I be the radial position at which the free surface returns to level . R_I is related to the standard deviation of the incoming jet flow by $R_I = \alpha_o b_i$, and α_o is evaluated from experiments. Let u_I and h_I be the velocity and depth of the upper layer and uniform distributions over the thickness h_I are assumed.

2.2.1 Analysis of the Control Volume

Continuity:

Neglecting entrainment in the surface impingement region and invoking the Boussinesq assumption, one obtains

$$b_i\ u_i = 2\ \alpha_o\ h_I\ u_I$$

Heat Conservation:

Assuming the linearized equation of state and equating the inflow and outflow heat fluxes:

$$\beta\ \rho_a \int_o^\infty u\ \Delta\rho 2\pi r dr \Bigg|_{\substack{\text{section}\\ i}} = \rho_a T_a \int_o^\infty u\ 2\pi r dr \Bigg|_{\substack{\text{section}\\ i}} - \pi b_i \rho_I (2\alpha_o h_I u_I) T_I$$

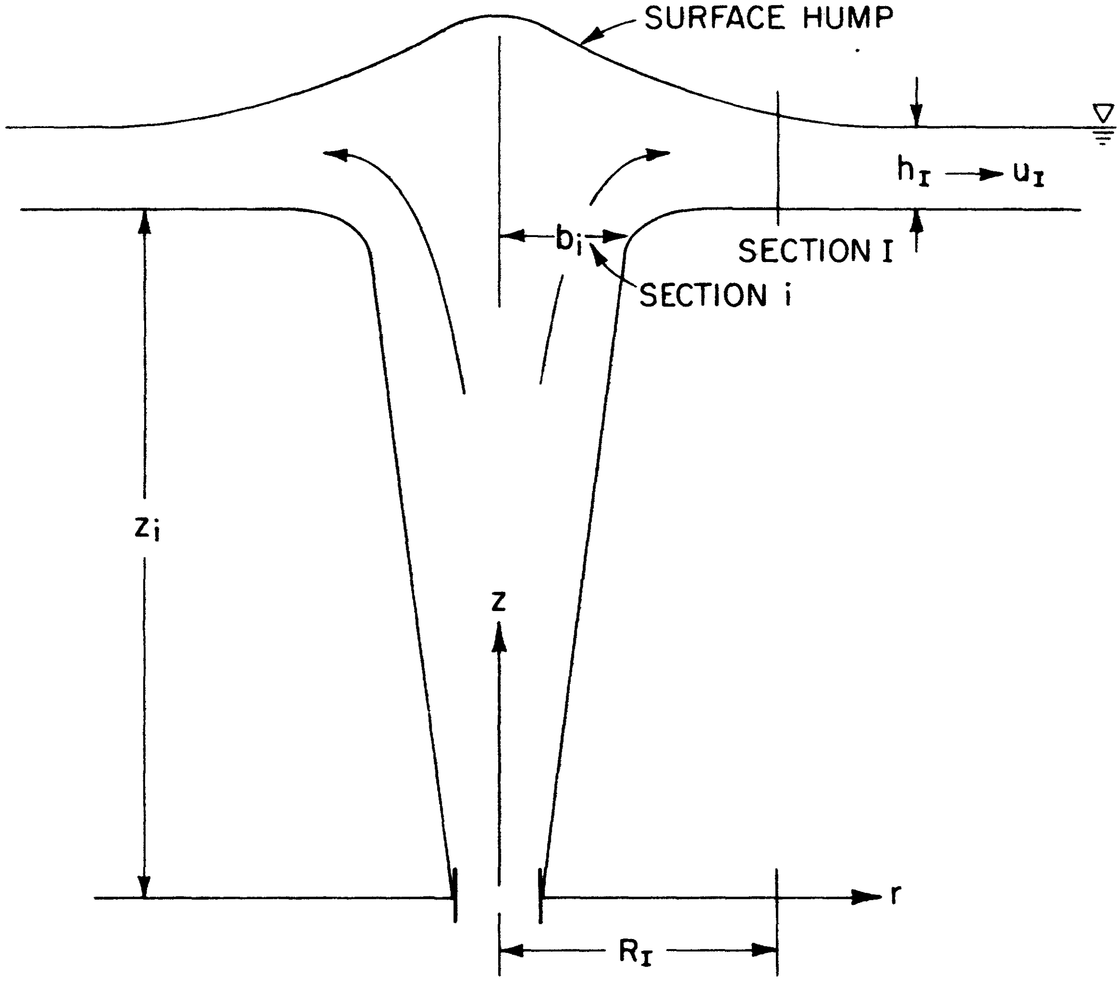

FIGURE (2-5) THE SURFACE IMPINGEMENT REGION

Invoking continuity, we have

$$\Delta\rho_I = \frac{\lambda^2}{1+\lambda^2} \Delta\rho_i$$

Conservation of energy:

In a conservative buoyant force field an energy potential $\Delta\rho gz$ can be defined.

Assuming an energy loss of the form $K_L \times$(Kinetic energy flux $|$in) where K_L is a head loss coefficient, conservation of energy then gives

$$(1 - K_L) \frac{u_i^2}{6g} = \frac{u_I^2}{2g} + \frac{h_I}{2} \Delta\rho_I g$$

Recapitulating the complete set of equations for the Surface Impingement Region:

$$b_i u_1 = 2h_I u_I \alpha_o \qquad (2.2.1)$$

$$\Delta\rho_i = \frac{1+\lambda^2}{\lambda^2} \Delta\rho_I \qquad (2.2.2)$$

$$\frac{\rho_a u_i^2}{2g} (1-K_L) = \rho_a \frac{u_I^2}{2g} + \frac{\Delta\rho_I}{2} h_I \qquad (2.2.3)$$

Eq. 2.2.1 - 2.2.3 can be solved iteratively with eq. 2.1.19 - 2.1.20 to find h_I and the densimetric Froude numbers of the upper and lower layers at the end of zone 2 (Fig. 2-1).

2.2.2 Limiting Cases

Insight can be gained by considering the two limiting cases of a momentum jet and a plume:

A. Momentum Jet: Setting $\Delta\rho = 0$ in eq. 2.1.1-2.1.3 gives

$$h_I = \sqrt{\frac{3}{4(1-K_L)\alpha_o^2}} \qquad (2.2.4)$$

Substituting $\frac{db}{dz} = \varepsilon$ into eq. (2.2.4) the following equation is obtained.

$$\frac{h_I}{H} = \frac{1}{1 + \frac{2}{3}\sqrt{\frac{(1-K_L)\alpha_o^2}{3}}}$$

For a momentum jet $\alpha = 0.057$ $\varepsilon = 0.114$

Evaluating $\frac{h_I}{H}$ for different values of K_L and α_o, we have

	$K_L = 0$	$K_L = 0.2$	$K_L = 0.4$	
$\frac{h_I}{H}$	0.09	0.0994	0.113	$\alpha_o = 1$
	0.05	0.06	0.07	$\alpha_o = 1.73$

$\alpha_o = 1.73$ corresponds to a R_I where the vertical velocity is 5% of the centerline velocity.

B. Plume: Assuming the asymptotic value of the local densimetric Froude number is reached before impinging the free surface

$$F_i^2 = \frac{5\lambda^2}{4\alpha}$$

From eq. 2.1.15 $\quad b_i = \frac{6\alpha}{5}(H - h_I)$

Substituting b_i into eq. 2.2.1 - 2.2.3, we obtain

$$F_i^2 \left\{ \frac{(1-K_L)}{3} - \left(\frac{b_i}{h_I}\right)^2 \frac{1}{4\alpha_o^2} \right\} = \frac{\lambda^2}{1+\lambda^2} \frac{1}{(b_i/h_I)}$$

For a plume $\lambda = 1.12$, $\alpha = 0.082$

By iteration, we get

	$K_L = 0$	$K_L = 0.2$	$K_L = 0.4$	
$\frac{h_I}{H}$	0.081	0.091	0.107	$\alpha_o = 1$
	0.048	0.053	0.06	$\alpha_o = 1.73$

The above analysis demonstrates the weak sensitivity of h_I/H to the range of densimetric Froude numbers. This approximately constant value can serve as a useful starting point in the numerical solution of eq. 2.2.1 - 2.2.3 and 2.1.19 - 2.1.20.

Lower bounds for the densimetric Froude numbers of the respective layers after surface impingement are given for the case of the plume as $F_1 = 4.12$, $F_2 = 0.21$ where subscript 1 refers to the upper layer and 2 the lower layer in the impingement zone.

In the theoretical solution $K_L = 0.2$ is assumed for a 90° bend and a wide range of curvature (Jirka and Harleman, 1973). As it is experimentally observed that $\frac{h_I}{H} \simeq 0.1$, $\alpha_o = 1$ is assumed in the subsequent analysis. Thus, the outer radius, section I, of the surface impingment region is assumed to be equal to the radius of the jet at section i.

2.3 Radial Stratified Flow

In this section the basic equations that govern the flow of a stratified two-layered system are derived and presented. A slowly-varying flow situation with a distinct interface is schematized as shown in fig. (2-6). For a two layer system with low densimetric Froude numbers there is very weak turbulent entrainment from the lower layer into the

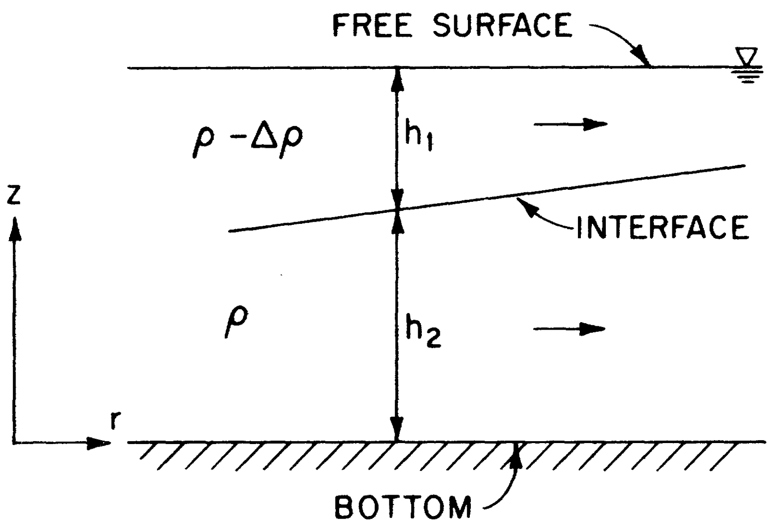

FIGURE (2-6) RADIAL STRATIFIED FLOW IN A TWO-LAYERED SYSTEM upper layer (Ellison and Turner, 1959). The densities of the two layers can hence be regarded as constants. The Navier Stokes equations are averaged in the vertical direction, and the resulting equations are further developed for the internal hydraulic jump as well as the stratified counterflow in later sections.

The steady state Navier-Stokes eq. in the radial direction in a cylindrical co-ordinate system (z,r) is

$$\rho\left(u \frac{\partial u}{\partial r} + w \frac{\partial u}{\partial z} \right) = - \frac{\partial p}{\partial r} + \rho \frac{\partial \tau_{zr}}{\partial z} \tag{2.3.1}$$

$\vec{q}$ = (u,w) : velocity vector at (z,r)

p = pressure

τ_{zr} = turbulent shear stress

The kinematic and dynamic boundary conditions are:

A) Kinematic Boundary Condition:

Surface $w_s = u_s \frac{\partial(h_1+h_2)}{\partial r}$

Interface $w_i = u_i \frac{\partial h_2}{\partial r}$

Bottom $w_b = 0$ (no bottom slope)

B) Dynamic Boundary Condition:

Surface $p = 0$ (free surface)

$\tau_s = \rho\varepsilon_z \frac{\partial u}{\partial z}\Big|_s \equiv \tau_{rz}\Big|_s$

Interface $\tau_i = \rho\varepsilon_i \frac{\partial u}{\partial z}\Big|_i \equiv \tau_{rz}\Big|_i$

Bottom $\tau_b = \rho\varepsilon_z \frac{\partial u}{\partial z}\Big|_b \equiv \tau_{rz}\Big|_b$

where τ_s = surface shear

τ_i = interfacial shear

τ_b = bottom shear

Defining the average velocities of the two layers as:

$$\text{Upper layer} = \quad u_1 = \frac{q_1}{h_1} = \frac{1}{h_1}\int_{h_2}^{h_1+h_2} u\,dz$$

$$\text{Lower layer} = \quad u_2 = \frac{q_2}{h_2} = \frac{1}{h_2}\int_{o}^{h_2} u\,dz$$

where q_1, q_2 are flow per unit width of the respective layers

$$q_1 = \frac{Q_1}{2r\pi}$$

$$q_2 = \frac{Q_2}{2r\pi} \qquad Q_1,\ Q_2 \text{ are constants}$$

h_1 = upper layer depth

h_2 = lower layer depth

Assuming hydrostatic pressure distribution; we have

$$\text{upper layer} = \quad p = \rho_1 g\ (h_1 + h_2 - z)$$

$$\text{lower layer} = \quad p = \rho_1 g\ h_1 + \rho_2 g\ (h_2 - z)$$

ρ_1 = density of upper layer

ρ_2 = density of lower layer

By continuity:

$$u\ \left(\frac{\partial u}{\partial r} + \frac{u}{r} + \frac{\partial w}{\partial z} \right) = 0$$

therefore

$$\frac{\partial u^2}{\partial r} - u\frac{\partial u}{\partial r} + \frac{\partial uw}{\partial z} - u\frac{\partial w}{\partial z} = \frac{\partial u^2}{\partial r} + \frac{\partial uw}{\partial z} + \frac{u^2}{r}$$

Integrating eq. 2.3.1 in the z-direction over the upper layer

$$\int_{h_2}^{h_1+h_2} \frac{\partial u^2}{\partial r}\, dz + \int_{h_2}^{h_1+h_2} \frac{\partial uw}{\partial z}\, dz + \int_{h_2}^{h_1+h_2} \frac{u^2}{r} dz = -\frac{g}{\rho_a} \int_{h_2}^{h_1+h_2} (\rho_1 (\frac{\partial h_1}{\partial r} + \frac{\partial h_2}{\partial r}))dz$$

$$+ \left(\varepsilon_z \frac{\partial u}{\partial z} \right) \Big|_{h_2}^{h_1+h_2}$$

$$\frac{\partial}{\partial r} \int_{h_2}^{h_1+h_2} u^2 dz \;-\; u_s^2 \frac{\partial (h_1+h_2)}{\partial r} + u_i^2 \frac{\partial (h_1+h_2)}{\partial r} + u_s w_s - u_i w_i + \frac{u_1^2}{r} h_1$$

$$= -\frac{g}{\rho_a} \frac{\partial \rho_1}{\partial r} (\frac{h_1^2}{2}) - \frac{g}{\rho_a} \rho_1 \frac{\partial (h_1+h_2)}{\partial r} h_1 + \frac{\tau_s - \tau_i}{\rho_a}$$

Carrying out a similar integration for the lower layer and invoking the kinematic and dynamic boundary conditions at the points of discontinuity, the following equations of motion for the two layers are obtained by neglecting surface shear ($\tau_s = 0$).

Upper layer:

$$(\frac{Q_1}{2\pi r})^2 \left[\frac{1}{h_1^2} \frac{\partial h_1}{\partial r} + \frac{1}{r h_1} \right] = g \frac{\rho_1}{\rho_a} \frac{\partial (h_1+h_2)}{\partial r} h_1 + \frac{\tau_i}{\rho_a} \qquad (2.3.2)$$

Lower layer:

$$(\frac{Q_2}{2\pi r})^2 \left[\frac{1}{h_2^2} \frac{\partial h_2}{\partial r} + \frac{1}{r h_2} \right] = \frac{g}{\rho_a} \left[\rho_1 \frac{\partial h_1}{\partial r} + \rho_2 \frac{\partial h_2}{\partial r} \right] h_2 - \frac{(\tau_i - \tau_b)}{\rho_a} \qquad (2.3.3)$$

2.4 The Radial Internal Hydraulic Jump

The internal hydraulic jump in a two-dimensional two-layered system has previously been treated by Yih (1955), Jirka and Harleman (1973). For an axi-symmetric jet in shallow water, a two-layered counterflow system consisting of a heated flow away in the upper layer and an ambient inflow induced by jet entrainment in the lower layer is set up in the near field. If a stable near field exists, an internal jump is always observed. The transition is accompanied by an energy loss and possibly turbulent entrainment at the interface. An approximate analysis is presented in this section to solve for the conjugate jump heights of the respective layers. These represent two possible dynamic states for the same given momentum flux. A simplified asymptotic solution is also derived as a special application to submerged discharge problems.

As a first approximation, a momentum analysis of the two layers is carried out by neglecting shear stresses. Because of the expanding cross-sections of a radial system, this assumption may introduce a substantial error in the computation of the exact conjugate jump height. It will be seen that this simplified analysis still gives valuable insight into the stability of the near field.

With the above-stated assumptions, the vertically averaged equations of motion for the radial stratified flow of an axisymmetric two-layered system eq. 2.3.2 - 2.3.3 become

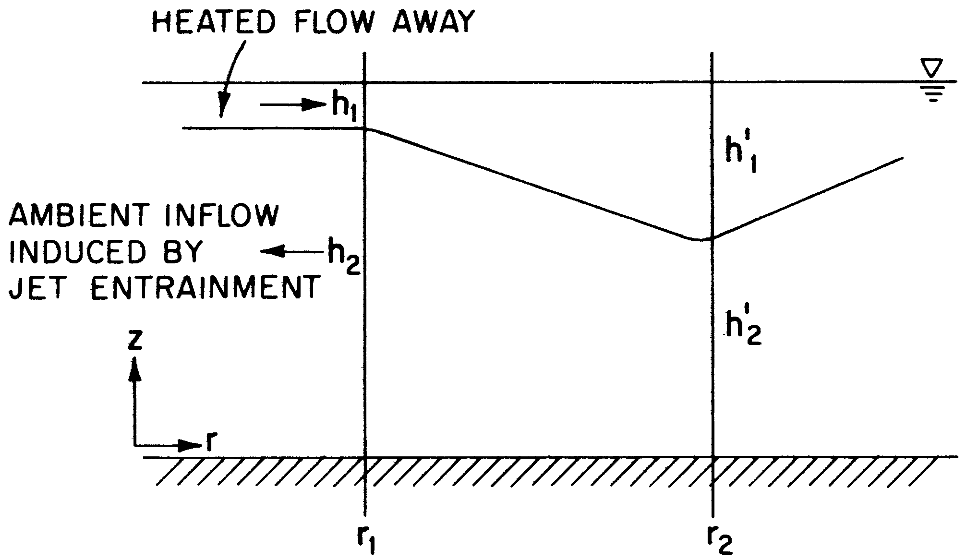

FIGURE (2-7) THE RADIAL INTERNAL JUMP

$$\left(\frac{Q_1}{2\pi r}\right)^2 \left[\frac{1}{h_1^2}\frac{dh_1}{dr} + \frac{1}{rh_1}\right] = g\,\frac{\rho_1}{\rho_a}\,\frac{d(h_1+h_2)}{dr}\,h_1 \qquad (2.4.1)$$

$$\left(\frac{Q_2}{2\pi r}\right)^2 \left[\frac{1}{h_2^2}\frac{dh_2}{dr} + \frac{1}{rh_2}\right] = \frac{g}{\rho_a}\left[\rho_1\frac{dh_1}{dr} + \rho_2\frac{dh_2}{dr}\right] h_2 \qquad (2.4.2)$$

where Q_1 , Q_2 are flows in the respective layers.

Noting that

$$\left[\frac{1}{h_1^2}\frac{dh_1}{dr} + \frac{1}{rh_1}\right] = -r\,\frac{d\left(\frac{1}{rh_1}\right)}{dr}$$

Eq. 2.4.1 becomes on simplification

$$\left(\frac{Q_1}{2\pi}\right)^2 \frac{d\left(\frac{1}{rh_1}\right)}{dr} = -g\,\frac{\rho_1}{\rho_a}\,\frac{d(h_1+h_2)}{dr}\,rh_1$$

Integrating from r_1 to r_2 , assuming $\bar{r} \simeq \frac{r_1+r_2}{2}$ and an average head $\bar{h}_1 \simeq \frac{h_1+h_2}{2}$ in the interval, we have

$$\left(\frac{Q_1}{2\pi}\right)^2 \left[\frac{1}{r_1h_1} - \frac{1}{r_2h_1'}\right] = g\,\frac{\rho_1}{\rho_a}\,\frac{(r_1+r_2)}{2}\,\frac{(h_1+h_1')}{2}\,(h_1'+h_2'-h_1-h_2) \qquad (2.4.3)$$

where h_1' , h_2' are the conjugate jump heights of the respective layers

A similar integration for the lower layer then gives

$$\left(\frac{Q_2}{2\pi}\right)^2 \left[\frac{1}{r_1h_2} - \frac{1}{r_2h_2'}\right] = g\,\frac{(h_2+h_2')}{2}\,\frac{(r_1+r_2)}{2}\left\{\frac{\rho_1}{\rho_a}(h_1'-h_1)+\frac{\rho_2}{\rho_a}(h_2'-h_2)\right\} \qquad (2.4.4)$$

Defining free surface Froude numbers as:

$$F_1^{*2} = \frac{\left(\frac{Q_1}{2\pi r_1 h_1}\right)^2}{g h_1}$$

$$F_2^{*2} = \frac{\left(\frac{Q_2}{2\pi r_1 h_2}\right)^2}{g h_2}$$

Equation 2.4.3-2.4.4 can then be reduced to:

Upper Layer:

$$F_1^{*2} r_1^2 \left[\frac{1}{r_1 h_1} - \frac{1}{r_2 h_1'}\right] = \frac{\rho_1}{\rho_a} \left(\frac{r_1+r_2}{2}\right)\left(\frac{h_1+h_1'}{2}\right) [\, h_1'+h_2'-h_1-h_2] \frac{1}{h_1^3} \qquad (2.4.5)$$

Lower Layer:

$$F_2^{*2} r_1^2 \left[\frac{1}{r_1 h_2} - \frac{1}{r_2 h_2'}\right] = \frac{(h_2+h_2')}{2} \; \frac{(r_1+r_2)}{2} \left[\frac{\rho_1}{\rho_a}(h_1'-h_1) + \frac{\rho_2}{\rho_a}(h_2'-h_2)\right] \frac{1}{h_2^3} \qquad (2.4.6)$$

Eq. 2.4.5 and 2.4.6 constitute an approximate momentum analysis of an internal hydraulic jump in a general two-layered system. Most submerged discharge designs, however, are characterised by small density differences and negligible free surface Froude numbers, but finite densimetric Froude numbers. An asymptotic solution can be obtained as follows:

Rearranging eq. 2.4.5 and eq. 2.4.6 we have

$$F_1^{*2}\left[1- \frac{r_2 h_1'}{r_1 h_1}\right] = \frac{1}{4} \left[1- \frac{\Delta\rho}{\rho}\right] \frac{r_2 h_1'}{r_1 h_1} \left[1+ \frac{r_2}{r_1}\right]\left[1+ \frac{h_1'}{h_1}\right] \left[\left(1- \frac{h_1'}{h_1}\right) + \left(1- \frac{h_2'}{h_2}\right)\frac{h_2}{h_1}\right]$$

$$F_2^{*2}\left[1- \frac{r_2 h_2'}{r_1 h_2}\right] = \frac{1}{4} \frac{r_2 h_2'}{r_1 h_2}\left[1+ \frac{r_2}{r_1}\right]\left[1+ \frac{h_2'}{h_2}\right] \left[\left(1- \frac{\Delta\rho}{\rho}\right)\left(1- \frac{h_1'}{h_1}\right)\frac{h_1}{h_2} + \left(1- \frac{h_2'}{h_2}\right)\right]$$

On further algebraic manipulation we obtain

$$\frac{h_2'}{h_2} = \frac{4F_1^{*2}\left[-1 + \frac{r_2 h_1'}{r_1 h_1}\right] \frac{h_1}{h_2}}{\left[1- \frac{\Delta\rho}{\rho}\right] \frac{r_2 h_1'}{r_1 h_1} \left[1+ \frac{r_2}{r_1}\right] \left[1+ \frac{h_1'}{h_1}\right]} + \left(1- \frac{h_1'}{h_1}\right)\frac{h_1}{h_2} + 1 \qquad (2.4.7)$$

$$\frac{h_1'}{h_1} = \frac{4F_2^{*2}\left[-1+\frac{r_2h_2'}{r_1h_2}\right]\frac{h_2}{h_1}}{\frac{r_2h_2'}{r_1h_2}\left[1+\frac{r_2}{r_1}\right]\left[1+\frac{h_2'}{h_2}\right]\left(1-\frac{\Delta\rho}{\rho}\right)} + \left(1-\frac{h_2'}{h_2}\right)\frac{h_2}{h_1}\frac{1}{\left(1-\frac{\Delta\rho}{\rho}\right)} + 1 \qquad (2.4.8)$$

It can be derived from eq. (2.4.7)

that
$$\frac{h_2'-h_1}{h_1'-h_1} = \frac{A\,h_2}{h_1'-h_1} - 1 \qquad (2.4.9)$$

where
$$A = \frac{4F_1^{*2}\left[-1+\frac{r_2h_1'}{r_1h_1}\right]\frac{h_1}{h_2}}{\frac{r_2h_1'}{r_1h_1}\left[1+\frac{r_2}{r_1}\right]\left[1+\frac{h_1'}{h_1}\right]\left(1-\frac{\Delta\rho}{\rho}\right)}$$

Two alternative expressions can be derived from eq. (2.4.8)

$$\frac{h_2'-h_2}{h_1'-h_1} = \frac{B\,h_1}{h_1'-h_1}\left(1-\frac{\Delta\rho}{\rho}\right) - \left(1-\frac{\Delta\rho}{\rho}\right) \qquad (2.4.10)$$

and

$$\frac{h_2'-h_2}{h_1'-h_1} = \frac{(h_2'-h_2)\left(1-\frac{\Delta\rho}{\rho}\right)}{\left(1-\frac{\Delta\rho}{\rho}\right)B\,h_1 - (h_2'-h_2)} \qquad (2.4.11)$$

where
$$B = \frac{4F_2^{*2}\left[-1+\frac{r_2h_2'}{r_1h_2}\right]\frac{h_2}{h_1}}{\frac{r_2h_2'}{r_1h_2}\left[1+\frac{r_2}{r_1}\right]\left[1+\frac{h_2'}{h_2}\right]\left[1-\frac{\Delta\rho}{\rho}\right]}$$

Subtracting eq. 2.4.9 from eq. 2.4.10 we get

$$\frac{4F_1^{*2}\left[\frac{r_2h_1'}{r_1h_1}-1\right]\frac{h_1}{h_2}}{\left[1-\frac{\Delta\rho}{\rho}\right]\frac{r_2h_1'}{r_1h_1}\left(1+\frac{r_2}{r_1}\right)\left(1+\frac{h_1'}{h_1}\right)}\frac{h_2}{h_1'-h_1} = \frac{4F_2^{*2}\left[\frac{r_2h_2'}{r_1h_2}-1\right]\frac{h_2}{h_1}}{\frac{r_2h_2'}{r_1h_2}\left(1+\frac{r_2}{r_1}\right)\left(1+\frac{h_2'}{h_2}\right)}\frac{h_1}{(h_1'-h_1)} \tag{2.4.12}$$

$$+\frac{\Delta\rho}{\rho}$$

Subtracting eq. 2.4.9 from eq. 2.4.11 we obtain an independent eq.

$$\frac{4F_1^{*2}\left[1-\frac{r_2h_1'}{r_1h_1}\right]}{\left(1-\frac{\Delta\rho}{\rho}\right)\frac{r_2h_1'}{r_1h_1}\left(1+\frac{r_2}{r_1}\right)\left(1+\frac{h_1'}{h_1}\right)\left(1-\frac{h_1'}{h_1}\right)} - 1 = \tag{2.4.13}$$

$$\frac{\frac{r_2h_2'}{r_1h_2}\left(1+\frac{r_2}{r_1}\right)\left(1+\frac{h_2'}{h_2}\right)\left(1-\frac{h_2'}{h_2}\right)\left(1-\frac{\Delta\rho}{\rho}\right)}{4F_2^{*2}\left(1-\frac{r_2h_2'}{r_1h_2}\right)-\frac{r_2h_2'}{r_1h_2}\left(1+\frac{r_2}{r_1}\right)\left(1+\frac{h_2'}{h_2}\right)\left(1-\frac{h_2'}{h_2}\right)}$$

In the limit when $\frac{\Delta\rho}{\rho}\to 0$, $F_1^*, F_2^* \to 0$

and
$$F_1^2 = \frac{F_1^{*2}}{\frac{\Delta\rho}{\rho}} \qquad \text{finite}$$

$$F_2^2 = \frac{F_2^{*2}}{\frac{\Delta\rho}{\rho}}$$

Eq. 2.4.12 and 2.4.13 reduce to

$$\frac{4F_1^2\left[1-\frac{r_2h_1'}{r_1h_1}\right]}{\frac{r_2h_1'}{r_1h_1}\left[1+\frac{r_2}{r_1}\right]\left[1+\frac{h_1'}{h_1}\right]\left[1-\frac{h_1'}{h_1}\right]} - 1 = \frac{4F_2^2\left[1-\frac{r_2h_2'}{r_1h_2}\right]\frac{h_2}{h_1}}{\frac{r_2h_2'}{r_1h_2}\left(1+\frac{r_2}{r_1}\right)\left(1+\frac{h_2'}{h_2}\right)\left(1-\frac{h_1'}{h_1}\right)} \tag{2.4.14}$$

$$\left[\frac{r_2h_1'}{r_1h_1}\left(1+\frac{r_2}{r_1}\right)\left(1+\frac{h_1'}{h_1}\right)\left(1-\frac{h_1'}{h_1}\right)-4F_1^2\left(1-\frac{r_2h_1'}{r_1h_1}\right)\right]\left[\frac{r_2h_2'}{r_1h_2}\left(1+\frac{r_2}{r_1}\right)\left(1+\frac{h_2'}{h_2}\right)\left(1-\frac{h_1'}{h_1}\right)-\right.$$
$$\left.-4F_2^2\left(1-\frac{r_2h_2'}{r_1h_2}\right)\right] = 16\,F_1^2\,F_2^2\left[1-\frac{r_2h_1'}{r_1h_1}\right]\left[1-\frac{r_2h_2'}{r_1h_2}\right] \tag{2.4.15}$$

These 2 equations describe an asymptotic solution to the radial internal jump problem. Given the densimetric Froude numbers of the respective layers, a numerical solution can be determined by relating the jump length (r_2-r_1) to the jump height $(h_1'-h_1)$.

The radial free surface hydraulic jump has been studied by Sadler et al (1963). The momentum equation assuming a finite jump length for this case is

$$\pi\, r_1y_1^2 + \frac{Q^2}{2\pi gry} = \pi\, r_2y_2^2 + \frac{Q^2}{2\pi gr_2y_2}$$

This can be gotten from eq. 2.4.4 by setting $\rho_1=0$ $\rho_2=\rho_a$ $Q_2=Q$

In the free surface case an experimentally determined coefficient of 4 is found for the ratio of the jump length to the jump height. The theoretical investigations of a radial two-layered system in the next section, however, shows a drastic difference in its behavior as compared to the free surface counterpart. No attempt is hence made in using this coefficient.

Valuable insight can be obtained by treating the case of negligible jump length, i.e., $r_2 = r_1$. A main concern of this study is to determine the criterion of the near field stability, that is, the locus of $(F_o, H/D)$ that characterises a stable-unstable near field transition. In view of the exclusion of shear stress in the momentum equations and the unknown relationship between jump length and jump height, it is judged that the solution of the radial internal jump problem in the context of a negligible jump length should furnish adequate information concerning the existence of a jump.

By setting $r_2 = r_1$ in eqs. 2.4.14-2.4.15 we obtain

$$2F_1^2 - \frac{h_1'}{h_1}\left(1+\frac{h_1'}{h_1}\right) = \frac{2F_2^2 \dfrac{h_1'}{h_1}\left(1+\dfrac{h_1'}{h_1}\right)\left(1-\dfrac{h_2'}{h_2}\right)}{\dfrac{h_2'}{h_2}\left(1+\dfrac{h_2'}{h_2}\right)\left(1-\dfrac{h_1'}{h_1}\right)} \frac{h_2}{h_1} \tag{2.4.16}$$

$$\left[\frac{h_1'}{h_1}\left(1+\frac{h_1'}{h_1}\right) - 2F_1^2\right]\left[\frac{h_2'}{h_2}\left(1+\frac{h_2'}{h_2}\right) - 2F_2^2\right] = 4\,F_1^2\,F_2^2 \tag{2.4.17}$$

The above equations are the same solution obtained for a two dimensional internal jump by Jirka and Harleman (1973). Combining the two eqs. we get

$$\frac{h_2'}{h_2}\left(\frac{h_2'}{h_2}+1\right) = \frac{4\,F_1^2\,F_2^2}{\dfrac{h_1'}{h_1}\left(\dfrac{h_1'}{h_1}+1\right) - 2\,F_1^2} + 2\,F_2^2 \tag{2.4.18}$$

From eq. (2.4.17), we have

$$\frac{h_2'}{h_2} = 1 + \frac{\frac{h_2'}{h_2}(\frac{h_2'}{h_2}+1)(\frac{h_1'}{h_1}-1)\ \frac{h_2}{h_1}\ [\frac{h_1'}{h_1}(\frac{h_1'}{h_1}+1) - 2\ F_1^2\ ]}{-2\ F_2^2\ \frac{h_1'}{h_1}\ (1+\frac{h_1'}{h_1})} \tag{2.4.19}$$

Substituting the value of $\frac{h_2'}{h_2}(\frac{h_2'}{h_2}+1)$ in eq. 2.4.18 into eq. 2.4.19 the following relationship is obtained

$$\frac{h_2'}{h_2} = 1 - (\frac{h_1'}{h_1} - 1)\ \frac{h_1}{h_2}$$

or $\quad h_1' + h_2' = h_2 + h_1$ (2.4.20)

Under such limiting conditions the total water depth remains unchanged. Substituting the value of h_2' in terms of h_1' into eq. 2.4.17 we have the single asymptotic form:

$$[\ \{(\frac{h_1'}{h_1}-1)\ \frac{h_1}{h_2} - \frac{3}{2}\}^2 - \frac{1}{4}\ ]\ [\frac{h_1'}{h_1}(\frac{h_1'}{h_1}+1) - 2\ F_1^2\ ] = \frac{h_1'}{h_1}(\frac{h_1'}{h_1}+1)2F_2 \tag{2.4.21}$$

which has been given by Jirka and Harleman (1973).

In the limiting case of a critical section $h_1' = h_1$ eq. 2.4.21 reduces to

$$F_1^2 + F_2^2 = 1 \tag{2.4.22}$$

Eq. 2.4.22 can be viewed as a defining statement of a critical section in a two-layered system.

For some combinations of F_1^2, F_2^2, $\frac{h_1}{h_2}$, eq. 2.4.21 does not yield a solution. This indicates a hydrodynamically unstable situation: even the longest waves at the interface amplify in magnitude; the excess kinetic energy is dissipated by turbulent diffusion over the near field region, leading to heat re-entrainment into the jet.

The implicitform of eq. 2.4.22 is plotted for a typical stable case and a typical unstable case (Fig. 2-8). In the case of a stable near field, two roots are always detected, the root with the larger value being disregarded by energy considerations. Numerical experience have shown that solving eq. 2.4.16 - 2.4.17 always gives the correct conjugate jump height.

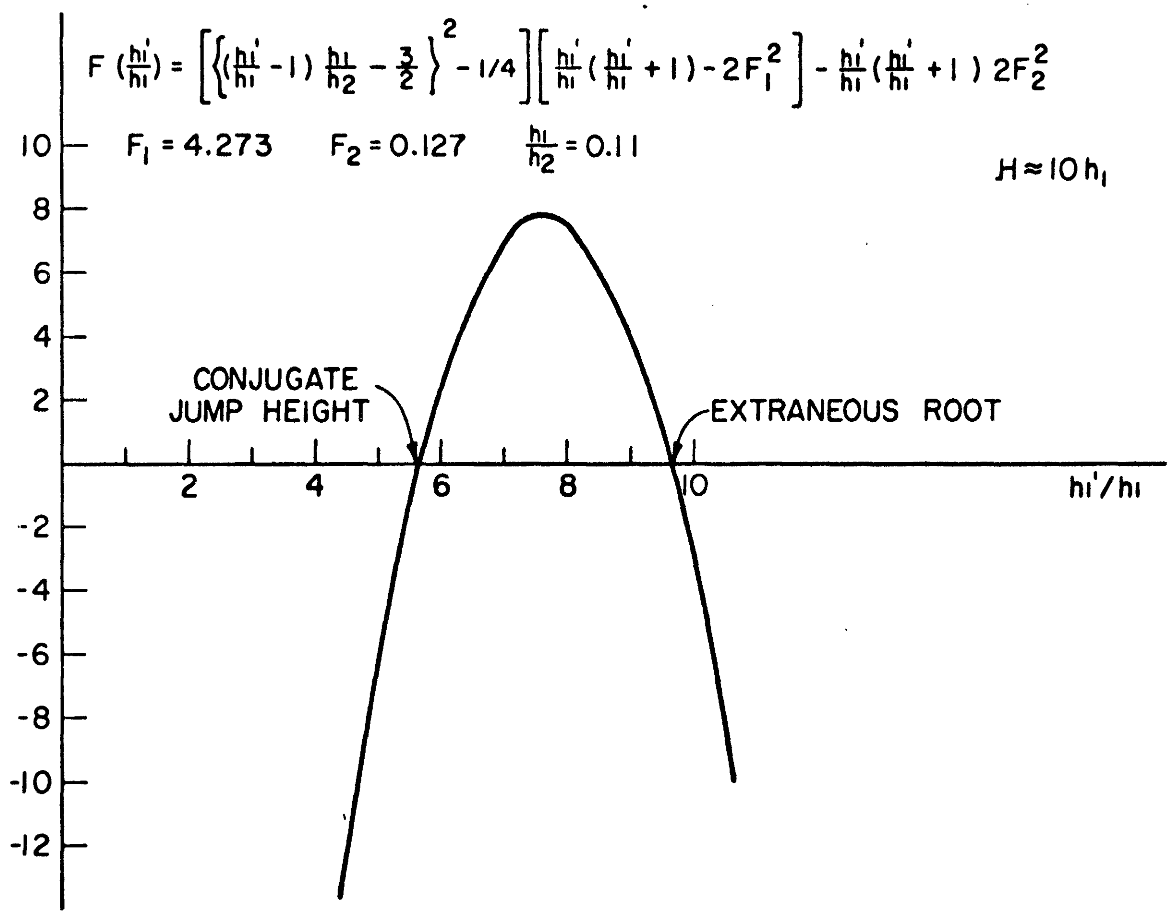

FIGURE (2-8a) BEHAVIOR OF ASYMPTOTIC SOLUTION: STABLE NEAR FIELD

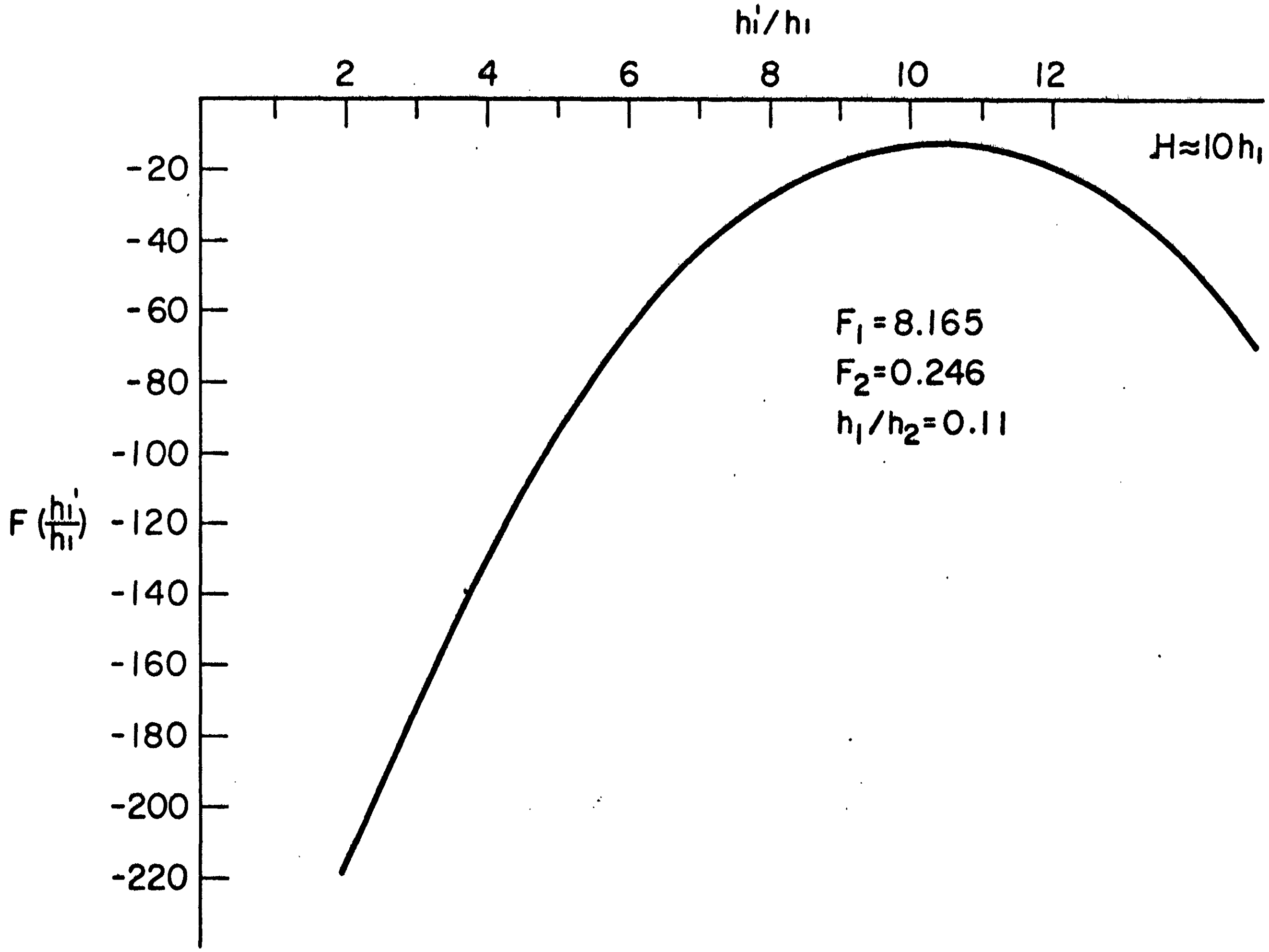

FIGURE (2-8b) BEHAVIOR OF ASYMPTOTIC SOLUTION UNSTABLE NEAR FIELD

2.5 Stratified Counterflow Region

When an unstable near field is present, there is heat re-entrainment of the jet, and a critical section is established near the discharge (at the critical section there is a sharp change in the interface)(Fig. 2-9). The subsequent fluid motion is described by a stratified counter-flow system. In the following sections the basic mechanics of the flow is discussed with respect to a far field condition similar to that in the experimental set up of this study (no imposed physical boundaries; ambient fluid at rest). In the prototype heat loss effects may govern the far field boundary condition. The fundamental behavior of the governing equations are presented and contrasted with the two-dimensional counterpart. Finally the predictions of the near field dilution for unstable jets are given.

2.5.1 The Momentum Equation for Axi-symmetric Stratified Flow

Noting that $\rho_2 = \rho_a$, $\rho_1 = \rho_a - \Delta\rho$ $\Delta\rho > 0$, eq. 2.3.1-2.3.2 can be simplified to give:

$$F_1^{*2} \left[\frac{dh_1}{dr} + \frac{h_1}{r}\right] = \left(1 - \frac{\Delta\rho}{\rho}\right) \frac{d(h_1+h_2)}{dr} + \frac{\tau_i}{\rho_a g h_1} \tag{2.5.1}$$

$$F_2^{*2} \left[\frac{dh_2}{dr} + \frac{h_2}{r}\right] = \frac{d(h_1+h_2)}{dr} - \frac{\Delta\rho}{\rho}\frac{dh_1}{dr} - \frac{(\tau_i-\tau_b)}{\rho g h_2} \tag{2.5.2}$$

Under the limiting conditions $\Delta\rho \to 0$, F_1^{*2}, $F_2^{*2} \to 0$. It was shown in a previous section that the total water depth is a constant

$$\frac{d(h_1+h_2)}{dr} = 0 \tag{2.5.3}$$

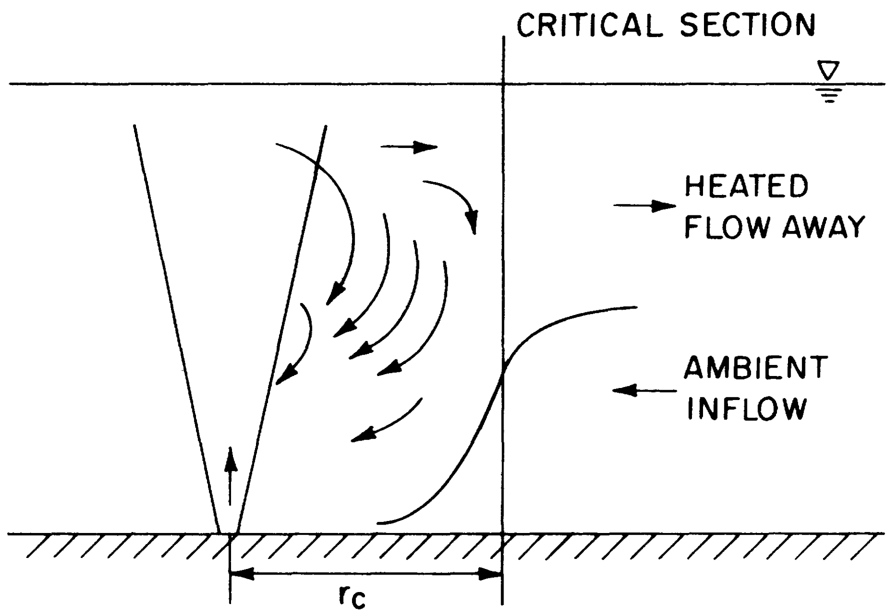

FIGURE (2-9) STRATIFIED COUNTER FLOW SYSTEM
IN AN UNSTABLE NEAR FIELD

Substituting eq. (2.5.3) in eq. 2.5.1-2.5.2 and rearranging, one obtains the following expression governing the radial variation of the interface

$$\frac{dh_2}{dr}\left[\frac{\Delta\rho}{\rho} - F_1^{*2} - F_2^{*2}\right] = F_2^{*2}\frac{h_2}{r} - F_1^{*2}\frac{h_1}{r} + \frac{\tau_i}{\rho g h_1} + \frac{(\tau_i-\tau_b)}{\rho g h_2}$$

Remembering $F_1^2 = F_1^{*2}/\frac{\Delta\rho}{\rho}$ $\quad F_2^2 = F_2^{*2}/\frac{\Delta\rho}{\rho}$, we get

$$\frac{dh_2}{dr} = \frac{F_2^2\frac{h_2}{r} - F_1^2\frac{h_1}{r} + \frac{\tau_i}{\rho g h_1}\frac{\rho}{\Delta\rho} + \frac{(\tau_i-\tau_b)}{\rho g h_2}}{1 - F_1^2 - F_2^2} \tag{2.5.4}$$

At the critical section, the sharp change in the interface can be described mathematically by $\frac{dh_2}{dr} \to \infty$, giving again the critical condition $F_1^2 + F_2^2 = 1.$

The interfacial and bottom shear are related to the velocities in the two layers in the usual quadratic friction relationships:

$$|\tau_i| \quad \frac{\rho f_i}{8}\,(u_1-u_2)^2 = \frac{\rho f_i}{8}\left(\frac{Q_1}{h_1} - \frac{Q_2}{h_2}\right)^2 \frac{1}{(2\pi r)^2}$$

Prefixing the known directions of our counterflow system, one obtains

$$\tau_i = \frac{\rho f_i}{8}\left(\frac{Q_1}{2\pi r}\right)^2 \frac{1}{h_2}\left(1 - \frac{Q_2}{Q_1}\frac{h_1}{h_2}\right)^2 \qquad Q_2 > 0 \quad Q_1 > 0$$

Similarly $\tau_o = \frac{\rho f_o}{8}\left(\frac{Q_2}{2\pi r}\right)^2\frac{1}{h_2}$

Substituting the expressions for τ_i and τ_o into eq. (2.5.4) we obtain the radial variation of the interface in the stratified counterflow system:

$$\frac{dh_2}{dr} = \frac{F_2^2\frac{h_2}{r} - F_1^2\frac{h_1}{r} + \frac{f_i}{8}F_1^2\left(1+\frac{h_1}{h_2}\right)\left(1-\frac{Q_2 h_1}{Q_1 h_2}\right)^2 + \frac{f_o}{8}F_2^2}{1 - F_1^2 - F_2^2} \tag{2.5.5}$$

2.5.2 Behavior of the counterflow system

The entire physical situation can be described by eq. 2.5.5 subject to a far field boundary condition which will be discussed later. At the critical section $r = r_c$, the critical flow condition $F_1^2 + F_2^2 = 1$ has to be satisfied.

In the sequel, the essential features of eq. 2.5.5 are discussed by considering the special case of equal counterflow $Q_1 = Q_2$, which indeed represents the case of high dilutions. For this case the problem can be shown to be dependent on a single dimensionless parameter.

Defining F_H^2 as $\dfrac{\left(\dfrac{Q}{2\pi r_c H}\right)^2}{g\dfrac{\Delta\rho}{\rho} H}$, constant densimetric Froude number based the total water depth

the problem can be cast in dimensionless form:

$$\frac{dH_2}{dR} = \frac{F_H^2 \dfrac{\left(\frac{R_c}{R}\right)^2}{H_2^3}\left(\dfrac{H_2}{R}\right) - \dfrac{F_H^2\left(\frac{R_c}{R}\right)^2}{(1-H_2)^3}\left(\dfrac{1-H_2}{R}\right) + \dfrac{f_i}{8}\dfrac{F_H^2\left(\frac{R_c}{R}\right)^2}{(1-H_2)^3}\dfrac{\left(1-\frac{(1-H_2)}{H_2}\right)^2}{H_2} + \dfrac{f_o}{8}F_H^2\dfrac{\left(\frac{R_c}{R}\right)^2}{H_2^3}}{1 - F_H^2\dfrac{\left(\frac{R_c}{R}\right)^2}{(1-H_2)^3} - F_H^2\dfrac{\left(\frac{R_c}{R}\right)^2}{H_2^3}}$$

s.t. at the critical section R_c

H_2 satisfies

$$F_H^2 \frac{1}{(1-H_2)^3} + \frac{1}{H_2^3} = 1$$

where $H_2 = h_2/H \qquad R = r/H \qquad R_c = r_c/H$

The radius r_c is to be determined from experimental results.

For a given F_H, $H_2(r = r_c)$ can be found by solving the critical flow condition. One H_{2c} is known, eq. 2.5.6 can then be solved numerically as an initial-value problem, using numerical methods, such as a fourth order Runga-Kutta scheme . Since the derivative $\frac{dH_2}{dR}$ is infinite at the starting point, the first few points of the interface is found by inverting the derivative and solving the inverse problem with $\frac{dR}{dH_2}$; after marching a few steps out, the formal derivative can be used again.

The change in the interface for different values of F_H and different friction coefficients is illustrated in fig. (2-10). Two remarks can be inferred:

1) For small R_c and in particular, $R_c \sim 0(1)$, which is experimentally observed, the inclusion of frictional effects has a negligible effect on the shape of the interface. In such cases the radial inertial effects predominate, and a frictionless flow situation can be adequately assumed.

2) The interface always approaches an asymptotic value horizontally. The value increases as F_H increases. In the limit as F_H approaches 0.25, the interface attains a maximum asymptotic value of 0.5 in the far field.

These behavior can be readily explained by studying eq. 2.5.5 in detail. For $R_c \sim 0(1)$ and H_2 finite the numerator of the derivative approaches zero as $r \to \infty$. Hence H_2 attains a constant value for large r.

Insight into the mechanics of the flow can be gained by contrasting eq. 2.5.5 with a radial free surface inward flow and a two-dimensional stratified counter-flow system. Sadler et al (1963) have derived the free surface curve for frictionless radial inward flow to be

$$\frac{dy}{dR} = \frac{F^2}{1 - F^2} \frac{y}{R} \tag{2.5.7}$$

where F = free surface Froude number

y = water depth

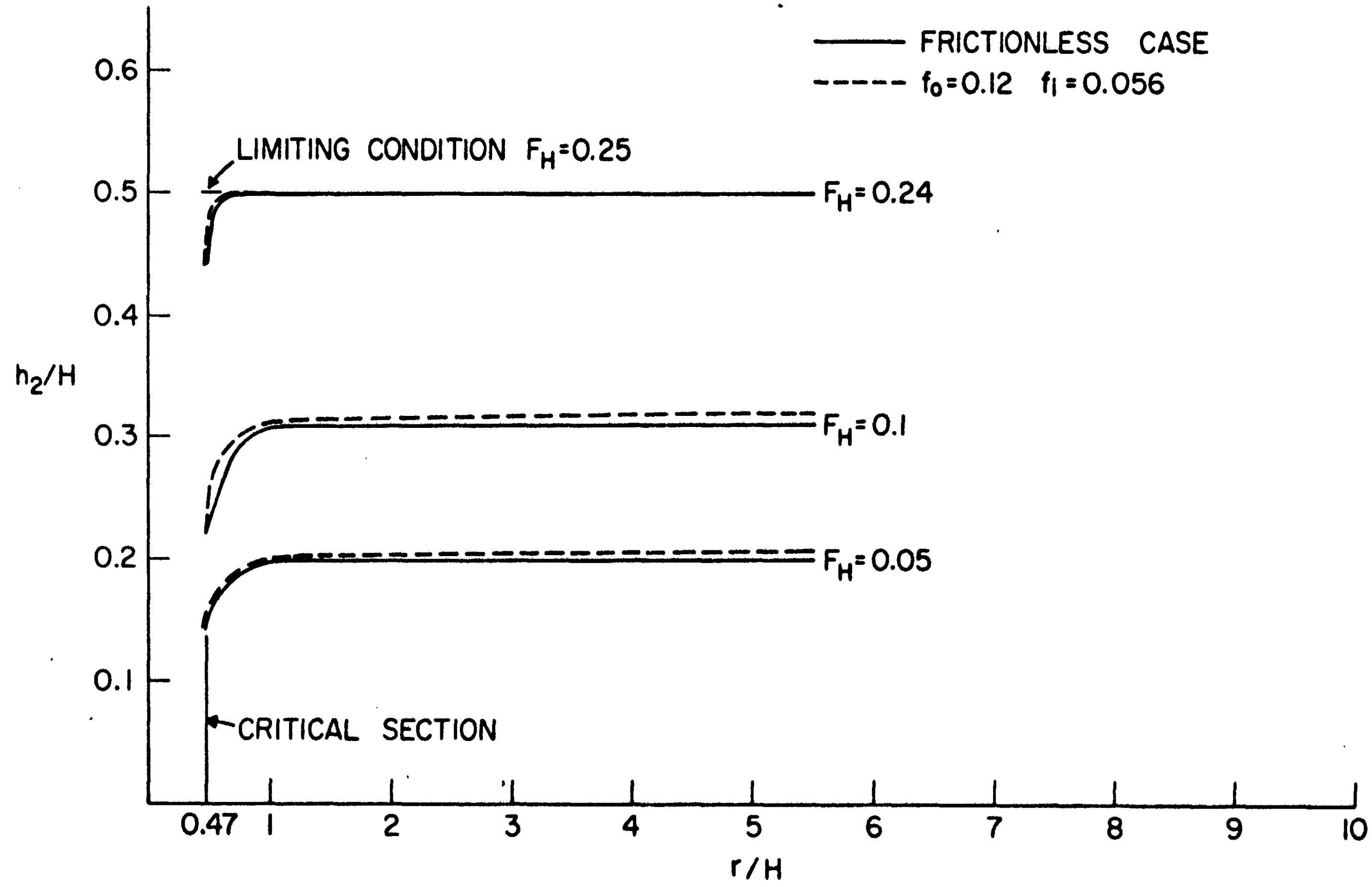

FIGURE (2-10) RADIAL VARIATION OF THE INTERFACE

This can be attained from the more general eq. 2.5.5 by setting $\frac{\Delta\rho}{\rho} = \frac{\rho}{\rho} = 1$ $f_i = f_o = 0$ and $F_1 = 0$.

It can be seen from eq. 2.5.7 that for subcritical flow ($F < 1$) the water depth is always increasing with $\frac{dy}{dR} = 0$ is asymptotically approached in the far field.

Jirka (1973) treated the two-dimensional counterpart of the present problem. For $r \to \infty$ eq. 2.5.5 reduced to this two-dimensional case, namely

$$\frac{dh_2}{dx} = \frac{\frac{f_o}{8} F_2^2 + \frac{f_i}{8} F_1^2 \left(1 - \frac{1}{Q_r} \frac{h_1}{h_2}\right)^2 \frac{H}{h_2}}{1 - F_1^2 - F_2^2} \tag{2.5.8}$$

where $Q_r = Q_1/Q_2$

Again eq. 2.5.8 can be obtained directly from eq. 2.5.5 by neglecting the radial components. In fact, equation 2.5.5 can be made to exhibit a two-dimensional behavior by artificially setting R_c very large, thus destroying the radial dependence of the equation. As illustrated in fig. (2-11), in these cases a second critical section is always found by marching out the solution. The interfacial height at this second critical section is approximately conjugate to the starting point. The physical implication is that in subcritical flow roughness effects always tend to raise the interface; however, because of the physical constraint imposed by the free surface, a critical section has to be formed some distance from the starting point.

In a radial stratified counterflow system with $R_c \sim O(1)$, however, the radial expansion allows one more degree of freedom; this stabilizes the flow and a second critical section is not formed near the starting point.

For the range of interest, $0.4 < R_c < 2$ strong self-similarity is

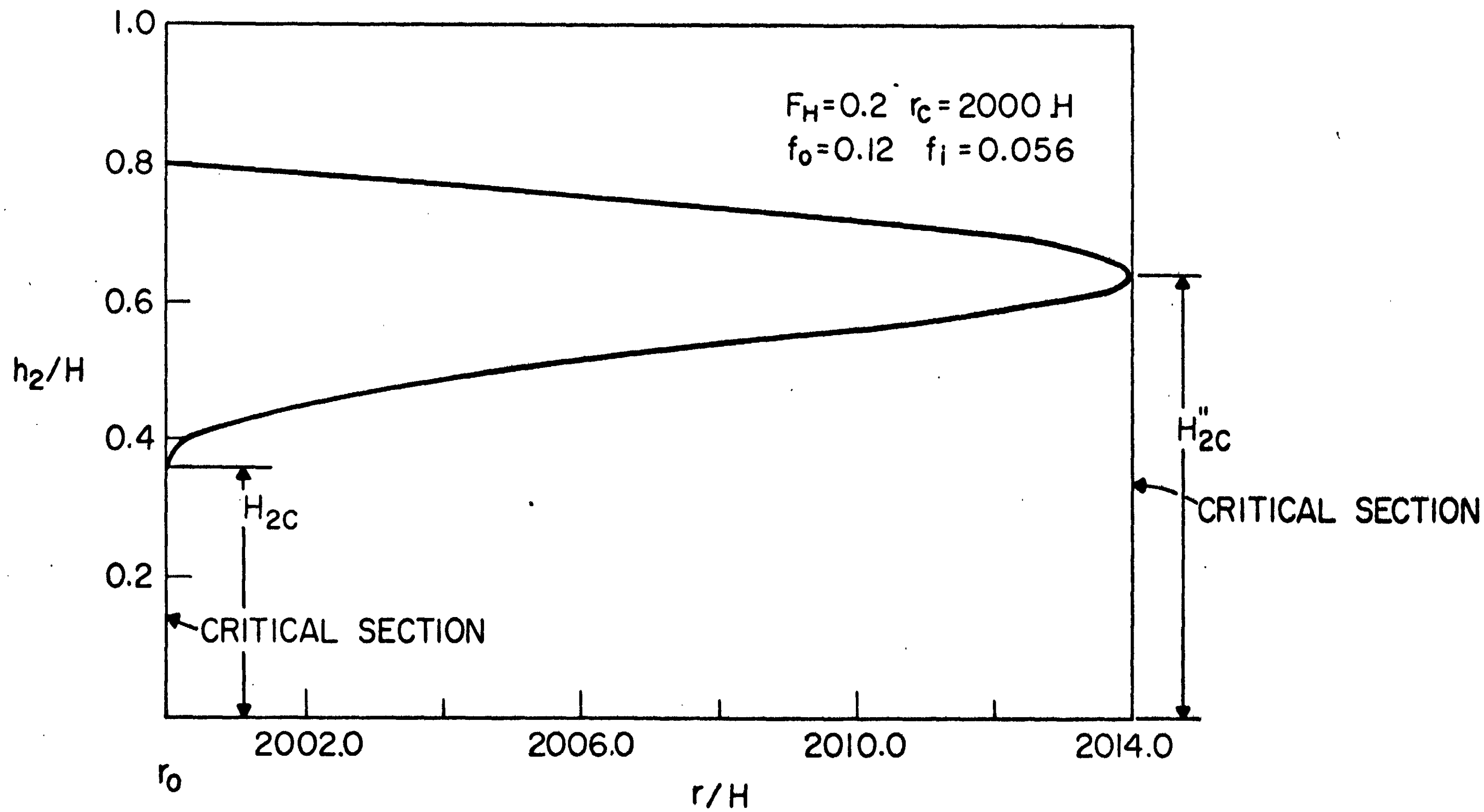

FIGURE (2-11) ILLUSTRATION OF TWO DIMENSIONAL COMPONENT FEATURE OF AXI-SYMMETRIC RADIAL STRATIFIED FLOW found in the behavior of eq. 2.5.5. All the information can be summarized by plotting h_2 against r/r_c (Fig. 2-12).

In the general case of non-equal counterflow the problem can be shown to be dependent on F_{2H} and Q_r, where $F_{2H}^2 = \dfrac{\left(\dfrac{Q_2}{2\pi r_c H}\right)^2}{g \dfrac{\Delta\rho}{\rho} H}$

The shape of the interface as a function of $Q_r = \dfrac{Q_1}{Q_2}$ is illustrated in fig. (2-13).

2.5.3 Critical Flow in a two layered system:

Since the critical flow condition is vital to the understanding of many stratified problems, and is very much related to the prediction of dilution in this study, a short discussion is deemed appropriate.

In open channel flow, as well as in two-layered systems, a critical section is often formed by an imposed control such as at a free overfall, sudden expansion from confinement into infinite space, etc. It has an implication on flow geometry, namely - a sharp change in the interface position. For the case of equal counterflow, the same governing condition can be derived from an independent energy principle (Appendix D). With respect to submerged buoyant discharges and other stratified flow problems the critical condition has the further implication of limiting the exchange flow. Consider the general case of a counterflow system:

At the critical section:

$$F_1^2 + F_2^2 = 1$$

or

$$F_{2H}^2 \left[\frac{Q_r^2}{(1-H_2)^3} + \frac{1}{H_2^{\,3}} \right] = 1 \qquad (2.5.9)$$

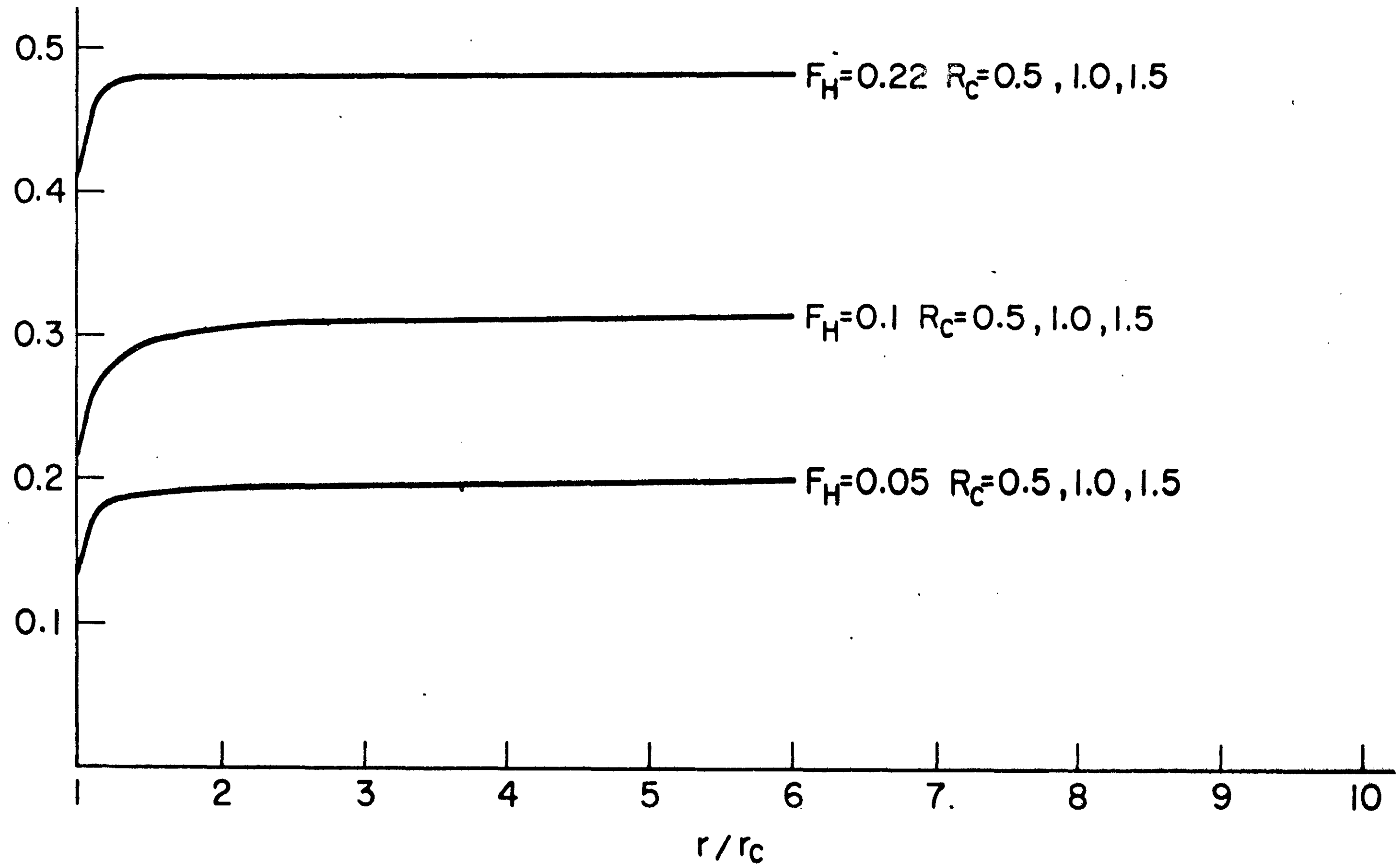

FIGURE (2-12) INTERFACE PROFILE AS A FUNCTION OF RADIAL DISTANCE NORMALIZED WITH RESPECT TO LOCATION OF CRITICAL SECTION

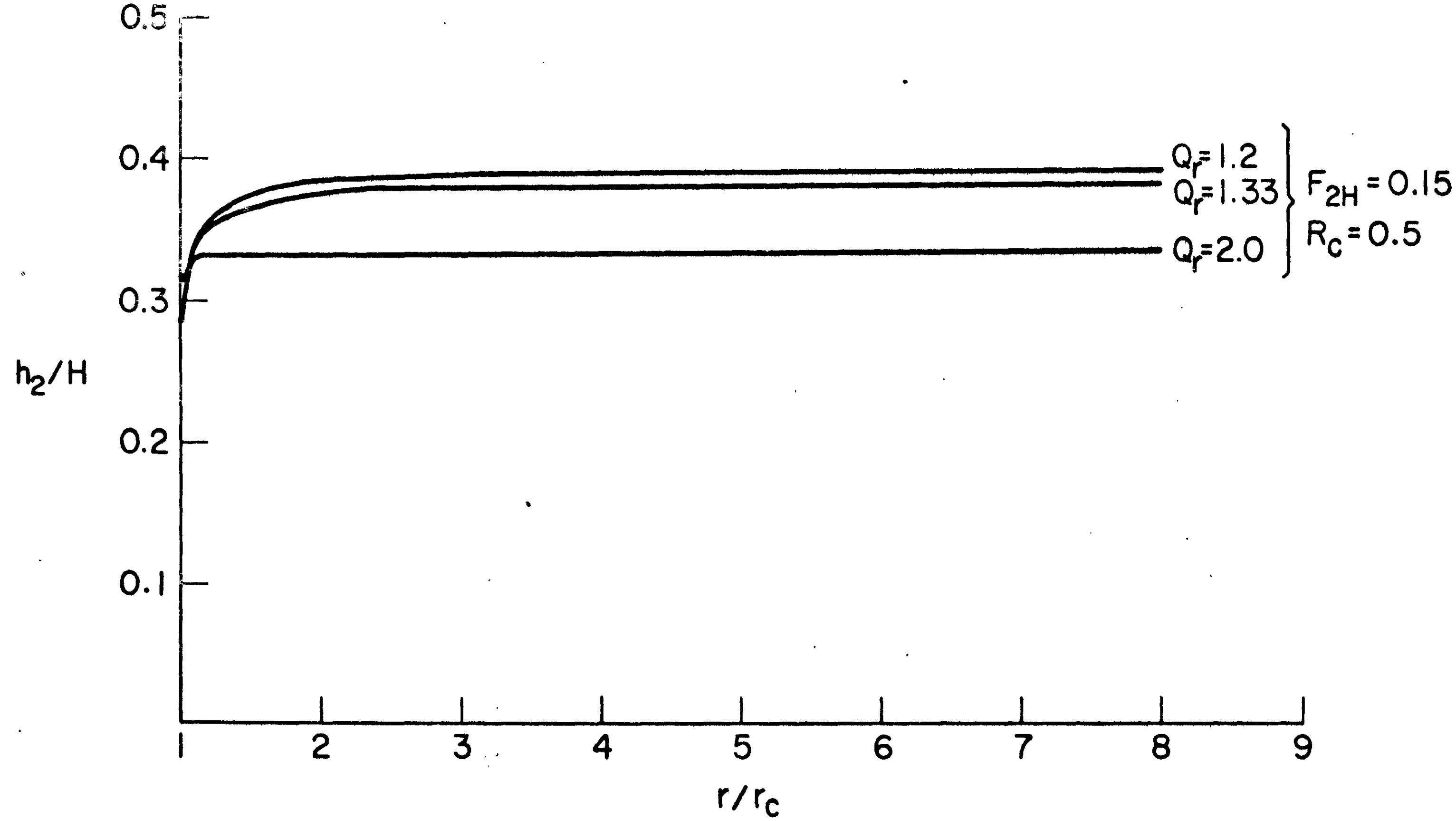

FIGURE (2-13) RADIAL VARIATION OF INTERFACE FOR NON - EQUAL COUTERFLOW where $F_{2H} = \frac{\left(\frac{Q_2}{2\pi r_c H}\right)^2}{g\frac{\Delta\rho}{\rho} H}$ $\quad Q_r = Q_1/Q_2$.

Fig. 2-14 shows the variation of H_{2c} as a function of F_{2H} for different values of Q_r . For a given ratio of flows in the two layers, Q_r a maximum exchange flow $Q_1 + Q_2$ corresponds to a maximum F_H. By rewriting eq. eq. 2.5.9 as

$$F_{2H}^2 = \frac{H_2^3(1-H_2)^3}{Q_r^2 H_2^3 + (1-H_2)^3} \tag{2.5.10}$$

and setting the derivative $\frac{dF_H^2}{dH_2}$ to zero we have

$$H_2 = \frac{1}{1 + Q_r^{\frac{1}{2}}} \tag{2.5.11}$$

Substituting eq. 2.5.11 into eq. 2.5.10 we obtain

$$F_{2H}^2 = \frac{1}{[1 + Q_r^{1/2}]^4} \tag{2.5.12}$$

Hence for a given Q_r we can compute the value of F_{2H} that will give the maximum exchange flow. In the special case of an equal counterflow $Q_r=1$

$F_{2H} = 0.25$ is the limiting condition when a maximum exchange flow is created.

In a two-dimensional two-layered system friction effects tend to oppose a condition of maximum exchange flow. The radial expansion of the flow in the three dimensional case (in the absence of physical boundaries), however, enhance the formation of such a condition at the critical section.

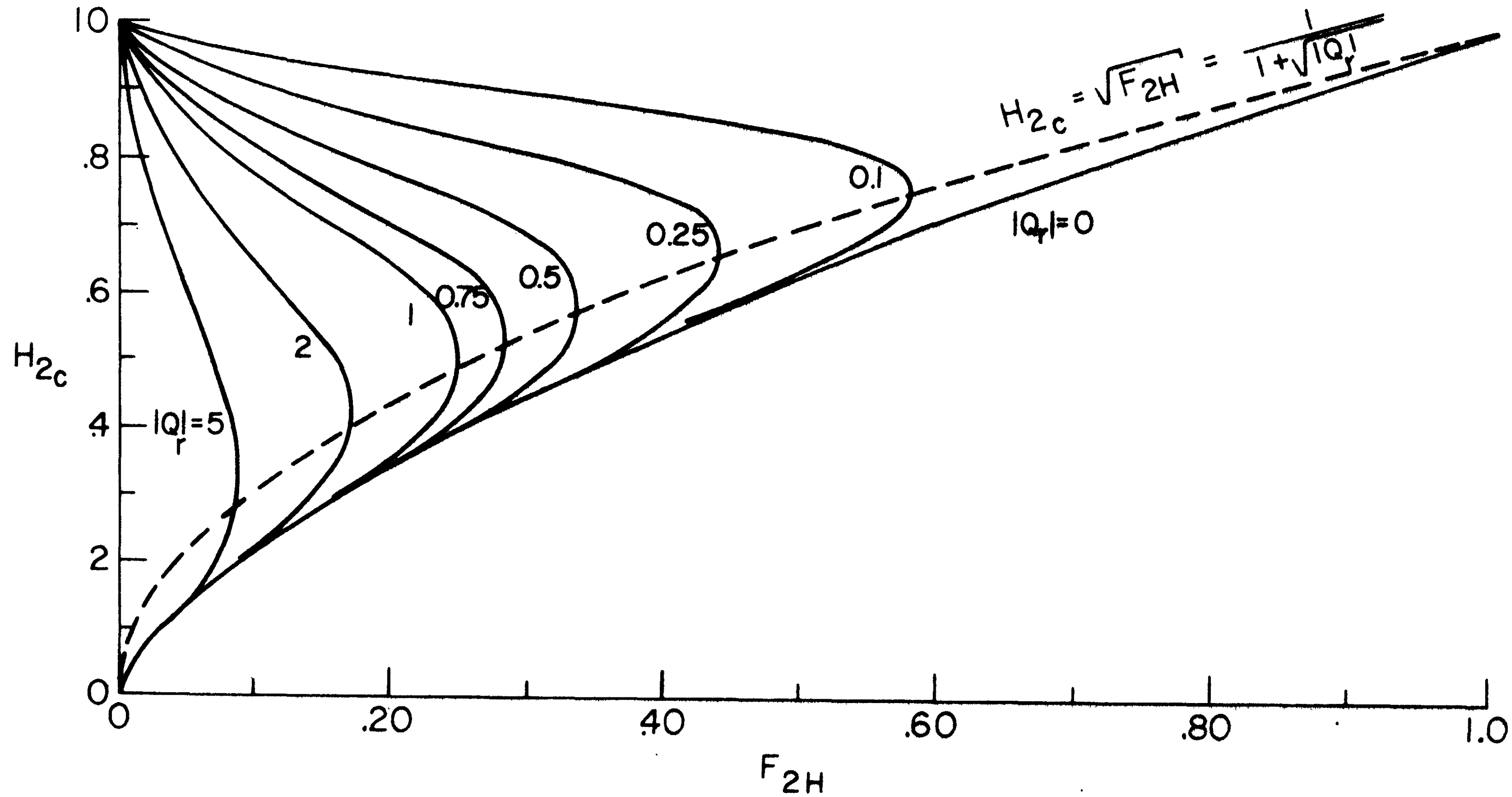

Fig. (2-14) CRITICAL DEPTH H_{2c} AS A FUNCTION OF F_{2H}, $|Q|_r$

2.5.4 Behavior of Flow at large distances

Fig. 2-10, 2-12, shows that at 'large distances' ($r \sim 10H$) from the jet discharge, an asymptotic behavior of the interface is approached. In the absence of any physical boundaries and ambient currents in the far field, flow is postulated at minimum energy dissipation.

The rate of energy dissipation, or work done against dissipative forces, can be expressed as:

$$E_{diss} = \rho\frac{f_i}{8}(u_1 + u_2)^3 + \rho\frac{f_o}{8}u_2^3$$

$$u_1 = \frac{Q_1}{2\pi r h_1} \qquad u_2 = \frac{Q_2}{2\pi r h_2}$$

Assuming $h_1 + h_2 =$ constant,

$$\frac{dE_{diss}}{dh_2} = 0 \quad \text{gives}$$

$$h_1^4 - \frac{f_i}{f_o}[Q_r h_2 + h_1]^2[Q_r h_2^2 - h_1^2] = 0 \qquad (2.5.13)$$

For the case of equal counterflow $Q_r = 1$ this reduces to

$$\left(\frac{h_i}{H}\right)^4 - \frac{f_i}{f_o}\left[\left(\frac{h_2}{H}\right)^4 - \left(\frac{h_1}{H}\right)^4\right] = 0 \qquad (2.5.14)$$

Since the interfacial shear is always about 4 times that of bottom shear ($f_i \simeq 0.5\ f_o$, $(2u)^3 \simeq 8u^3$), a limiting approximation of $f_i/f_o \to \infty$ gives $\frac{h_1}{H} = \frac{h_2}{H} = 0.5.$ Fig. 2-15 illustrates the weak sensitivity of h_2/H to f_i/f_o.

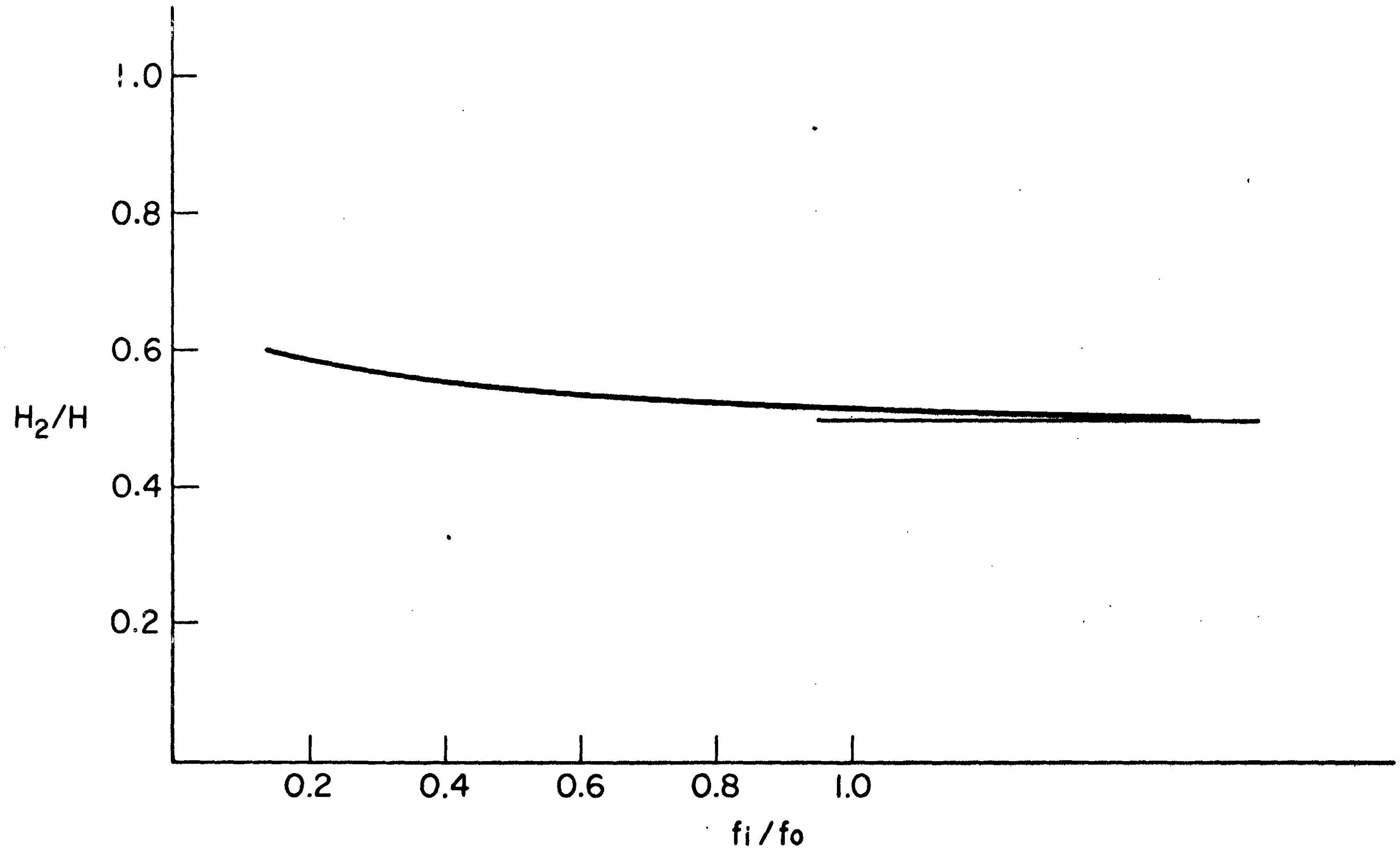

FIGURE (2-15) VARIATION OF THE FAR FIELD INTERFACE AS A FUNCTION OF f_i/f_o

In the prototype far field ($r >> H$) the boundary condition may be determined by heat loss effects. In view of the small areal extent within which asymptotic behavior of the interface is established, the boundary condition presented in this section is judged to be independent of heat loss in the far field.

2.6 Summary of Theoretical Framework

The coupling of the theory outlined for the four regions to give the near field dilution is described in the following sections.

2.6.1 Definition of the Near Field Dilution

The near field dilution S is defined volumetrically as the ratio of the flow away in the upper layer to the initial jet discharge flow, $S = Q_1/Q_o$. In the absence of heat losses, heat conservation implies this definition is equivalent to $S = \frac{\Delta T_o}{\Delta T}$, where

ΔT = temperature rise above ambient in the near field

ΔT_o = discharge temperature rise above ambient

2.6.2 Stable Near Field Dilution

For a given (F_o, H/D) the velocity and the upper layer thickness in the surface impingement region can be obtained by solving eq. 2.2.1-2.2.3 in conjunction with eq. 2.1.19-2.1.20. By visual observation, confirmed by temperature data, it is found that the internal jump occurs at $r_j = 0.57\ H$ from the jet axis. F_1, F_2 and h_1/h_2 can then be computed and used as input to the internal jump equations. Existence of a conjugate height implies a stable near field.

It can be inferred from the two-dimensional buoyant jet experiments done by Jirka and Harleman (1973) that the ratio of the jump length to jump height is approximately 4. It is expected that this number is smaller for a three dimensional buoyant jet. Unfortunately, the arrangement of the temperature probes in the near field is not dense enough to resolve the shape of the jump interface from temperature data. A zero jump length is assumed as a first approximation in the theoretical solution. This is chosen in light of the stability analysis, with the main purpose of evaluating the near field stability rather than the exact shape of the internal jump region.

For submergence (H/D) less than the length of the zone of flow establishment, the theory outlined in sec. 2.1 is not directly applicable. A simplified analysis based on the assumption of a momentum jet is substituted as an approximation in this range (Appendix C).

If a stable near field exists, the dilution is given by the solution of the surface impingement region. A different theory for the prediction of near-field dilution is posed in the next section for the case of an unstable near field.

The prediction of the near field stability is shown in fig. 2-16 along with the near field dilutions. For $H/D > 6.0$ the stability transition can be described by the criterion

$$F_o = 4.4\ H/D \qquad (2.6.1)$$

In view of the assumptions embodied in the analytical framework, the stability criterion should be interpreted as a narrow band rather than a

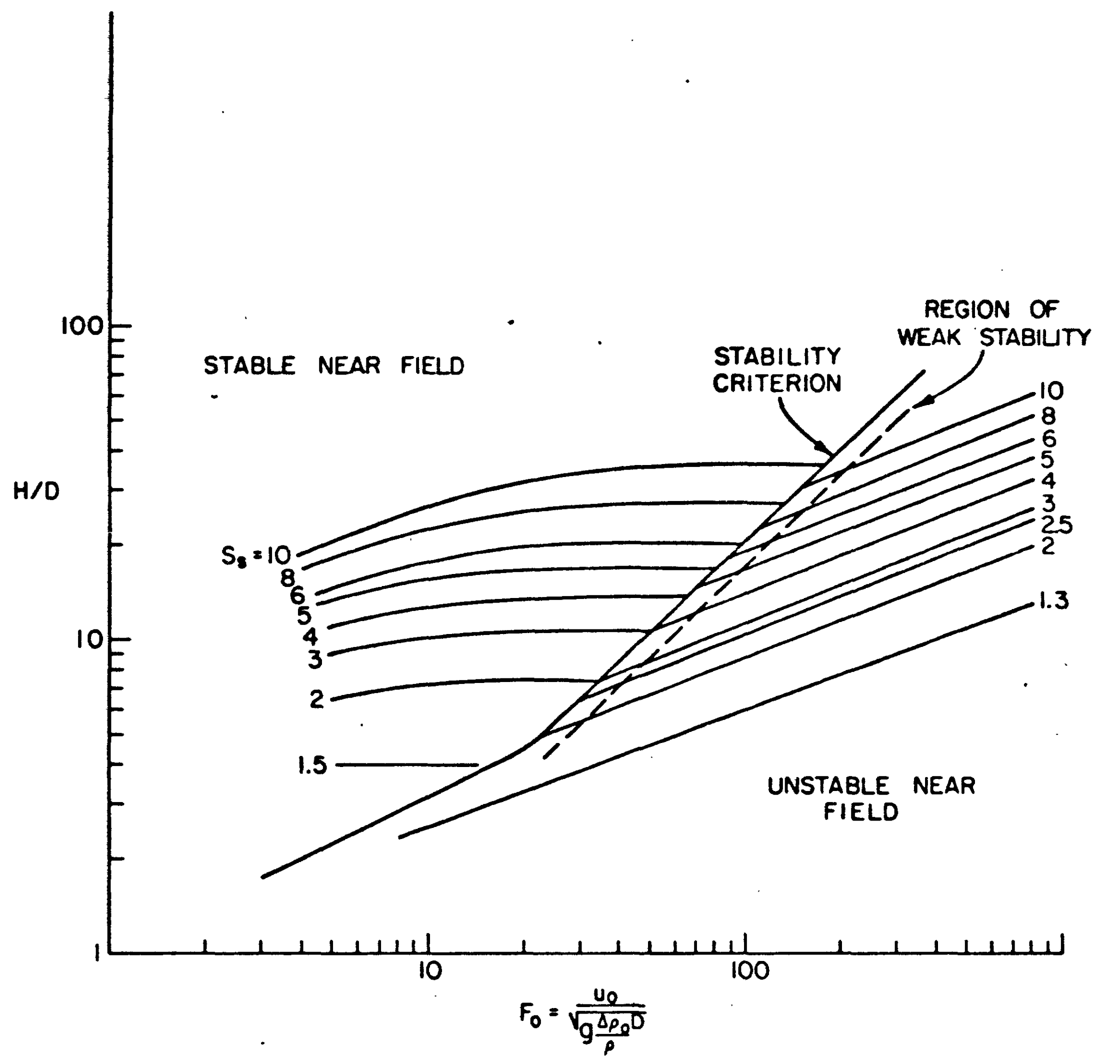

FIGURE (2-16) GENERAL THEORETICAL SOLUTION OF NEAR FIELD DILUTION single line delimiting the stable region on the graph from the unstable region. The 'transition' from a point in the stable region to one in the unstable region is continuous in nature, as exemplified by the weak instability (submerged jump) observed (Ch. 3). The same statements apply to the two-dimensional case (Jirka and Harleman, 1973).

For low submergences ($H/D < 5$), the stability criterion is determined by a line with a different slope. This is due to the fact a different model is assumed for the zone of flow establishment.

Fig. 2-17 illustrates the sensitivity of the stability criterion to the assumed location of the internal jump at r_j. As this is well established from experimental data, this sensitivity should not have an important effect of the overall prediction.

2.6.3 Unstable Near Field Dilution

Based on the theoretical discussions presented in sec. 2.5, two assumptions are made:

1) the radial variation of the interface can be described by a frictionless flow situation.
2) at large distances from the jet, bottom shear is negligible compared with interfacial shear.

2.6.4 Equal Counterflow

For the case of high dilutions, an equal counterflow system can be assumed: the far field boundary condition is $\frac{h_2}{H} = 0.5$; given the behavior of the interface, a limiting condition of $F_H = 0.25$ has to be established

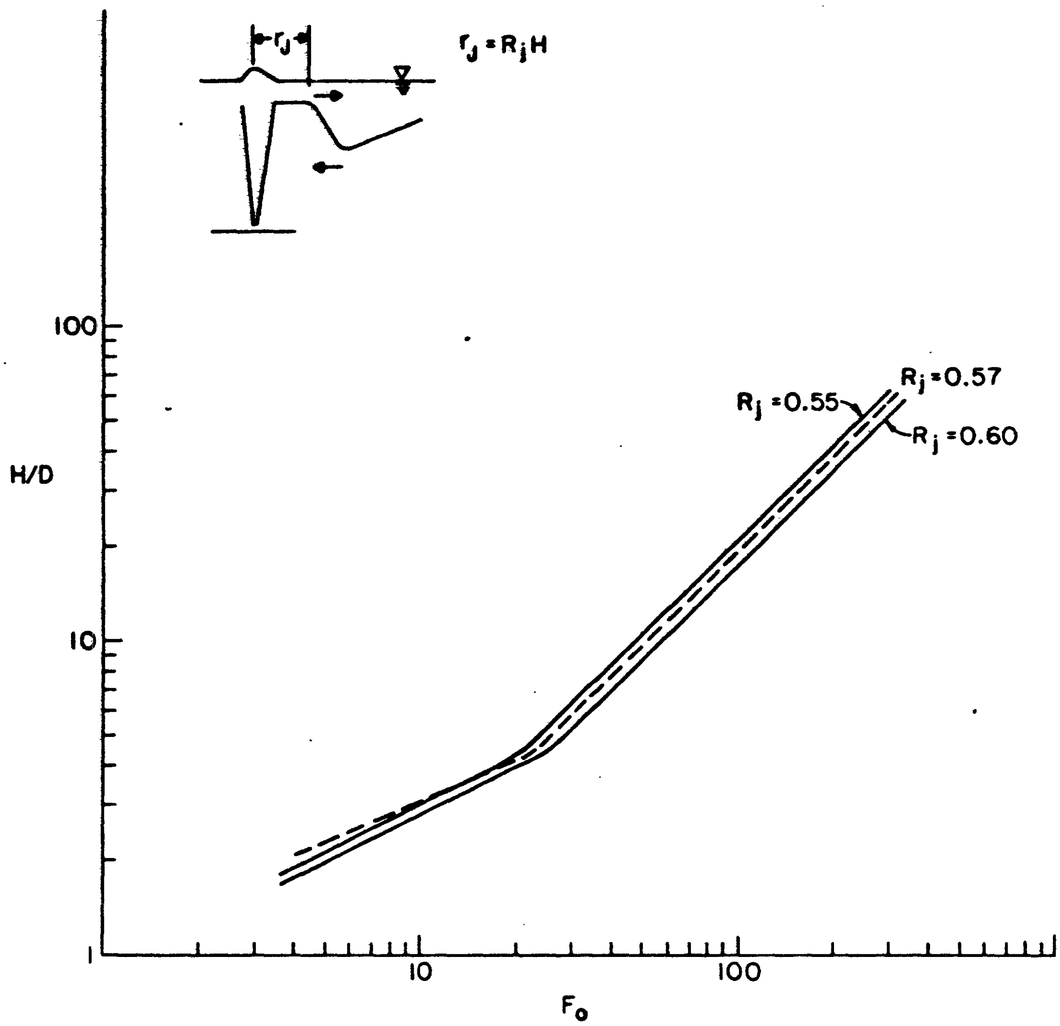

FIGURE (2-17) SENSITIVITY OF STABILITY TRANSITION TO THE LOCATION OF THE JUMP TOE at the critical section r_c in order to match the boundary condition at large distances. This has the physical implication that a maximum exchange flow is generated in the counterflow system. By definition

$$F_H^2 = \frac{\left(\frac{Q}{2\pi r_c H}\right)^2}{g \frac{\Delta\rho}{\rho} H} = \frac{S^3 F_o^2}{64R_c^2 (H/D)^5} \qquad R_c = r_c/H$$

The solution for high dilutions is given by the limiting condition $F_H^2 = (0.25)^2 = 1/16$.

i.e.

$$S = \left[\frac{4\, R_c^2 (H/D)^5}{F_o^2} \right]^{1/3} \tag{2.6.2}$$

R_c is the second experimentally determined coefficient.

2.6.5 Non-equal Counterflow

For low dilutions the equal counterflow approximation is not valid and the general case of non-equal counterflow has to be considered.

The formal approach is to assume a starting value for the dilution, solve the initial value problem defined by eq. 2.5.5 iteratively until the asymptotic value of h_2 in the far field matches with that obtained by solving the far field boundary condition. The large numerical efforts involved is deemed not necessary. Instead a concept derived in the equal counterflow case is postulated to carry over to the non-equal counterflow case: a condition of maximum exchange flow has to be created.

By definition

$$F_{2H}^2 = \frac{S(S-1)^2 F_o^2}{64R_c^{\,2} (H/D)^5} \tag{2.6.3}$$

Combining eq. 2.6.3 with eq. 2.5.12 and noting that $Q_r = \frac{S}{S-1}$, the near field dilution for unstable buoyant jets can be solved numerically.

III. Experimental Investigation

A series of experiments were conducted to test the behavior of the axisymmetric buoyant jet in stagnant ambient water. In an experimental basin of limited extent boundary effects will influence the stratified flow pattern in the far field. In order to minimize these effects a plane of symmetry was assumed at one basin wall and a half jet in lieu of the full round jet was used. This has the additional advantage of being able to visually observe the physical phenomenon through the water and the plane of symmetry.

3.1. The Experimental Setup

The experiments were carried out in a 37' x 18' x 1' hydraulic model basin. Fig. 3-1 illustrates the general experimental setup. To ensure good heat insulation, the bottom of the model basin was covered with 1" thick styrofoam material. A plastic liner was laid on top of the insulation material to prevent any possible leakage of water. An additional layer of 1" thick styrofoam and $1\frac{5}{8}$" thick concrete blocks formed a false floor.

Near one wall of the basin a partition was constructed along the whole length of the model. This created a 16' x 34' area on one side of the partition. In order to visualize the flow pattern of the jet, the center portion of the partition was constructed of two 6' x 10" plexiglass pieces ($\frac{1}{2}$" thick). The rest of the partition was made from 14" high plywood sheets and styrofoam material, both of which were braced and weighted by concrete blocks. The partition formed a plane of symmetry of the axi-symmetric jet.

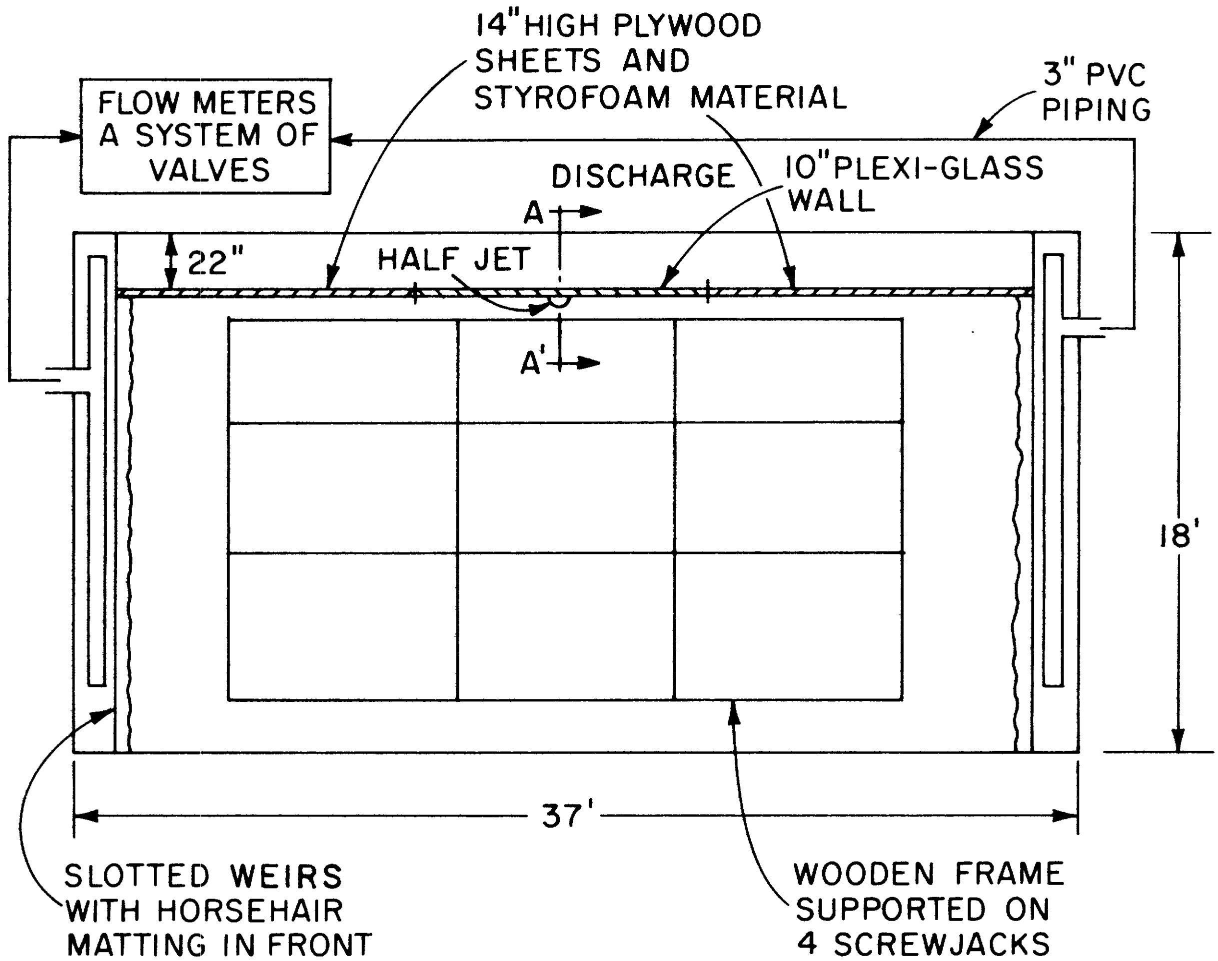

FIGURE (3-1a) PLAN VIEW OF EXPERIMENTAL SET-UP

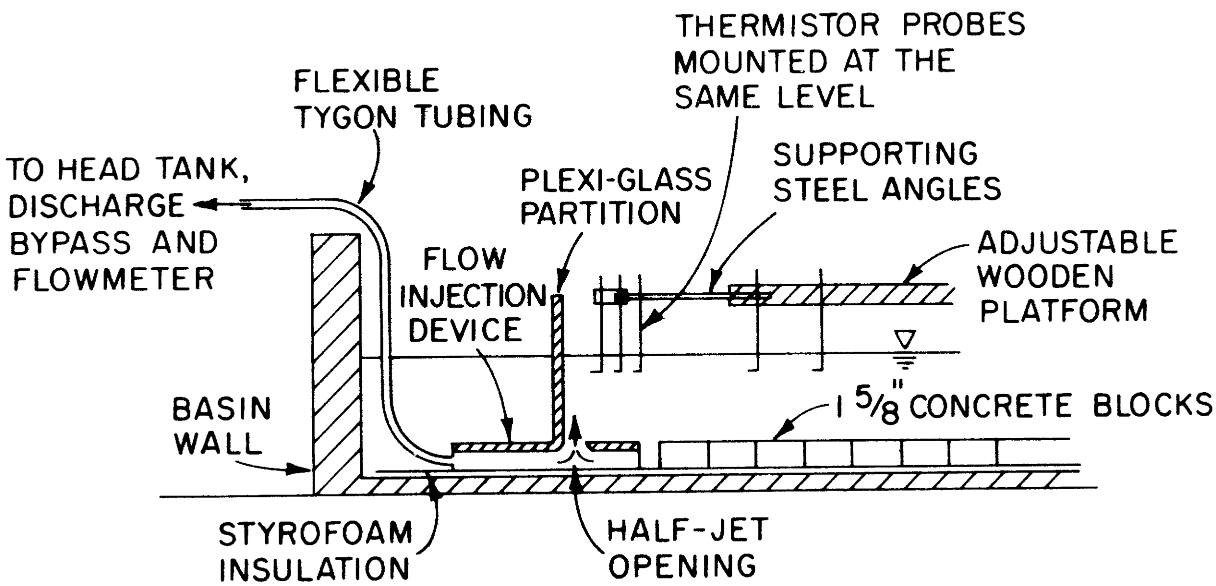
THERMISTOR PROBES
MOUNTED AT THE
SAME LEVEL
FLEXIBLE
TYGON TUBING
SUPPORTING
STEEL ANGLES
TO HEAD TANK,
DISCHARGE
BYPASS AND
FLOWMETER
PLEXI-GLASS
PARTITION
ADJUSTABLE
WOODEN
PLATFORM
FLOW
INJECTION
DEVICE
BASIN
WALL
1 5/8" CONCRETE BLOCKS
STYROFOAM
INSULATION
HALF-JET
OPENING

FIGURE (3-1 b)

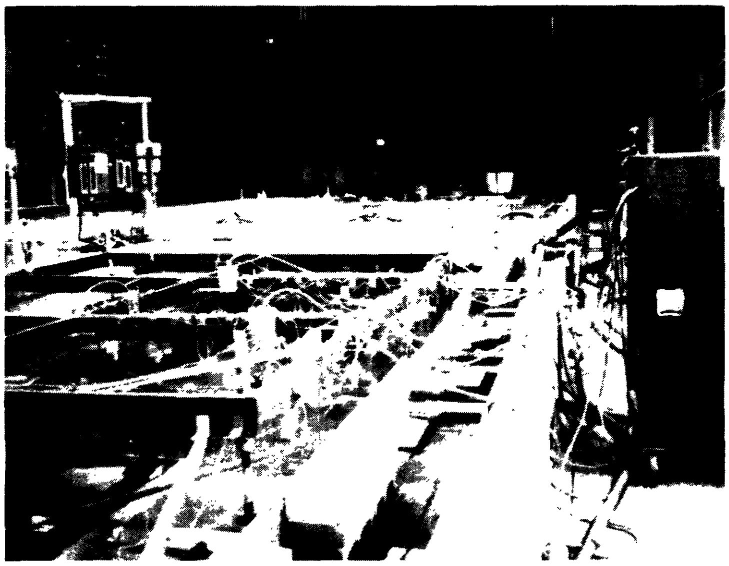

←tempera-
ture
scanner

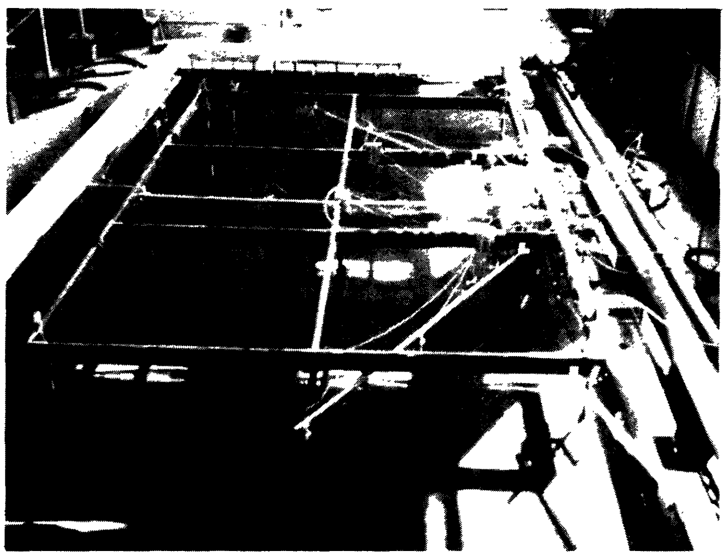

Fig. 3-1(c) Experimental Set-up

An existing circulating water system capable of generating currents across the model was used to mix the water in the basin. This ensured a uniform ambient water temperature before the experiment starts. Two 4" x 14.5' diffuser pipe manifolds were installed in two 1.3' wide channels at either end of the basin. The two pipe manifolds were connected by 3" PVC piping to a flow meter system. Flow is generated by a large pump (25 HP, 500 GPM). The lateral uniformity of the crossflow was improved by horsehair matting and vertical slotted weirs at the basin ends.

The flow injection device for the half-jet is a rectangular plexiglass box composed of two parts, as illustrated in fig. 3-2. Flow enters the box at one end and exits upwards through a semi-circular hole. Fig. 3-2a illustrates the core part of the box. The other part consisted of a glass plate of the same thickness as the upper face of the central core with a semi-circular hole cut in fig. 3-2b. Different pieces of semi-circular plexiglass with the desired semi-circular opening (0.25", 0.5", 1") cut at the center can then be fitted onto the glass plate. A half-jet of a desired diameter is formed by fitting the appropriate glass plate onto the core part and sealed with construction sealant. A $\frac{5}{8}$ " x 6" slot is cut off the center portion of the partition. The injection device was then sealed onto the plexiglass wall by fitting it inside the slot and aligning the dividing line E-E of the box with the inner edge of the plexiglass wall. The device was then installed in place such that the upper face of the box is level with the floor. Jets of different diameters are obtained by changing the plexiglass piece. To avoid flow separation the exit section of the half jet was rounded off smoothly.

Hot water obtained from a heat exchanger flows to a discharging

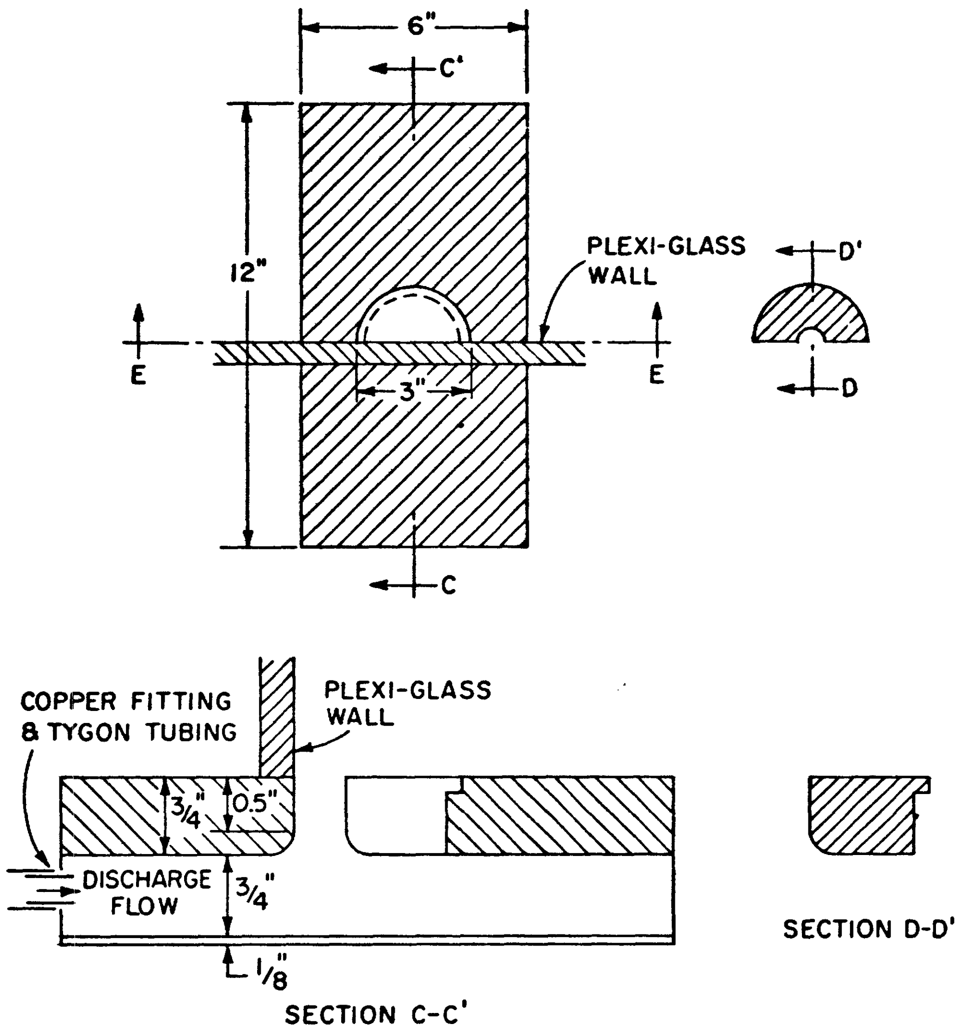

FIGURE (3-2) THE FLOW INJECTION DEVICE

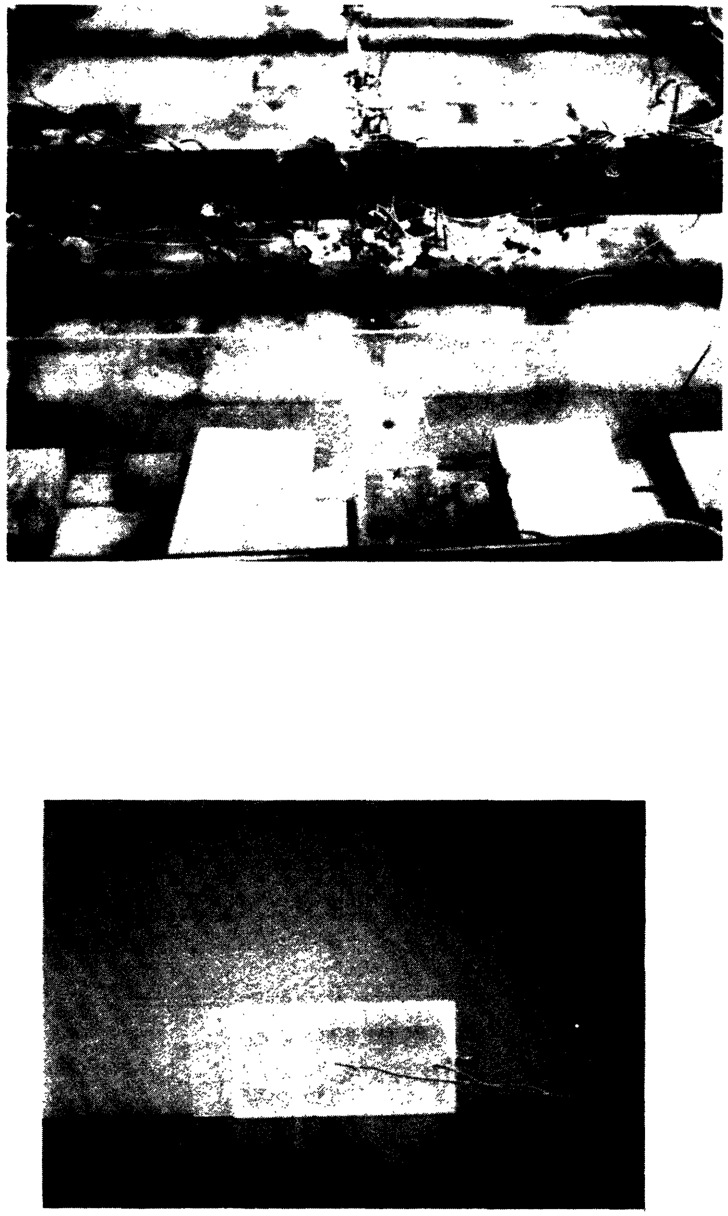

Fig. 3-2(c) The Flow Injection Device

piping system that consists of a bypass and a connection to the flow injection device via a flexible tygon tubing and copper fittings. Depending on the amount of flow needed, two types of flowmeters were used to monitor the flow. For flows higher than 0.5 GPM, a calibrated Brooks rotameter is used. A different type of rotameter (Brooks, Model 1560) was used to monitor flows below 0.5 GPM accurately.

Forty-four Yellow Springs therimistor probes (Series 701, Time Constant = 9.0 sec., accuracy 0.3°F) for temperature measurement were set up and mounted at the same horizontal level on a wooden platform supported on four screw jacks. The probes were identically mounted on four different radial lines, as shown in fig. 3-3. Six additional probes were used to monitor the discharge and ambient water temperature at fixed positions. Temperature readings were recorded by an electronic scanner and printed on paper to the nearest 0.01 F. By turning the screw jacks manually, the elevation of the wooden platform can be adjusted. Thus through the movement of the wooden platform vertical temperature profiles can be taken.

Temperature data was punched on cards and processed by a data reduction computer programme that prints out the experimental run parameters and the temperature excess along the radial lines for different vertical positions (see Appendix E).

3.2. Experimental Procedure

Before the start of each run the circulating water system was operated to mix the water in the basin. Hot water was allowed to flow through the bypass at the desired rate until a steady desired hot water temperature was attained. The depth of the water in the basin was measured by

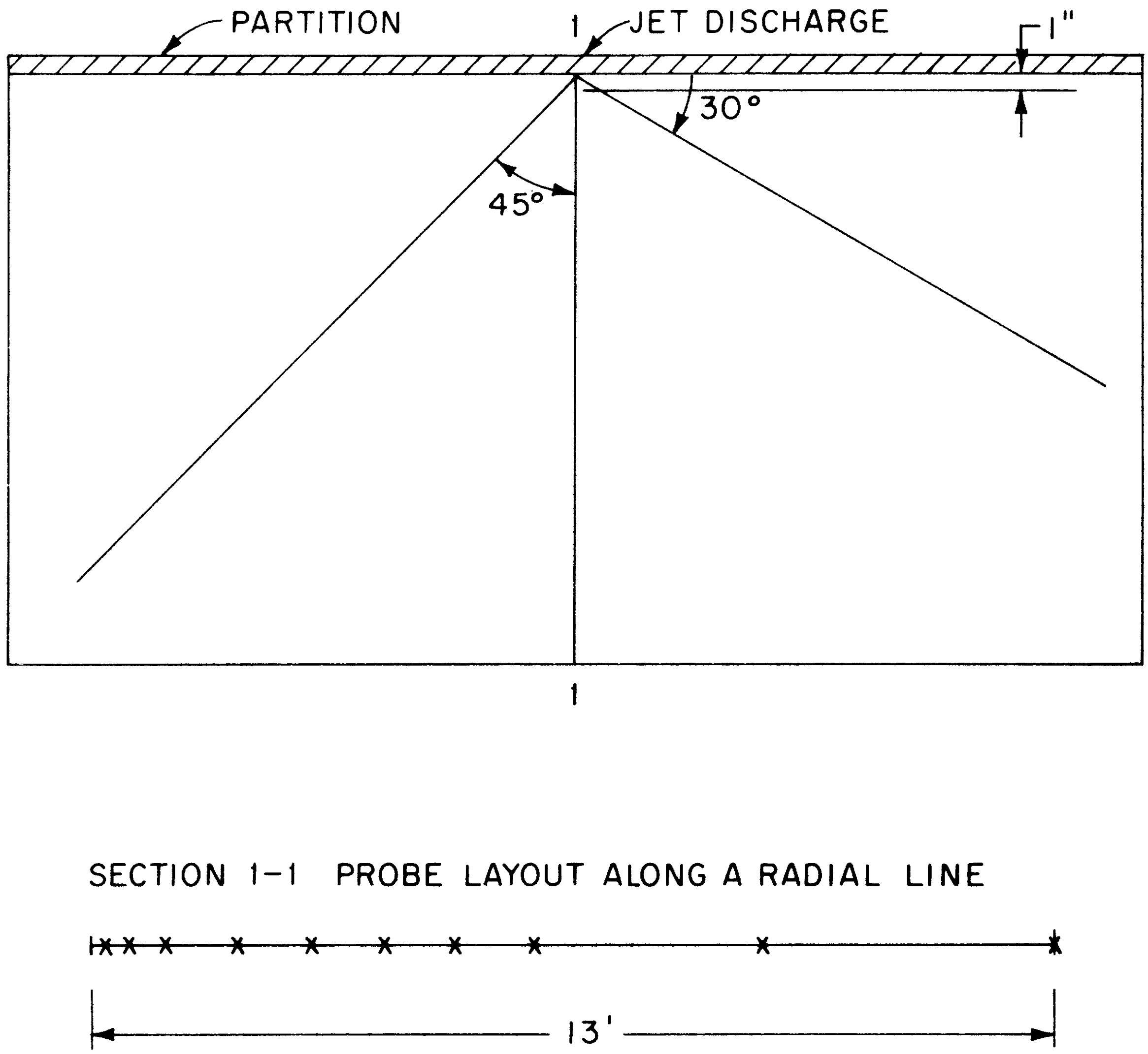

FIGURE (3-3) SCHEMATIC OF TEMPERATURE PROBE SET-UP taking readings with a point gauge.

When the temperature scanner indicated a uniform ambient temperature, the bypass was turned off and the jet discharge was initialized. Shortly after the experiment started, dye was injected to observe the flow pattern. The first scan of the surface temperatures was started when the dye front had gone past a substantial area. After two or three surface scans had been taken, the wooden platform was then lowered to record vertical temperature profiles. The experiment was stopped shortly after the dye cloud had reached the basin boundaries. This took about 20 minutes for the majority of runs. Since the response time of the thermistor probes is 9 sec., 15 sec. was allowed to elapse after each adjustment of the platform before starting the scan.

To ensure that some kind of quasi-steady state situation was reached in the experiment, a surface scan was always taken at the end of the experiment. In all the runs the temperature recordings of the last surface scan in the near field were very close to those of the first few initial scans. As a confirming check, a particular run was carried out for as long as an hour. Fig. 3-4 illustrates that the near field temperature reduction remains fairly stable with time.

As no suction device had been installed to withdraw the basin water, the water depth was increasing during the course of the experiment. Due to the large size of the basin, the maximum and average relative deviation in water depth was only 0.04 and 0.01 respectively for the range of water depths and flow rates used in the set of experiments performed.

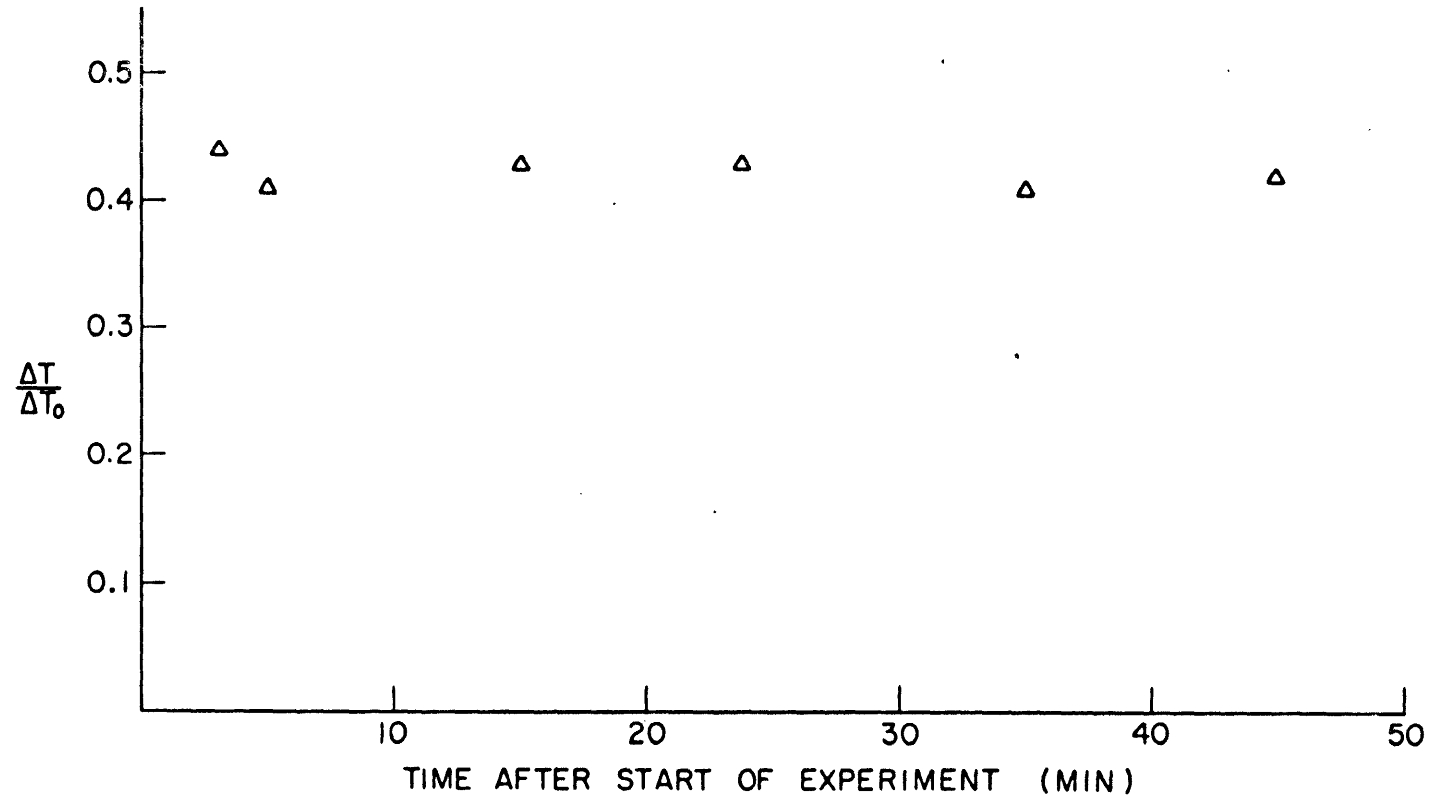

FIGURE (3-4) VARIATION OF NEAR FIELD TEMPERATURE RISE WITH TIME (RUN 32)

3.3. Experimental Program

Experiments were conducted for a sufficiently wide range of densimetric Froude numbers and submergence in order to cover the stable-unstable transition region. Runs were made in the highly unstable region to obtain experimental comparison with the theoretical prediction of near field dilution for unstable jets.

The summary of run parameters and observed near field dilution for the experiments performed in this study is presented in Table 3-1. The near field dilution corresponds to the temperature recordings of the thermistor probes at the nearest radial position (2" from the jet axis).

3.4. Experimental Observation

Dye injections were used to visually observe the flow pattern of the jets. However, due to the oblique angle of observation it was difficult to obtain good quality photographs of the cross-sectional flow profile through the water and the plexiglass partition.

A turbulent jet is always observed for the range of the Reynold's numbers tested. The erratic, eddying motion of the fluid particles accompany the linear spread of the jet. As the jet impinges on the free surface, a surface boil is observed, which fluctuates in intensity, creating a disturbance that generates easily observable circular wave fronts on the free surface.

As outlined in Ch. 2, the stability of the near field depends on two dimensionless parameters, the submergence of the jet H/D and the discharge densimetric Froude number F_o . For high submergence and low Froude numbers, a weak surface boil is observed, followed by a jet like horizontal

	Physical Variables				Secondary Parameters				
Run No.	Jet Diameter (in) D	Initial ambient temp. T_a °F	Temp. difference ΔT_o °F	Flow rate (GPM)	densimetric Froude number F_o	Submergence H/D	Reynold's number $R \times 10^3$	Near field stability	Observed near field dilution
1	0.5	72.5	28.2	0.95	38.9	10.6	12.9	S	4.4
2	0.5	74.9	26.5	1.07	44.6	10.8	14.7	S	4.3
3	0.5	76.2	26.0	1.55	64.8	10.8	21.1	SJ	3.8
4	0.5	74.8	28.1	1.60	64.5	8.7	21.8	U	2.0
5	0.5	74.9	26.8	1.50	62.2	12.4	20.4	S	5.2
6	0.5	76.0	29.0	2.05	80.4	12.7	27.9	SJ	4.2
7	0.5	78.3	21.4	0.83	38.3	13.0	11.3	S	4.3
8	0.5	73.2	27.1	2.30	95.9	10.6	31.3	U	2.1
9	0.5	75.7	24.2	2.48	46.0	11.1	14.3	S	4.5
10	0.5	78.0	25.8	0.60	24.9	11.2	8.2	S	5.5
11	0.5	72.8	27.8	2.52	103.9	13.9	34.3	SJ	4.3
12	0.5	73.9	26.9	3.20	131.9	14.1	43.5	U	3.5

S = Stable
U = Unstable
SJ = Submerged jump

TABLE 3-1 Summary of Run Parameters and Experimental Results

	Physical Variables			Secondary Parameters					
Run No.	Jet Diameter (in) D	Initial ambient temp. T_a °F	temp. difference ΔT_o °F	Flow rate (GPM)	densimetric Froude number F_o	Submergence H/D	Reynold's number $R \times 10^3$	Near field stability	Observed near field dilution
13	0.5	75.0	24.8	1.38	59.7	14.4	18.8	S	4.5
14	0.5	75.7	23.2	0.88	39.5	14.5	12.0	S	4.0
15	0.5	71.3	26.2	1.15	49.7	6.2	15.7	U	1.9
16	0.5	73.3	23.9	0.90	40.4	6.3	12.2	U	2.2
17	0.25	70.2	28.7	0.65	151.8	19.3	17.7	U	4.6
18	0.25	72.1	23.1	0.31	81.2	19.3	8.4	S	7.7
19	0.25	73.4	23.5	0.59	146.6	23.5	16.0	SJ	9.1
20	0.25	74.7	22.4	0.80	208.8	23.4	21.7	U	7.1
21	0.25	73.2	26.8	1.10	261.6	24.1	29.9	U	4.2
22	0.25	75.4	24.7	1.30	318.6	24.2	35.3	U	3.6
23	0.25	76.0	34.8	0.78	154.8	32.3	21.2	S	8.6
24	0.25	77.9	22.6	2.30	583.4	32.3	62.5	U	3.3

TABLE 3-1 Continued

	Physical Variables ,			Secondary Parameters					
Run No.	Jet Diameter (in) D	Initial ambient temp. T_a °F	Temp. difference ΔT_o °F	Flow rate (GPM)	densimetric Froude number F_o	Submergence H/D	Reynold's number $R \times 10^3$	Near field stability	Observed near field stability
25	0.25	79.1	26.5	1.29	295.3	32.7	35.0	U	7.1
26	0.25	71.9	27.1	0.86	205.2	10.1	23.4	U	2.2
27	0.25	73.9	28.4	1.30	296.7	15.8	35.3	U	2.6
28	0.25	75.5	26.3	0.93	219.5	17.7	25.3	U	3.1
29	0.25	76.3	26.3	1.05	246.4	19.7	28.5	U	2.6
30	1.0	78.9	25.1	1.62	11.9	2.4	11.0	U	2.1
31	1.0	74.5	23.2	2.37	19.0	2.6	16.1	U	1.2
32	1.0	76.1	28.2	1.15	8.0	2.2	7.8	SJ	2.04
33	1.0	76.1	21.9	1.00	8.2	4.0	6.8	S	2.5

TABLE 3-1 Continued

spreading, usually accompanied by a weak jump. As the submergence is decreased and (or) the Froude number is increased while still maintaining near field conditions, the near field structure is even more clearly observed, namely a thin upper layer of approximately 1/10 of the total water depth in the surface impingement region is found. This thin layer spreads out horizontally with no apparent change in thickness, and an internal jump is always observed at a radial distance of approximately 0.6 H.

As H/D is decreased further and (or) F_o is increased, a weak instability is observed in the near field. This is characterised by a thickening of the upper layer in the near field, followed by an internal jump possessing a conjugate depth that touches the bottom (submerged jump). Weak re-entrainment of the upper layer water is observed. The region of instability extends some distance off the jet axis, and a critical section is observed at the end of the field of instability.

For sufficiently high F_o and (or) low H/D an instantaneously unstable near field is observed. Intense re-entrainment occurs and the linear spread of the jet is no longer visible. The region of instability is concentrated near the jet axis, with the establishment of a critical section at some distance from the jet. The intense instability creates a strong counterflow system which results in a critical section close to the jet. The observations are schematized in Fig. 3-5.

Fig. 3-6 shows temperature transects for a typical case of each of the three cases mentioned above. The normalized temperature rise $\frac{\Delta T}{\Delta T_o}$ is plotted beside the location of each thermistor probe.

Radial symmetry of the dye pattern was not obtained in all runs. For runs with an unstable near field, reasonable symmetry was observed.

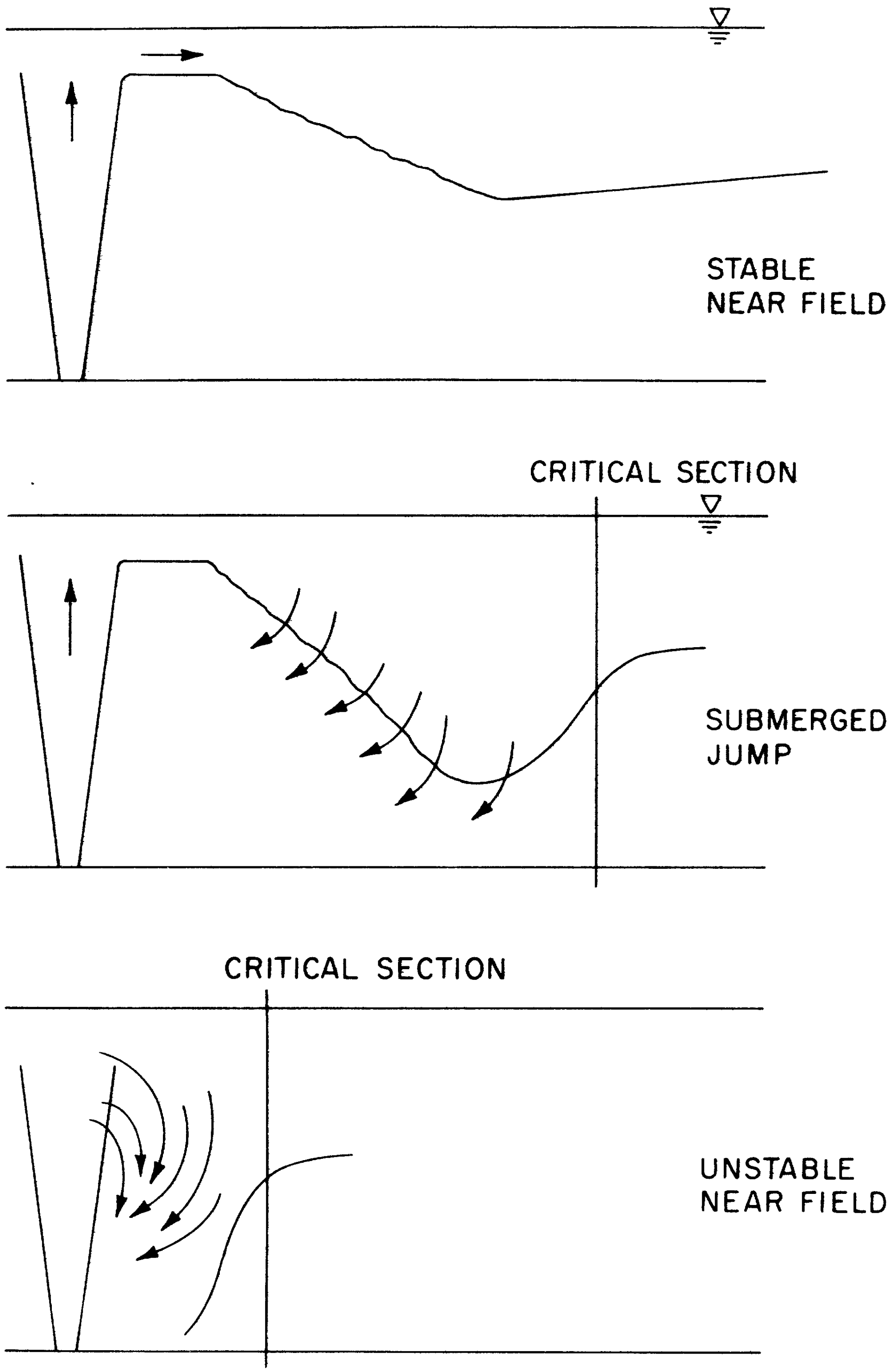

FIGURE (3-5) OBSERVED NEAR FIELD STABILITY

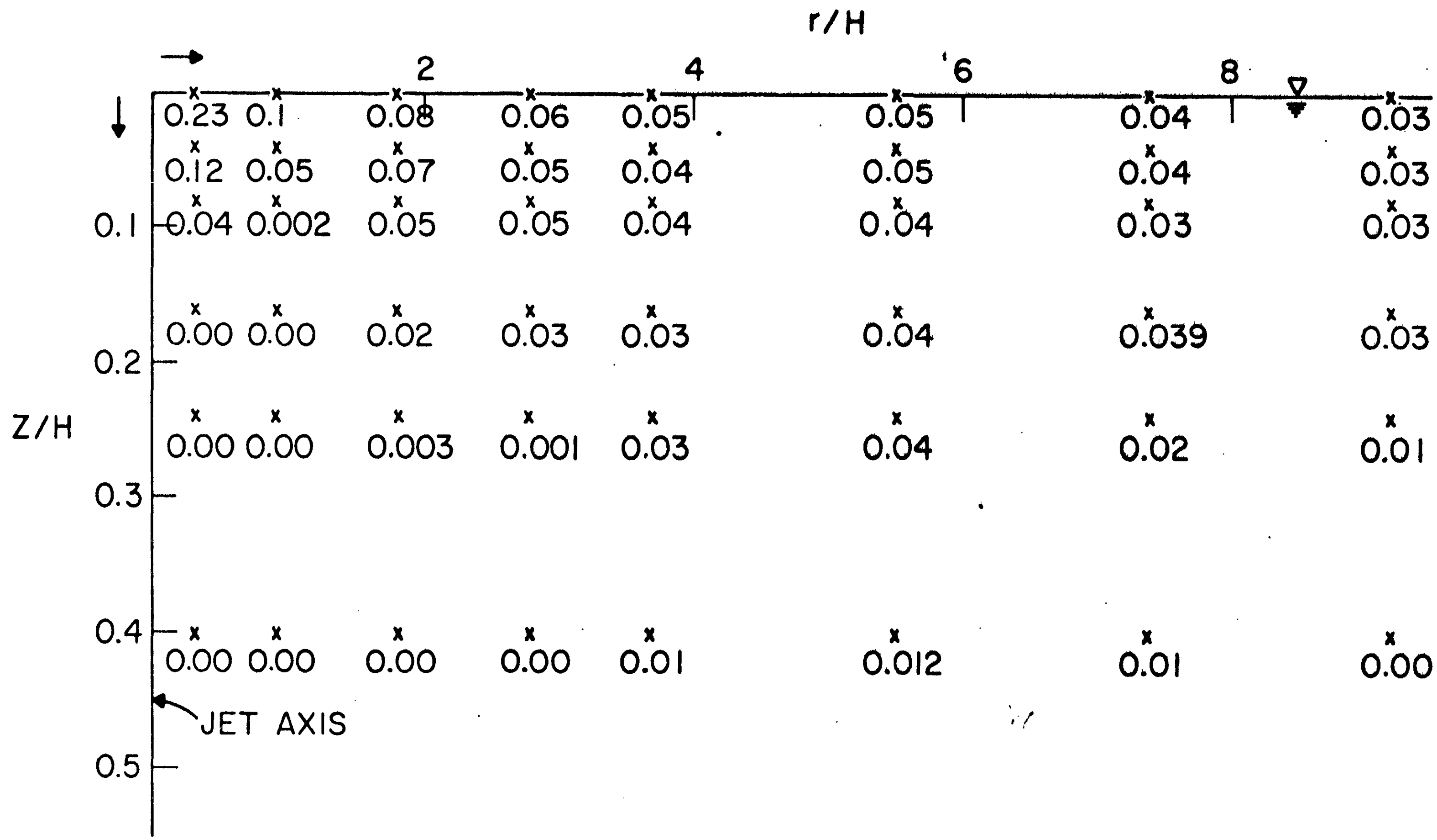

FIGURE (3-6a) TEMPERATURE TRANSECT FOR A TYPICAL STABLE NEAR FIELD (RUN 7)

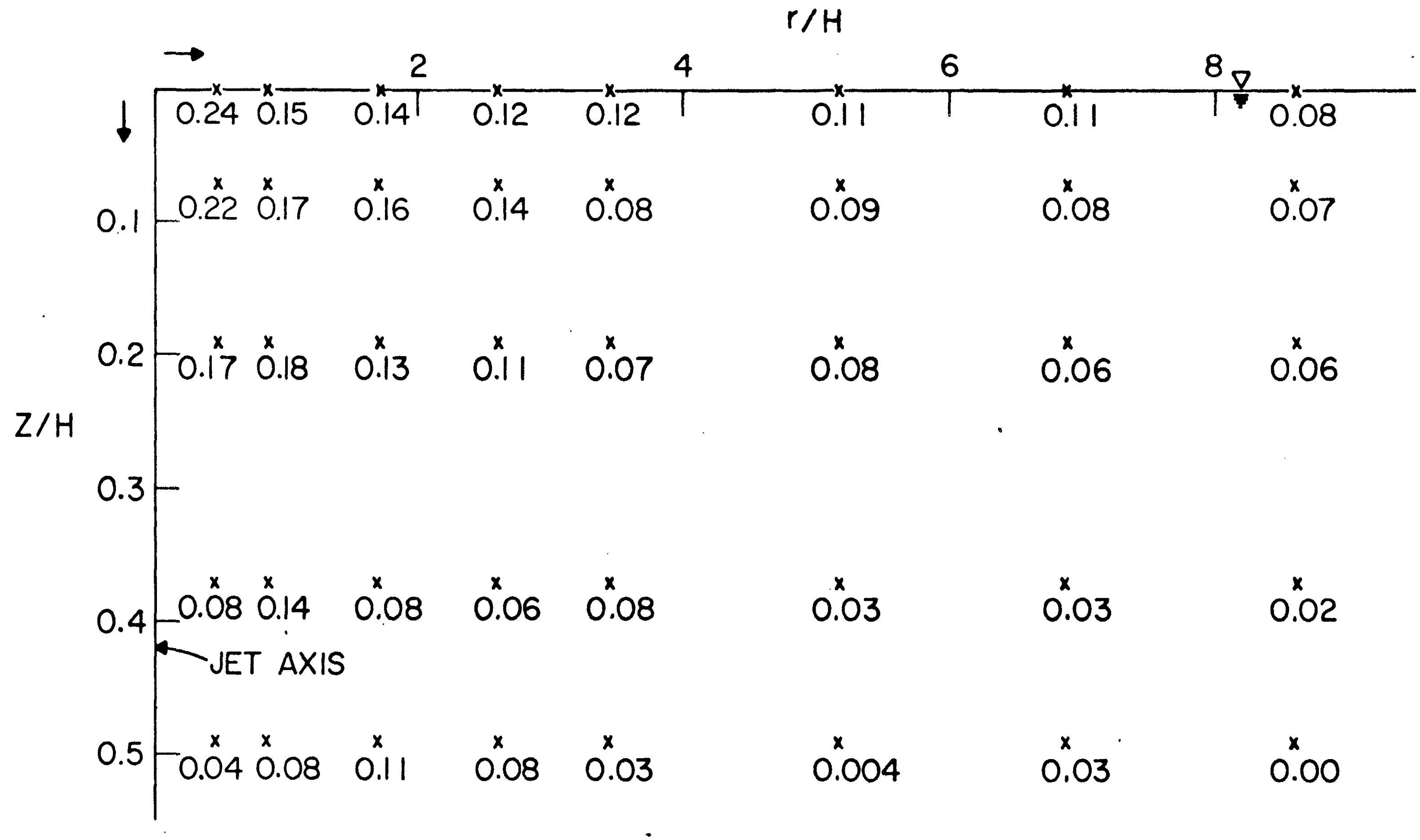

FIGURE (3-6b) TEMPERATURE TRANSECT FOR A TYPICAL WEAK INSTABILITY (SUBMERGED JUMP) (RUN 11)

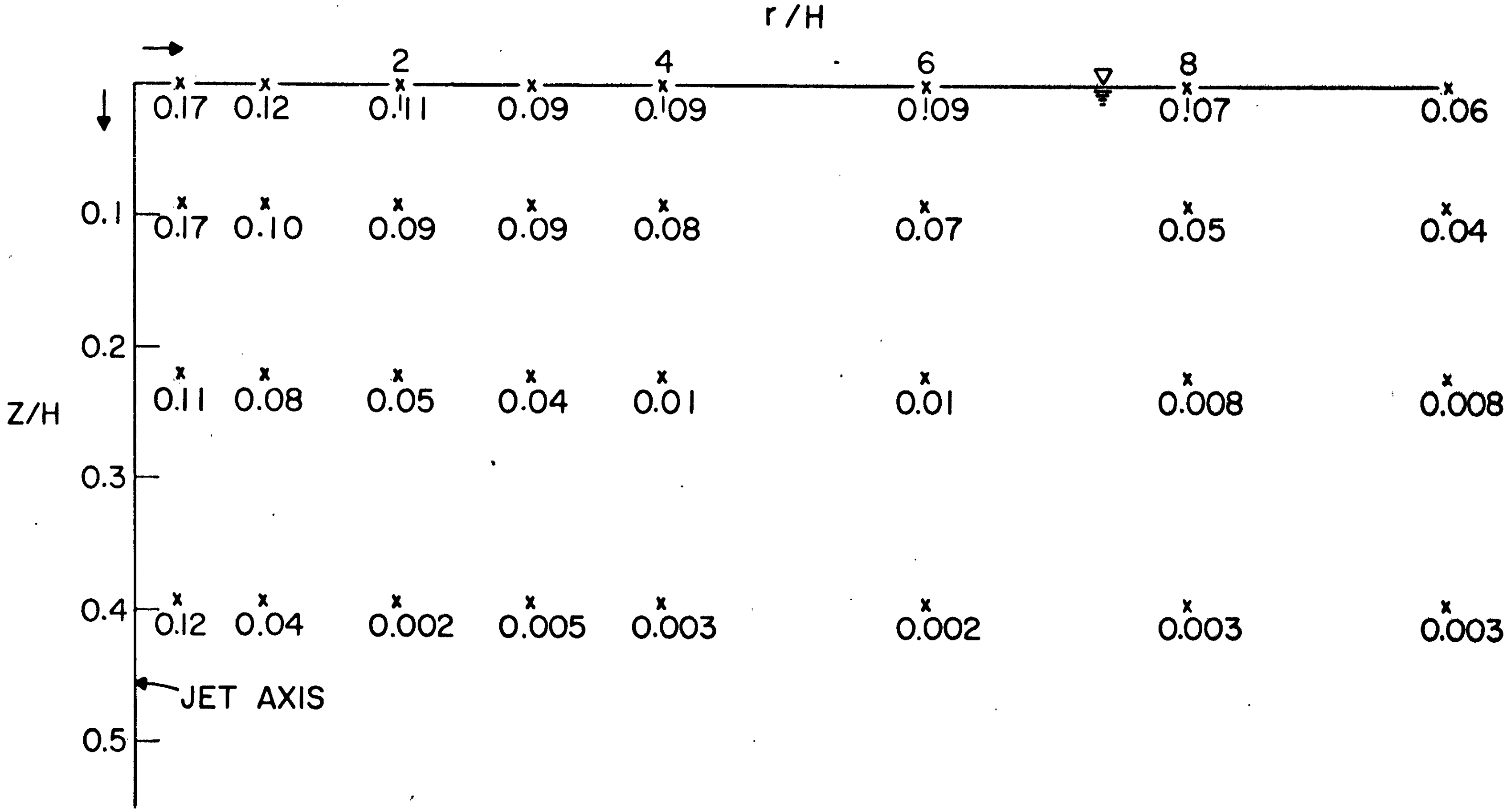

FIGURE (3-6c) TEMPERATURE TRANSECT FOR AN UNSTABLE NEAR FIELD (RUN - 21)

For runs with a stable near field, protruded fronts near the partition and normal to it are frequently observed, with a slight dent in a narrow portion of the circumference, as illustrated in fig. 3-7. Possible explanations for this phenomenon are: the presence of the basin boundary has the effect of creating a recirculation into the near field, causing the observed dent, fig. 3-8. Constrained by the model geometry, the exit section of the injection device (0.5" long) is not large compared with the jet diameter. The exit flow may have a stronger component in the forward direction ($\theta = 90°$), again creating a weak recirculation into the near field for a narrow portion of the circumference.

In every case the temperature rise of the four radial lines for different vertical positions delimits very distinctly the three cases of a stable, weakly stable (submerged jump) or an unstable near field.

The effect of the partition wall, which was located at one jet symmetry plane, can be assumed as negligible for the submergence tested (max. 32). This is based on a consideration of the wall jet data on centerline velocity by Rajaratnam (1974), which can be compared to the free jet solution by Albertson et al. (1950), as shown in fig. 3-9. For the range of submergence tested, the deviation due to additional wall shear can be neglected.

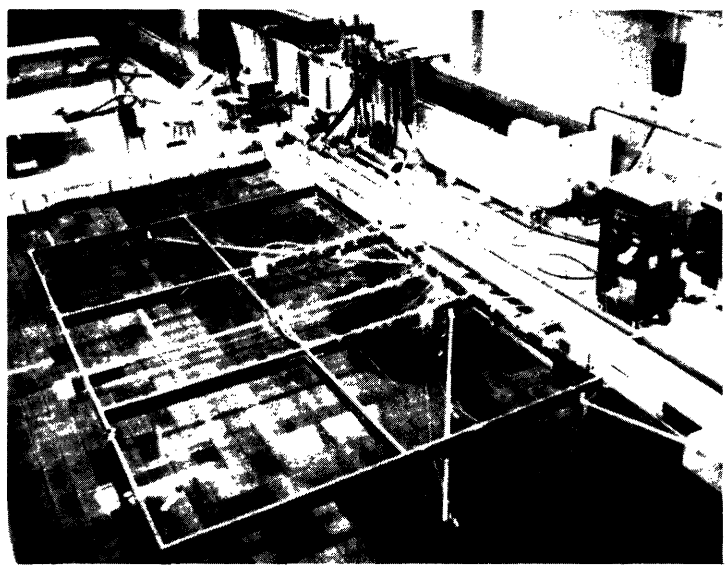

Fig. 3-7: Observed Indentation:
Slight Asymmetry of The Dye Front

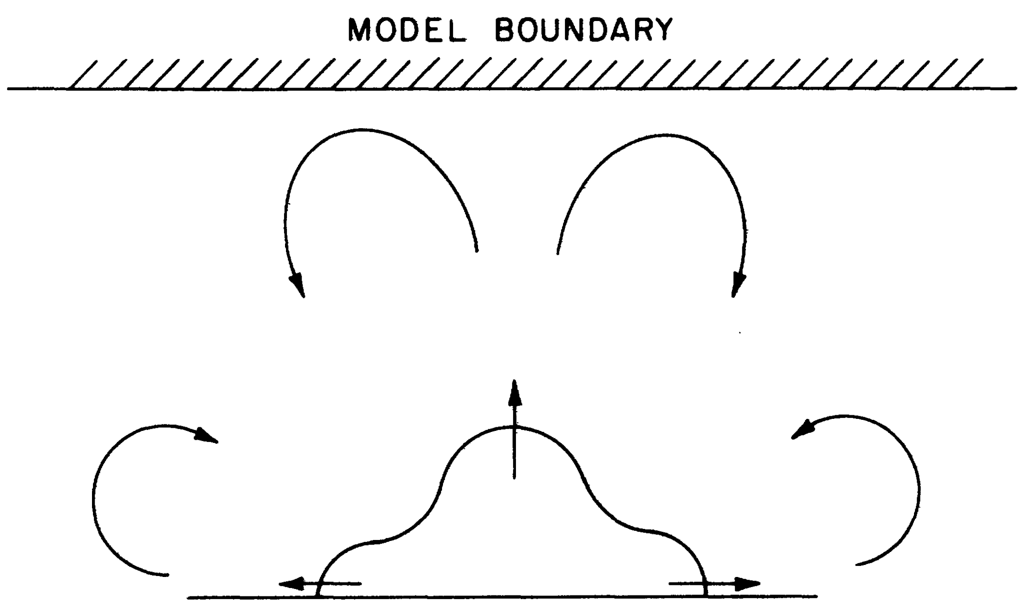

FIGURE (3-8) WEAK ENTRAINMENT INDUCED BY MODEL BOUNDARY

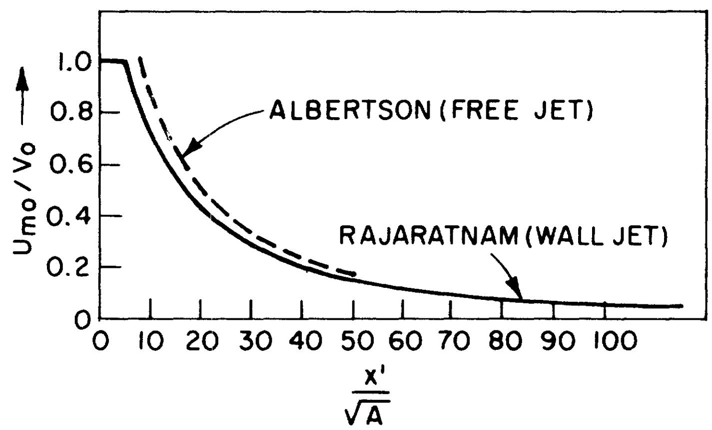

x' – CENTERLINE DISTANCE

A – AREA OF NOZZLE

U_{mo} – CENTERLINE VELOCITY

V_o – NOZZLE VELOCITY

FIGURE (3-9) COMPARISON OF WALL JET DATA WITH ALBERTSON'S FREE JET DATA: DECAY OF MAXIMUM VELOCITY ALONG CENTER PLANE

IV. Comparison of Theory and Experimental Results

The experimental observation of the near field dilution in relation to the theoretical prediction outlined in Ch. 2 is discussed in the sequel. The results of the theoretical solution are then compared with experimental data and empirical coefficients are evaluated.

4.1. Near Field Stability

The prediction of the near field stability as discussed in sec. 2.6. is compared with experimental data in fig. (4-1). It can be seen that the stability is well-predicted by the theory.

4.2. Near Field Dilution

The theoretical predictions for the near field dilutions are evaluated for the exact densimetric Froude numbers and submergences of the experimental runs. The results are compared with the observed near field dilutions in Table 4-1.

Stable Jets: In general reasonable agreement is obtained. Observed dilutions are always higher than predicted. This may be ascribed to additional entrainment in the surface impingement region and the weak re-entrainment on the surface caused by the slight asymmetry observed.

Unstable Jets: Using experimental results of runs with an unstable near field and near field dilution greater than 3.0, an average value of $R_c = 0.47$ is obtained by fitting the data with eq. 2.6.2. Theoretical predictions computed with this value of R_c are compared to the observed dilutions.

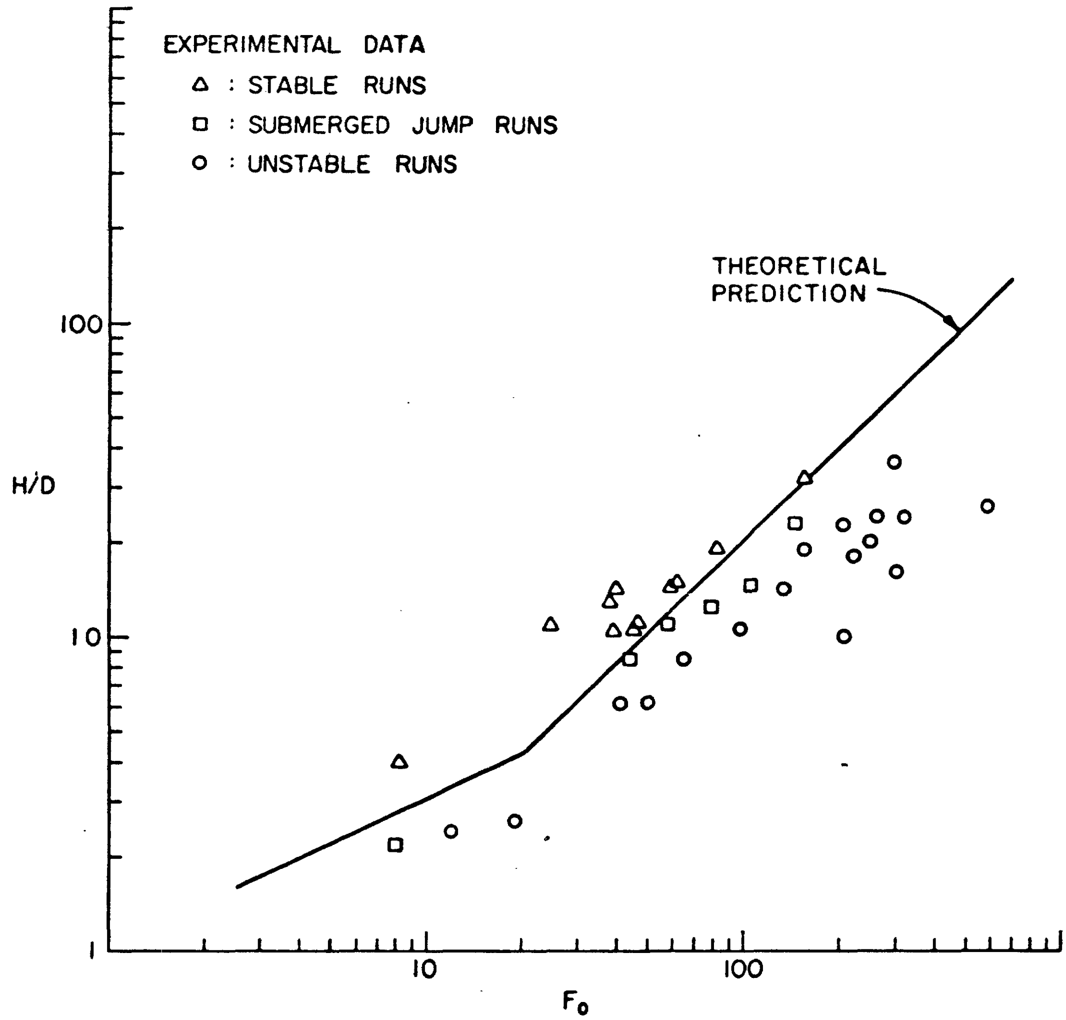

FIGURE (4-1) NEAR FIELD STABILITY OF AN AXI-SYMMETRIC JET IN SHALLOW WATER

Although the coefficient R_c is derived from experimental results with dilutions greater then 3.0, very good agreement is obtained with data characterised by dilutions less than 3.0. This confirms the validity of the postulated structure of the theory for the stratified counterflow system in an unstable near field.

Although the theory requires two experimentally determined coefficients: namely the location of the jump R_j for a stable near field and the length of the mixing region for an unstable near field R_c, the near field dilution predictions as well as the experimental data demonstrate a consistent trend which could be understood in terms of our physical notions of buoyant jets in shallow water.

As a turbulent jet was always observed for the range of Reynold's number tested and frictional effects are shown to be unimportant at large distances from the jet (sec. 2.5, stratified counterflow region), the findings of this study can be extended to prototype conditions.

The experimental data is compared with the general theoretical predictions in fig. 4-2.

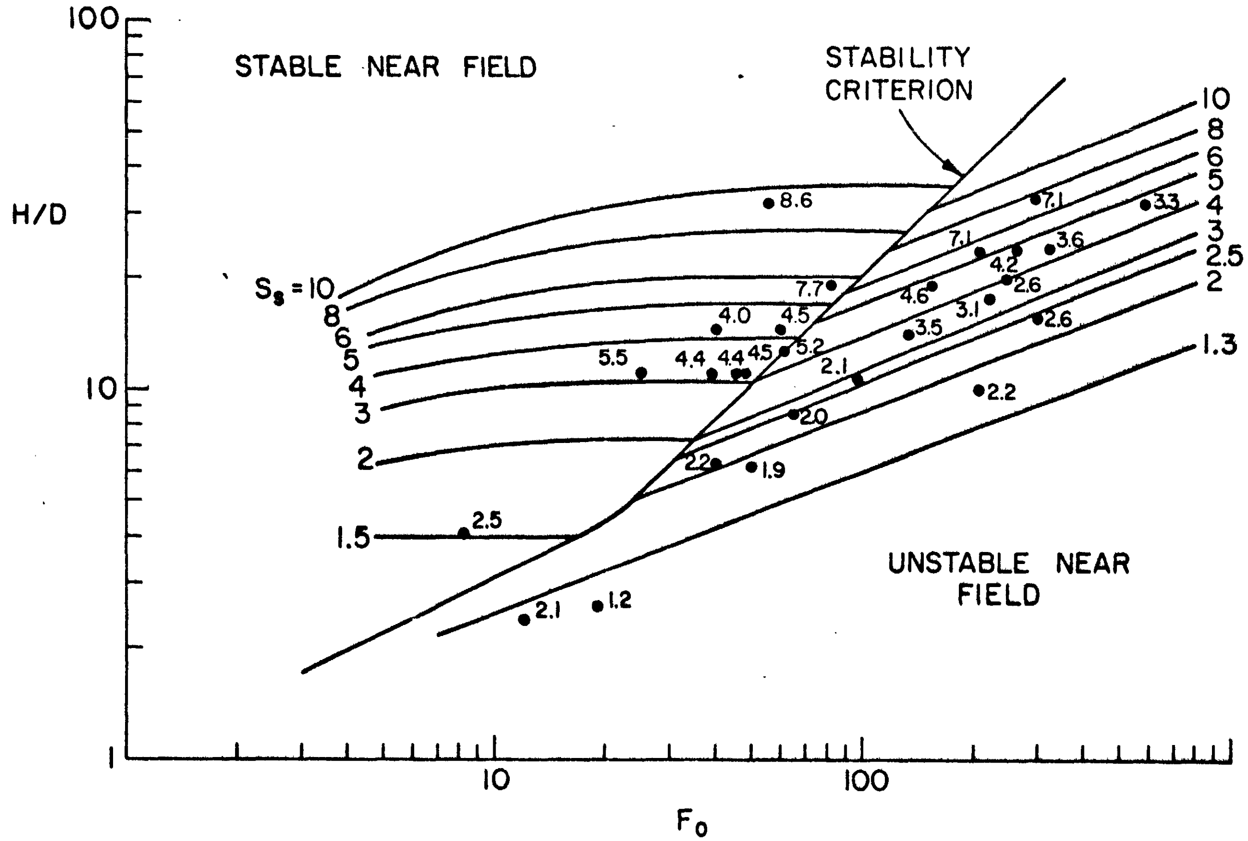

FIGURE (4-2) NEAR FIELD DILUTION AS A FUNCTION OF F_o, H/D VERTICAL AXI-SYMMETRIC JET IN STAGNANT WATER

Physical Variables				Secondary Parameters					
jet diameter (in)	initial ambient temperature	temp. difference	Flow rate	densimetric Froude number	submergence	Reynold's number	Near Field Instability	Observed Near Field Dilution	Predicted Near Field Dilution
D	T_a °F	ΔT_o °F	(GPM)	F_o	H/D	R x 10^3		S	S^*
0.5	72.5	28.2	0.95	38.9	10.6	12.9	S	4.4	3.1
0.5	74.9	26.5	1.07	44.6	10.8	14.7	S	4.3	3.1
0.5	76.2	26.0	1.55	64.8	10.8	21.1	SJ	3.8	NA
0.5	74.8	28.1	1.60	64.5	8.7	21.8	U	2.0	2.5
0.5	74.9	26.8	1.50	62.2	12.4	20.4	S	5.2	3.6
0.5	76.0	29.0	2.05	80.4	12.7	27.9	SJ	4.2	NA
0.5	78.3	21.4	0.83	38.3	13.0	11.3	S	4.3	3.8
0.5	73.2	27.1	2.30	95.9	10.6	31.3	U	2.1	2.7
0.5	75.7	24.2	2.48	46.0	11.1	14.3	S	4.5	3.2
0.5	78.0	25.8	0.60	24.9	11.2	8.2	S	5.5	3.3
0.5	72.8	27.8	2.52	103.9	13.9	34.3	SJ	4.3	NA
0.5	73.9	26.9	3.20	131.9	14.1	43.5	U	3.5	3.4

TABLE 4-1 Summary of Run Parameters and Experimental Results

Physical Variables				Secondary Parameters					
jet diameter (in)	initial ambient temperature	temp. difference	Flow rate	densimetric Froude number	submergence	Reynold's number	Near Field Instability	Observed Near Field Dilution	Predicted Near Field Dilution
D	T_a °F	ΔT_o °F	(GPM)	F_o	H/D	$R \times 10^3$		S	S^*
0.5	75.0	24.8	1.38	59.9	14.4	18.8	S	4.5	4.2
0.5	75.7	23.2	0.88	39.5	14.5	12.0	S	4.0	4.2
0.5	71.3	26.2	1.15	49.7	6.2	15.7	U	1.9	1.9
0.5	73.3	23.9	0.90	40.4	6.3	12.2	U	2.2	2.1
0.25	70.2	28.7	0.65	151.8	19.3	17.7	U	4.6	5.0
0.25	72.1	23.1	0.31	81.2	19.3	8.4	S	7.7	5.6
0.25	73.4	23.5	0.59	146.6	23.5	16.0	SJ	9.1	NA
0.25	74.7	22.4	0.80	208.8	23.4	21.7	U	7.1	5.6
0.25	73.2	26.8	1.10	261.6	24.1	29.9	U	4.2	5.0
0.25	75.4	24.7	1.30	318.6	24.2	35.3	U	3.6	4.5
0.25	76.0	34.8	0.78	154.8	32.3	21.2	S	8.6	9.4
0.25	77.9	22.6	2.30	583.4	32.3	62.5	U	3.3	4.8

TABLE 4-1 Continued

Physical Variables			Secondary Parameters						
jet diameter (in) D	initial ambient temperature Ta °F	temp. difference T_o °F	Flow rate (GPM)	densimetric Froude number F_o	submergence H/D	Reynold's number $R \times 10^3$	Near Field Instability	Observed Near Field Dilution S	Predicted Near Field Dilution S^*
0.25	79.1	26.5	1.29	295.3	32.7	35.0	U	7.1	7.6
0.25	71.9	27.1	0.86	205.2	10.1	23.4	U	2.2	1.7
0.25	73.9	28.4	1.30	296.7	15.8	35.3	U	2.6	2.5
0.25	75.5	26.3	0.93	219.5	17.7	25.3	U	3.1	3.5
0.25	76.3	26.3	1.50	246.4	19.7	28.5	U	2.6	3.8
1.0	78.9	25.1	1.62	11.9	2.4	11.0	U	2.1	1.3
1.0	74.5	23.2	2.37	19.0	2.6	16.1	U	1.2	1.1
1.0	76.1	28.2	1.15	8.0	2.2	7.8	SJ	2.04	NA
1.0	76.1	21.9	1.00	8.2	4.0	6.8	S	2.5	1.5

TABLE 4-1 Continued

V. Conclusion

The mechanics of a vertical axisymmetric jet in stagnant water is investigated both theoretically and experimentally. Four flow regimes with distinct hydrodynamic properties are discerned in the near field of the jet: the Buoyant Jet region, the Surface Impingement region, the Internal Hydraulic Jump region, the Stratified Counterflow region. The mechanics of the flow in each region are formulated analytically. Insight is gained by examining in detail the mathematical behavior of the theoretical framework. The solutions of the four regions are coupled to give a prediction of the near field stability and the near field dilution as a function of the jet characteristics. To verify this theory, a series of experiments were carried out with a half-jet.

It is found that the near field stability is dependent on the densimetric Froude number and the submergence of the jet. For certain combinations of the two, an instability is detected. The criterion that governs the stable-unstable transition is found to be $F_o = 4.4\ H/D$ for $H/D > 6$. In the case of a stable near field, the dilution is governed only by the jet characteristics. When an unstable near field exists, there is heat re-entrainment from the stratified flow away, and the dilution is correspondingly lessened. In this case the dilution is governed by the far field boundary condition in addition to the jet characteristics. The basic mechanics of the flow for an axisymmetric buoyant jet can be understood in terms of the theory developed in this study.

The theory is solved on a generic basis and the general results presented. The characteristics of the four flow regimes and the phenomenon of instability are experimentally confirmed. The observed near field dilution are compared with the theoretical predictions. Good agreement is obtained.

Recommendations for future research include: investigation of the behavior of buoyant jets in an ambient crossflow, the effect of the angle of discharge on the near field stability, and testing the theory in this study against experiments carried out with a full round jet.

References:

1. Abraham, F., "Jet Diffusion in Stagnant Ambient Fluid", Delft Hyd. Lab., Publ. No. 29 (1963)

2. Albertson, M. L., Dai, Y. N., Jensen, R. A. and Rouse, H., "Diffusion of Submerged Jets", Trans. ASCE, 115 (1950)

3. Brooks, N. H., "Dispersion in Hydrologic and Coastal Environments", Keck Lab. of Hydraulics and Water Resources, Report No. KH-R-29, California Institute of Technology

4. Ellison, T. H. and Turner, J. S., "Turbulent Entrainment in Stratified Flows", J. F. M., Vol. 6, Pt. 3, Oct. (1959)

5. Jirka, G. and Harleman, D. R. F., "The Mechanics of Submerged Multi-port Diffusers for Buoyant Discharges in Shallow Water", R. M. Parsons Lab. of Water Resources and Hydrodynamics, Report No. 169 (1973)

6. Morton, B. R., G. I. Taylor and J. S. Turner, "Turbulent Gravitational Convection from Maintained and Instantaneous Sources", Proc. Roy. Soc. of London, Series A, 1956, No. 1196, Jan., pp. 1-23.

7. Rajaratnam, N. and Pani, B., "Three Dimensional Turbulent Wall Jets", ASCE, Vol. 100, No. HY1, Jan. 1974.

8. Rouse, H., C. S. Yih and H. W. Humphreys, "Gravitational Convection from a Boundary Source", Tellus 4, 1952, No. 3, Aug., pp. 201-210.

9. Sadler, C. D. and Higgins, M., "Radial Free Surface Flow", M.S. Thesis, Dept. of Civil Engineering, M.I.T., 1963.

10. Trent, D. and Welty, J., "Numerical Thermal Plume Model for Vertical Outfalls in Shallow Water", EPA-R2-73-162, Environmental Protection Technology Series, March 1973.

11. Ungate, C., "Temperature Reduction in a Submerged Vertical Jet in the Laminar-Turbulent Transition", S.M. Thesis, Dept. of Civil Engineering, M.I.T., Aug. 1974.

12. Yih, C. S. and Guha, C. R., "Hydraulic Jump in a Fluid System of Two Layers", Tellus, VII (1955).

LIST OF FIGURES AND TABLES

Fig.		Page
1-1	Illustration of near field stability	11
2-1	Flow structure in the plane of symmetry of a vertical axisymmetric jet in shallow water	13
2-2	An axisymmetric jet discharging vertically	15
2-3	Schematized structure of an axisymmetric buoyant jet	18
2-4	Length of zone of flow establishment as a function of the exit densimetric Froude number	30
2-5	The surface impingement region	32
2-6	Radial stratified flow in a two-layered system	36
2-7	The radial internal jump	41
2-8	Behavior of asymptotic solution	50
2-9	Stratified counterflow system in an unstable near field	53
2-10	Radial variation of the interface	57
2-11	Illustration of two dimensional component feature of axisymmetric radial stratified flow	59
2-12	Interface profile as a function of radial distance normalised with respect to location of critical section	61
2-13	Radial variation of interface for non-equal counterflow	62
2-14	Critical depth H_{2c} as a function of F_{2H}, $\|Q_r\|$	64
2-15	Variation of the far field interface as a function of f_i/f_o	66
2-16	General theoretical solution of near field dilution	69
2-17	Sensitivity of stability transition to the location of the jump toe	71
3-1	Experimental set-up	75
3-2	The flow injection device	79
3-3	Schematic of temperature probe set-up	82
3-4	Variation of near field temperature rise with time	84

Fig. Page

3-5 Observed near field stability 90

3-6 Temperature transect for the near field 91

3-7 Observed indentation of dye front 95

3-8 Weak entrainment induced by model boundary 96

3-9 Comparison of wall jet data with Albertson's free jet data: decay of maximum velocity along centerplane 97

4-1 Near field stability of an axisymmetric jet in shallow water 99

4-2 Near field dilution as a function of F_o, H/D; vertical axisymmetric jet in stagnant water 101

TABLES

3-1 Summary of run parameters and experimental results 86

4-1 Summary of run parameters and experimental results 102

LIST OF SYMBOLS

Subscripts:

1,2	upper, lower layers in stratified flow
c	critical section in stratified flow
e	end of region of flow establishment
s,i,b	surface, interface, bottom boundary conditions
j	internal jump section in stratified flow
i	inflow section of impingement zone
I	outflow section of impingement zone
a	ambient variables
o	discharge variables
z	vertical direction
r	radial direction

---

b	jet width
b'	width of mixing region in zone of flow establishment
c	dimensionless length of zone of flow establishment
c_p	specific heat
D	jet diameter
F	layer densimetric Froude number
F_H	densimetric Froude number based on total water depth
F^*	free surface Froude number
f_i	interfacial stress coefficient
f_b	bottom stress coefficient
g	acceleration due to gravity
H	total water depth

LIST OF SYMBOLS (Continued)

h	layer depth in stratified flow
h'	conjugate jump height
h_I	thickness of jet impingement layer
K_L	head loss coefficient for impingement
M	momentum flux
p	pressure
Q	layer flow in 2 layer system
Q_e	entrainment flux
Q_r	flow ratio in 2 layered system
q	flow per unit width
q_H	heat flux
r_c	location of critical section for unstable jet
r_j	location of internal jump
r	radial co-ordinate
R	Reynolds number
R_I	radial position of outflow section of surface impingement region
r_1, r_2	toe and end of internal jump
S	dilution
T	temperature
T_e	equilibrium temperature
(u,w)	velocities in axisymmetric cylindrical co-ordinate system
u_1, u_2	averaged layer velocities for stratified 2-layered system
u_c	jet centerline velocity

LIST OF SYMBOLS (Continued)

u_i	jet velocity at inflow section of impingement zone
y	water depth for free surface flow
z	vertical coordinate
α	entrainment coefficient
ε	jet spreading angle
λ	jet spreading ratio between mass and momentum
ΔT	temperature rise above ambient
ΔT_o	discharge temperature rise
$\Delta\rho$	density deficiency
ρ	density
τ	shear stress
β	coefficient of thermal expansion

Appendix A

Stable Near Field Solution:

The solution for the average dilution in a stable near field can be obtained by solving eq. 2.2.1-2.2.3 in conjunction with eq. 2.1.19-2.1.20. The following set of non-dimensionalized algebraic equations are arrived at. These two equations are solved numerically by the Newton Ralphson method.

$$u = \frac{1}{H^*z} \left[\left\{\frac{1+\lambda^2}{\lambda^2} \frac{1}{4\varepsilon^2} \frac{1}{c}\right\}^3 + \frac{3(1+\lambda^2)}{8\varepsilon^2 F_o^2} \{z^2 H^{*2} - c^2\} \right]^{\frac{1}{3}}$$

$$\frac{u^2(1-K_L)}{6} = \frac{1}{z} \left[\frac{\varepsilon z u}{z(1-z)\alpha_o} \right]^2 + \frac{(1-z)}{2H^*(4\varepsilon^2)z^2F_o^2u}$$

where $u = \dfrac{u_i}{u_o}$ $\quad z = z_i/H \quad H^* = H/D \quad c = z_e/D$

Having solved for u, z the densimetric Froude numbers of the upper and lower layer can be computed and used as input for obtaining the conjugate jump height.

Assuming that the internal jump occurs at $r_j = R_j H$ from the jet axis, and experimental observation indicates there is practically no change in the thickness of the upper layer prior to the jump. The densimetric Froude numbers of the respective layers can then be related to the jet characteristics:

$$F_1^2\bigg|_{r_j} = \frac{u_1^2}{g\frac{\Delta\rho}{\rho} h_1}\bigg|_{r_j} = \left(\frac{\varepsilon^3}{zR_j^2}\right) \frac{z^4}{(1-z)^3} \frac{u^2 S F_o^2}{H^*}$$

$$F_2^2 = \left(\frac{S-1}{S}\right)^2 \left(\frac{1-z}{z}\right)^3 F_1^2$$

Appendix B

The Internal Hydraulic Jump

The conjugate jump height of the radial internal jump can be solved numerically by the Newton Raphson method. By assuming

$$r_2 - r_1 = T(h_1' - h_1) \qquad T \text{ constant}$$

such that

$$R^* = \frac{r_2}{r_1} = 1 + a\left(\frac{h_1'}{h_1} - 1\right)$$

$$\text{where} \qquad a = \frac{Th_1}{r_1}$$

By rearranging eq. (2.4.14) and (2.4.15), we obtain the following set of two algebraic equations.

$$F_1(x_1, y_1) = \frac{4F_1^2[1-R^*x_1]}{R^*(1+R^*)x_1(1-x_1^2)} - 1 - \frac{4F_2^2\frac{h_2}{h_1}[1-R^*y_1]}{R^*(1+R^*)y_1(1+y_1)(1-x_1)} = 0$$

$$F_2(x_1, y_1) = \frac{4F_z^2 x_1(1+x_1)(1-R^*y_1)}{y_1(1+y_1)} - R^*(1+R^*)(1+x_1)(1-y_1)x_1 - 4F_1^2\frac{h_1}{h_2}(1-R^*x_1) = 0$$

$$\text{where} \qquad x_1 = \frac{h_1'}{h_1} \qquad y_1 = \frac{h_2'}{h_2}$$

Having evaluated the partial derivatives of $F_1(x_1, y_1)$ and $F_2(x_1, y_1)$ the two equations can be solved by iteration.

```
C     AXISYMMETRIC BUOYANT JET IN SHALLOW WATER                           STAB0001
      REAL LAMDA,K,HL                                                     STAB0002
      COMMON LAMDA,EPS                                                    STAB0003
      COMMON/DL/ALP,HL                                                    STAB0004
      COMMON /FT/FR                                                       STAB0005
      COMMON /D1/S                                                        STAB0006
      COMMON/RJ/FR1,FR2,APH                                               STAB0007
      COMMON/RJ1/Z,SLOPE,K                                                STAB0008
      READ(8,1) LAMDA,EPS,K,BETA                                          STAB0009
    1 FORMAT(4F10.3)                                                      STAB0010
      WRITE(5,2) LAMDA,EPS,K,BETA                                         STAB0011
    2 FORMAT(2X,'LAMDA=',F10.3,1X,'EPS=',F10.3,1X,'K=',F10.3,'BETA ',     STAB0012
     5 F10.3)                                                             STAB0013
      READ(8,10) ALP,HL                                                   STAB0014
   10 FORMAT(2F10.3)                                                      STAB0015
      WRITE(5,11) ALP,HL                                                  STAB0016
   11 FORMAT(2X,'ALP=',F10.3,1X,'HL=',F10.3)                              STAB0017
      SLOPE= 0.0                                                          STAB0018
      WRITE(5,25) SLOPE                                                   STAB0019
   25 FORMAT(3X,'SLOPE=',F10.3)                                           STAB0020
      READ(8,5) FR,S                                                      STAB0021
    5 FORMAT(2F10.3)                                                      STAB0022
      WRITE(5,7) FR,S                                                     STAB0023
    7 FORMAT(////2X,'FR=',F10.3,1X,'S=',F10.3)                            STAB0024
      IF(S.LE.6.0) GO TO 100                                              STAB0025
      CALL FLENG(FR,C)                                                    STAB0026
      CALL DILUT(C ,Z,U,DELRO)                                            STAB0027
      XD= EPS**2/(2.0*K)                                                  STAB0028
      XD= XD**2                                                           STAB0029
      FR1 = XD*Z**4/(1.0-Z)**3                                            STAB0030
      FR1 = FR1*DELRO*(U*FR)**2/S                                         STAB0031
      XD1 = (DELRO-1.0)/DELRO                                             STAB0032
      XD2 = (1.0-Z)/Z                                                     STAB0033
      FR2 = (XD1**2)*(XD2**3)*FR1                                         STAB0034
      FR1= SQRT(FR1)                                                      STAB0035
      FR2 = SQRT(FR2)                                                     STAB0036
```

```
      APH= (1.0-Z)/Z                                                    STAB0037
      GO TO 200                                                         STAB0038
   10 XS= 1.0 - BETA                                                    STAB0039
      SD= 1.0 + 0.083*XS*S + 0.0128*(XS*S)**2                           STAB0040
      WRITE(5,20)SD                                                     STAB0041
   20 FORMAT(5X,'NEAR FIELD DILUTION= ',F10.3)                          STAB0042
      DUM1= 64.0*(K**2)*(BETA**3)                                       STAB0043
      FR1 = (SD**3)*(FR**2)                                             STAB0044
      FR1 = FR1/(DUM1*S**5)                                             STAB0045
      DUM2= (SD-1.0)/SD                                                 STAB0046
      DUM3 = BETA/(1.0-BETA)                                            STAB0047
      FR2= (DUM2**2)*(DUM3**3)*FR1                                      STAB0048
      FR1= SQRT(FR1)                                                    STAB0049
      FR2= SQRT(FR2)                                                    STAB0050
      APH= DUM3                                                         STAB0051
      Z= 1.0 - BETA                                                     STAB0052
  200 WRITE(5,15) FR1,FR2,APH                                           STAB0053
   15 FORMAT(2X,'FR1=',F10.3,1X,'FR2=',F10.3,1X,'APH=',F10.3)           STAB0054
      CALL RJUMP                                                        STAB0055
      CALL EXIT                                                         STAB0056
      END                                                               STAB0057
      SUBROUTINE FLENG(FR,C)                                            STAB0058
C     SOLVING THE DIMENSIONLESS LENGTH OF FLOW ESTABLISHMENT,C          STAB0059
C     INPUT: DENSIMETRIC FROUDE NUMBER,FR                               STAB0060
C     SCHMIDT NUMBER,LAMDA                                              STAB0061
C     ANGLE OF SPREAD OF STANDARD DEVIATION OF CROSS-SECTIONAL          STAB0062
C     VELOCITY PROFILE, EPS                                             STAB0063
      REAL LAMDA                                                        STAB0064
      EXTERNAL FCT                                                      STAB0065
      COMMON LAMDA,EPS                                                  STAB0066
C     FA IS THE ASYMPTOTIC VALUE OF THE LOCAL DENSIMETRIC FROUDE NO OF A PLUME STAB0067
      FA= SQRT( (1.5*LAMDA**2)/EPS)                                     STAB0068
      WRITE(5,11) FA                                                    STAB0069
   11 FORMAT(3X,'FA=',F6.3)                                             STAB0070
      CALL RTNI(C,F,DERF,FCT,6.2,0.001,200,IER)                         STAB0071
      WRITE(5,3) C,F,IER                                                STAB0072
```

```
    3 FORMAT(2X,'C=',F10.3,1X,'F=',F10.3,1X,I2)
      RETURN
      END
      SUBROUTINE FCT(X,F,DERF)
      COMMON AL,EPS
      COMMON /FT/FR
      XX= AL*EPS
      YY= 3.0*FR**2
      A1= 1.0/YY
      A2 = SQRT(3.1416)*XX/YY
      A3= 4.0*XX**2/YY
      A4 = (1.0+AL**2)/(4.0*XX**2)
      A4 = (A4**2)*2.0*EPS**2
      F= 1.0 + A1*X + A2*X**2 + A3*X**3 - A4/(X**2)
      DERF= A1 + 2.0*A2*X + 3.0*A3*X**2 + 2.0*A4/X**3
      RETURN
      END
      SUBROUTINE DILUT(C ,Z,U,DELRO)
      REAL LAMDA
      COMMON /FT/F
      COMMON /D1/S
      COMMON LAMDA,EPS
      COMMON/DL/ALP,HL
C     THIS SUBPROGRAM COMPUTES THE THICKNESS OF THE UPPER LAYER IN THE
C     SURFACE IMPINGEMENT REGION. THE NEAR FIELD DILUTION IS ALSO
C     COMPUTED, IF A STABLE NEAR FIELD EXISTS.
      DUM= 1.0 + LAMDA**2
      XDUM= DUM/(C*(LAMDA*2.0*EPS)**2)
      D1 = XDUM**3
      D2 = 0.375*DUM/(EPS*F)**2
      D3 = 0.75*EPS**2/( (1.0-HL)*ALP**2)
      D4 = (0.75/(1.0-HL))/(S*(F*EPS)**2)
      Z= 0.9
      U= D1 + D2*((Z*S)**2 - C**2)
      U= U**0.333/(Z*S)
      WRITE (5,6) U
```

```
    6 FORMAT(2X,'U=',F6.3)                                              STAB0109
      I= 1                                                              STAB0110
C     Z AND U ARE STARTING VALUES IN THE PREVIOUS STATEMENT             STAB0111
C     ITERATION BY NEWTON RALPHSON METHOD                               STAB0112
C     EVALUATING THE FUNCTION AND JACOBIAN VALUES                       STAB0113
C     I IS A COUNTER                                                    STAB0114
   20 X= D1 + D2*((Z*S)**2 - C**2)                                      STAB0115
      F1= Z - (X**0.333)/(U*S)                                          STAB0116
      Y= D3*(U*Z/(1.0-Z) )**2                                           STAB0117
      Y= Y + D4*(1.0 -Z)/(U*Z**2)                                       STAB0118
      F2 = U - SQRT(Y)                                                  STAB0119
      F1Z= 1.0 - 0.667*D2*S*Z/(U*X**0.667)                              STAB0120
      F1U= (X**0.333)/(S*U**2)                                          STAB0121
      XX= 2.0*D3*Z*U**2/(1.0-Z)**3                                      STAB0122
      XX= XX + D4*(Z-2.0)/(U*Z**3)                                      STAB0123
      F2Z= -XX/(2.0*SQRT(Y))                                            STAB0124
      F2U= 2.0*D3*U*(Z/(1.0-Z))**2                                      STAB0125
      F2U= F2U - D4*(1.0-Z) /(Z*U)**2                                   STAB0126
      F2U= 1.0 - F2U/(2.0*SQRT(Y) )                                     STAB0127
C     FINISHED EVALUATING EXPRESSIONS  START FINDING ITERATION INCREMENTS  STAB0128
      DET= F1U*F2Z - F1Z*F2U                                            STAB0129
      DELU= ( F2*F1Z - F1*F2Z) /DET                                     STAB0130
      DELZ= (F1*F2U - F2*F1U)/DET                                       STAB0131
      TEST= ABS(DELU)                                                   STAB0132
      IF(TEST .LE.0.0001) GO TO 120                                     STAB0133
      U= U + DELU                                                       STAB0134
      Z= Z + DELZ                                                       STAB0135
      IF(Z.LE.1.0) GO TO 50                                             STAB0136
      WRITE(5,5)                                                        STAB0137
      Z= 1.0                                                            STAB0138
    5 FORMAT('TRIAL VALUE FOR Z HAS REACHED PHYSICAL LIMIT')            STAB0139
   50 I = I + 1                                                         STAB0140
      IF ( I.GT. 50) GO TO 201                                          STAB0141
      GO TO 20                                                          STAB0142
  120 TEST = ABS(DELZ)                                                  STAB0143
      IF (TEST.LE.0.0001) GO TO 150                                     STAB0144
```

```
      U= U + DELU                                                        STAB0145
      Z= Z + DELZ                                                        STAB0146
      IF(Z.LE.1.0) GO TO 60                                              STAB0147
      Z= 1.0                                                             STAB0148
      WRITE(5,5)                                                         STAB0149
   60 I = I + 1                                                          STAB0150
      IF ( I.GT  50) GO TO 201                                           STAB0151
      GO TO 20                                                           STAB0152
  150 WRITE (5,2)  I                                                     STAB0153
    2 FORMAT(10X,'ITERATION CONVERGED AFTER',I3, 'STEPS')                STAB0154
      WRITE(5,3) F1,F2                                                   STAB0155
    3 FORMAT( 5X,'F1=',F6.3, 3X,'F2=',F6.3)                              STAB0156
      DELRO= U*(2.0*EPS*Z*S)**2                                          STAB0157
      ZX= 1.0 - Z                                                        STAB0158
      WRITE(5,10) ZX                                                     STAB0159
   10 FORMAT(3X,'S.I.REGION THICKNESS=  ',1X,F6.3)                       STAB0160
      WRITE(5,11) DELRO                                                  STAB0161
   11 FORMAT(3X,'NEAR FIELD DILUTION= ',1X,F6.2)                         STAB0162
      GO TO 200                                                          STAB0163
  201 WRITE(5,202)                                                       STAB0164
  202 FORMAT(2X,'ITERATION DID NOT CONVERGE AFTER  50 STEPS')            STAB0165
  200 RETURN                                                             STAB0166
      END                                                                STAB0167
      SUBROUTINE RJUMP                                                   STAB0168
      COMMON/RJ/FR1,FR2,APH                                              STAB0169
      COMMON/RJ1/Z,SLOPE,K                                               STAB0170
C     THIS PART COMPUTES THE CONJUGATE JUMP HEIGHT, TAKING INTO ACCOUNT  STAB0171
C     JUMP LENGTH; IN EFFECT THIS IS A TEST FOR THE STABILITY OF THE     STAB0172
C     NEAR FIELD; NON-CONVERGENCE OR NO SOLUTION WOULD INDICATE AN       STAB0173
C     INSTABILITY                                                        STAB0174
C     THE INPUTS TO THIS PART ARE THE DENSIMETRIC FROUDE NUMBERS OF THE  STAB0175
C     RESPECTIVE LAYERS AT THE JUMP LOCATION, AND THE RATIO OF THE LAYER STAB0176
C     DEPTHS BEFORE THE JUMP                                             STAB0177
      REAL K                                                             STAB0178
      X1 = 1.2                                                           STAB0179
      Y1= 0.8                                                            STAB0180
```

```
      I= 1                                                                  STAB0181
      XLIMIT= (1.0 + APH) /APH                                              STAB0182
C     X1 IS THE RATIO OF THE UPPER LAYER DEPTH AFTER AND BEFORE THE JUMP    STAB0183
C     Y1 IS THE SAME RATIO FOR THE LOWER LAYER                              STAB0184
C     X1 AND Y1 ARE STARTING VALUES IN THE PREVIOUS STATEMENT               STAB0185
C     ITERATION BY NEWTON RALPHSON METHOD                                   STAB0186
C     EVALUATING THE FUNCTION AND JACOBIAN VALUES                           STAB0187
C     I IS A COUNTER                                                        STAB0188
      A= SLOPE*(1.0-Z)/K                                                    STAB0189
      A1 = 4.0*FR1**2                                                       STAB0190
      A2 = 4.0*(FR2**2)/APH                                                 STAB0191
      A3= 4.0*FR2**2                                                        STAB0192
      A4= 4.0*(FR1**2)*APH                                                  STAB0193
   10 D= 1.0 + A*(X1-1.0)                                                   STAB0194
      D1 = 1.0 + D                                                          STAB0195
      P1 = 1.0 + X1                                                         STAB0196
      P2 = 1.0 -X1                                                          STAB0197
      P3 = 1.0 + Y1                                                         STAB0198
      P4= 1.0 - Y1                                                          STAB0199
      F1 = A1*(1.0-D*X1)/(D*D1*X1*P1*P2)                                    STAB0200
      F1 = F1 -1.0                                                          STAB0201
      F1 = F1 - A2*(1.0-D*Y1)/(D*D1*Y1*P3*P2)                               STAB0202
      F2 = A3*X1*P1*(1.0-D*Y1)/(Y1*P3)                                      STAB0203
      F2 = F2 - D*D1*P1*P4*X1 - A4*(1.0-D*X1)                               STAB0204
C     FINISHED EVALUATING FUNCTION VALUES                                   STAB0205
      DUM= -D*D1*X1*P1*P2*(D+A*X1)                                          STAB0206
      DUM= DUM -(1.0-D*X1)*(D*D1*(1.0-3.0*X1**2)+X1*P1*P2*(1.0+2.0*D)       STAB0207
     2 *A)                                                                  STAB0208
      DUM= DUM*A1/(D*D1*X1*P1*P2)**2                                        STAB0209
      DUM1 = -D*D1*P2*A*Y1                                                  STAB0210
      DUM1 = DUM1 - (1.0-D*Y1)*(-D*D1 + P2*(1.0+2.0*D)*A)                   STAB0211
      DUM1 = DUM1/(D*D1*P2)**2                                              STAB0212
      DUM1 = -A2*DUM1/(Y1*P3)                                               STAB0213
      F1X1 = DUM + DUM1                                                     STAB0214
      DUM2= -Y1*D*P3                                                        STAB0215
      DUM2= DUM2 - (1.0-D*Y1)*(1.0+2.0*Y1)                                  STAB0216
```

```
      DUM2 = DUM2/(Y1*P3)**2                                              STAB0217
      DUM2 = -A2*DUM2/(D*D1*P2)                                           STAB0218
      F1Y1= DUM2                                                          STAB0219
      DUM3= -X1*P1*A*Y1                                                   STAB0220
      DUM3 = DUM3 + (1.0-D*X1)*(1.0+2.0*X1)                               STAB0221
      DUM3 = A3*DUM3/(Y1*P3)                                              STAB0222
      DUM3 = DUM3-P4*(X1*P1*A*(1.0+2.0*D)+D*D1*(1.0+2.0*X1))              STAB0223
      F2X1= DUM3 + A4*(D+X1*A)                                            STAB0224
      DUM4= A3*X1*P1*(-Y1*P3*D -(1.0-D*Y1)*(1.0+2.0*Y1))                  STAB0225
      DUM4 = DUM4/(Y1*P3)**2                                              STAB0226
      F2Y1= DUM4 + D*D1*X1*P1                                             STAB0227
C     FINISHED EVALUATING DERIVATIVES; START FINDING ITERATION INCREMENTS STAB0228
      DET= F1X1*F2Y1 - F1Y1*F2X1                                          STAB0229
      DELX1= (F2*F1Y1-F1*F2Y1)/DET                                        STAB0230
      DELY1= (F1*F2X1 - F2*F1X1)/DET                                      STAB0231
      TEST= ABS(DELX1)                                                    STAB0232
      IF (TEST.LE.0.0001) GO TO 20                                        STAB0233
      X1 = X1 + DELX1                                                     STAB0234
      Y1 = Y1 + DELY1                                                     STAB0235
      IF(X1.LE.XLIMIT) GO TO 50                                           STAB0236
      X1= XLIMIT - 0.05                                                   STAB0237
      GO TO 50                                                            STAB0238
   50 XTEST= X1 - 1.0                                                     STAB0239
      IF(XTEST.LE.0.1   ) X1= 1.05                                        STAB0240
      I= I + 1                                                            STAB0241
      IF(I.GT.70) GO TO 200                                               STAB0242
      GO TO 10                                                            STAB0243
   20 TEST= ABS(DELY1)                                                    STAB0244
      IF(TEST.LE.0.0001) GO TO 102                                        STAB0245
      X1 = X1 + DELX1                                                     STAB0246
      Y1 = Y1 + DELY1                                                     STAB0247
      I= I+1                                                              STAB0248
      IF(I.GT.70) GO TO 200                                               STAB0249
      GO TO 10                                                            STAB0250
  102 IF(F1.LE.0.001) GO TO 103                                           STAB0251
      X1 = X1 + DELX1                                                     STAB0252
```

```
      Y1 = Y1 + DELY1                                                   STAB0253
      I= I + 1                                                          STAB0254
      IF(I.GT.70) GO TO 200                                             STAB0255
      GO TO 10                                                          STAB0256
  103 IF( F2.LE.0.001) GO TO 100                                        STAB0257
      X1 = X1 + DELX1                                                   STAB0258
      Y1 = Y1 + DELY1                                                   STAB0259
      I= I + 1                                                          STAB0260
      IF(I.GT.70) GO TO 200                                             STAB0261
      GO TO 10                                                          STAB0262
  100 WRITE(5,2) I                                                      STAB0263
    2 FORMAT(10X,'ITERATION CONVERGED AFTER',I3,'STEPS')                STAB0264
      WRITE(5,3) F1,F2                                                  STAB0265
    3 FORMAT(5X,'F1=',F6.3,3X,'F2=',F6.3)                               STAB0266
      WRITE(5,6) X1,Y1                                                  STAB0267
    6 FORMAT(5X,'X1=',F6.3,3X,'Y1=',F6.3)                               STAB0268
      GO TO 300                                                         STAB0269
  200 WRITE(5,15)                                                       STAB0270
   15 FORMAT(2X,'ITERATION DID NOT CONVERGE AFTER 70 STEPS')            STAB0271
  300 RETURN                                                            STAB0272
      END                                                               STAB0273
```

Appendix C

For H/D smaller than approximately 6.0 the theory outlined in ch. 2 and the previous appendix does not strictly hold as the flow is not fully established when the jet reaches the free surface. By assuming momentum dominates in such cases, a simplified analysis is done to derive an average dilution in the near field.

From Albertson et al (1950),

$$Q/Q_o = 1.0 + 0.083 \frac{z}{D} + 0.0128 \frac{z^2}{D^2}$$

where Q is the total flow of the jet.

Assuming the depth of the upper layer = βH , the dilution in the near field is given by

$$S = 1.0 + 0.083(1-\beta)H^* + 0.0128\ (1-\beta)^2 H^{*2}$$

Assuming that the jump occurs at $r_j = R_j H$ from the jet axis, the densimetric Froude numbers of the respective layers prior to the internal jump can be related to the jet characteristics and experimental coefficients:

$$F_1^2 = \frac{u_1^2}{g \frac{\Delta\rho}{\rho} h_1} = \frac{1}{64 R_j^2 \beta^3} \frac{S^3 F_o^2}{H^{*5}}$$

$$F_2^2 = \frac{u_2^2}{g \frac{\Delta\rho}{\rho} h_2} = \left(\frac{S-1}{S}\right)^2 \left(\frac{\beta}{1-\beta}\right)^3 F_1^2$$

In the numerical solution β is assumed to be 0.1.

Appendix D

Energy Approach to critical flow in a two-layered counterflow system:

It is well known that for open channel flows, the critical flow condition can be interpreted as that which minimizes the specific energy for a given flow. The following is an extension of the same principle to a two-layered counterflow system.

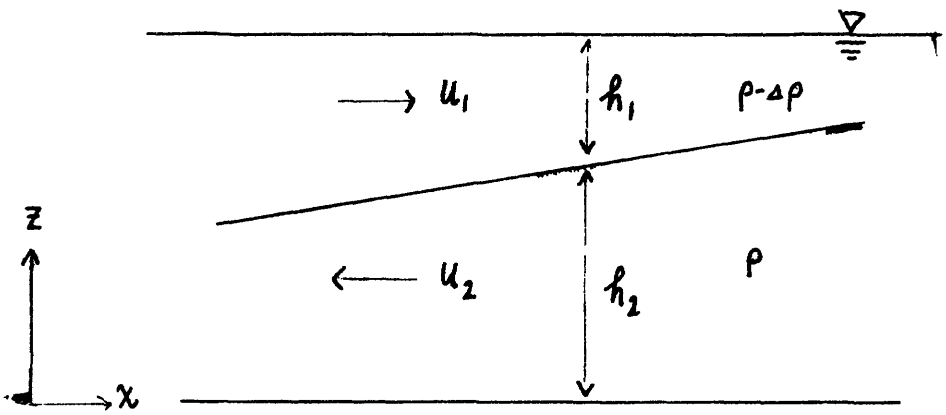

The two dimensional case is treated here. However, the analysis is also applicable to axi-symmetric flows.

Kinematic Boundary Condition:

free surface: $$w_s = u_s \frac{d(h_1 + h_2)}{dx}$$

interface: $$w_i = u_i \frac{dh_2}{dx}$$

A small fluid particle of mass $\rho\delta V$ possesses potential and kinetic energy: $E\delta V = \{\rho g z + \frac{1}{2}\rho(u^2 + w^2)\}\ \delta V$

First Law of Thermodynamics:

$$\frac{DE}{Dt}\,\delta V = \left(\frac{\partial E}{\partial t} + u\,\frac{\partial E}{\partial x} + w\,\frac{\partial E}{\partial z}\right)\delta V = \frac{\delta(\text{Work})}{\delta t}$$

$$= -\left(\frac{\partial \rho u}{\partial x} + \frac{\partial \rho w}{\partial z}\right)\delta V$$

Assuming steady state and neglecting friction losses: we have

$$\frac{\partial}{\partial x}(E+p)u + \frac{\partial}{\partial z}(E+p)w = 0$$

Integrating this vertically and applying Leibnitz rule:

$$\frac{d}{dx}\int_0^{h_1+h_2}\{(E+p)u\}\,dz - (E+p)_s\,u_s\,\frac{d(h_1+h_2)}{dx} + (E+p)_s w_s = 0$$

Invoking the kinematic boundary condition at the free surface,

$$\frac{d}{dx}\int_0^{h_1+h_2}\{(E+p)u\}dz = 0$$

$$\int_0^{h_2}(E+p)udz = \int_0^{h_2}\{\rho gz + \frac{1}{2}\rho(u^2+w^2) + (\rho-\Delta\rho)gh_1 + \rho g(h_2-z)\}udz$$

Assuming $w << u$ and $\overline{u_2^3} \simeq \overline{u}_2^{\,3}$ we have

$$= \frac{1}{2}\rho\overline{u_2}^{\,3}\,h_2 + \{\rho g(h_1+h_2) - \Delta\rho g\,h_1\}\,h_2\,\overline{u_2}$$

For the counterflow system: we have $q_2 = -\,|q_2|$

therefore

$$\int_0^{h_2}(E+p)\,udz = -\frac{1}{2}\rho\frac{q_2^3}{h_2^3}\,h_2 - \{\rho g(h_1+h_2) - \Delta\rho gh_1\}\,h_2\left(\frac{q_2}{h_2}\right)$$

Similarly,

$$\int_0^{h_1+h_2} (E+p)u\,dz = \int_{h_2}^{h_1+h_2} u\{(\rho-\Delta\rho)gz + \tfrac{1}{2}\rho u^2 + (\rho-\Delta\rho)g(h_1+h_2-z)\}dz$$

$$= \tfrac{1}{2}\rho\left(\frac{q_1^3}{h_1^3}\right) h_1 + (\rho-\Delta\rho)g(h_1+h_2)\left(\frac{q_1}{h_1}\right) h_1$$

$$q_1 > 0$$

Total energy at any x can be defined as:

$$E(x) = -\tfrac{1}{2}\rho\frac{q_2^3}{h_2^2} - \{\rho g(h_1+h_2) - \Delta\rho g h_1\} q_2$$

$$+ \tfrac{1}{2}\rho\left(\frac{q_1^3}{h_1^3}\right) + (\rho-\Delta\rho)g(h_1+h_2)\, q_1$$

For extremum, $\frac{\partial E}{\partial h_1} = 0$ $\quad \frac{\partial E}{\partial h_2} = 0$ We have

$$-(\rho-\Delta\rho)\, g\, q_2 + (\rho-\Delta\rho)\, g\, q_1 - \frac{\rho q_1^3}{h_1^3} = 0 \tag{1}$$

$$-\rho g\, q_2 + (\rho-\Delta\rho)\, g\, q_1 + \frac{\rho q_2^3}{h_2^3} = 0 \tag{2}$$

(1) - (2):

$$\frac{-\rho q_1^3}{h_1^3} - \frac{\rho q_1^3}{h_2^3} + \Delta\rho g\, q_2 = 0$$

$q_1 = q_2$ gives

$$F_1^2 + F_2^2 = 1 .$$

Appendix E: Sample Output of Data-Reduction Program

```
    RUN N11
INITIAL AMBIENT TEMP
   73.29      73.23      73.21      73.16      73.04      73.04      73.06      72.98      73.13      73.50
   75.65      73.18      73.16      73.33      73.15      73.19      73.17      73.23      73.17      73.17
   73.21      73.31      73.14      73.21      73.12      73.21      73.15      73.18      73.21      73.17
   73.29      73.55      73.48      73.46      73.11      73.28      73.20      73.25      73.42      74.86
   73.19      72.85      73.15      73.22      73.04      73.15     103.72      73.24      73.29      73.23
INITIAL AMBIENT TEMP  : 73.24F
INITIAL DISCHARGE TEMP:100.32F
INITIAL TEMP DIFF.    : 27.08F
JET SUBMERGENCE       : 10.65
DISCHARGE FLOW        :875.50CC/MIN
NOZZLE DIAMETER       :  0.50IN
DENSIMETRIC FROUDE NO.:  95.98
```

```
   TEMP. DATA
 0.00BELOW SURFACE
 79.79     79.66     78.77     78.21     78.65     78.45     79.00     78.09     73.04     73.36
 81.28     79.03     78.28     78.10     79.09     76.41     75.78     77.18     74.31     72.97
 80.83     78.01     75.85     75.63     77.39     76.51     76.87     74.73     72.91     73.00
 82.54     77.83     76.53     77.15     77.60     75.86     76.49     76.50     74.64     74.54
 82.85     83.78     85.60     82.63     99.92     72.82    103.36     72.59     72.79     72.73
R=      0.38      1.13      2.25      3.38      4.51      6.76      9.02     11.27     13.53     20.29
      THETA= 00.0
      0.365     0.246     0.244     0.211     0.191     0.215     0.209     0.219     0.191     0.200
      THETA= 30.0
      0.404     0.217     0.219     0.197     0.182     0.223     0.137     0.109     0.151     0.247
      THETA= 90.0
      0.465     0.284     0.181     0.110     0.103     0.165     0.127     0.140     0.067     0.220
      THETA=135.0
      0.357     0.272     0.161     0.121     0.145     0.178     0.110     0.130     0.127     0.250
  0.000  0.000  0.200  0.000
      AVERAGED TEMP RISE

      0.396     0.298     0.202     0.160     0.155     0.195     0.146     0.150     0.134     0.224
```

Appendix F

Heat loss effects in the Near Field:

In this section it is shown that heat loss effects are insignificant in the near field of the bouyant jet.

Neglecting molecular transport process, heat conservation implies:

$$u \frac{\partial T}{\partial r} + w \frac{\partial T}{\partial z} = - \frac{\overline{T'u'}}{r} - \frac{\overline{T'w'}}{z} \qquad (F.1)$$

where u_1' w' = velocity fluctuations

T' = temperature fluctuation

Integrating eq. F.1 vertically for the upper layer, using Leibnitz rule and invoking kinematic boundary conditions at the free surface and the interface (assuming no free surface slope) it can be shown that

$$u_1 \frac{d\ T_1}{dr} = \frac{q_{H_s} - q_{H_i}}{\rho_a c_\rho h_1}$$

where

q_{H_s} = surface heat flux

q_{H_i} = interfacial heat flux

T_1 = average temperature of upper layer

c_p = specific heat of water

Putting the heat fluxes in the form:

$$q_{H_s} = - k(T_1 - T_e)$$

$$q_{H_i} = k_z(T_1 - T_2)$$

where k = surface heat loss coefficient

k_z = interfacial heat loss coefficient

T_2 = average temperature of lower layer

T_e = Equilibrium air temperature

Doing a scaling and replacing T_1 with the temperature excess above ambient ΔT_1, we have

$$u_1^* \frac{d\Delta T_1^*}{dr^*} = -\left[\frac{k\ R}{\rho_a c_\rho\ Hu_o}\right] \frac{(\Delta T_1^* - \Delta T_e^*)}{h_1^*} - \left[\frac{k_z\ R}{\rho_a c_\rho\ Hu_o}\right] \frac{(\Delta T_1^* - \Delta T_2^*)}{h_1^*} \tag{F.2}$$

where

$u_1^* = u_1/u_o$ $\quad$ $\Delta T_1^* = \Delta T/\Delta T_o$

$r^* = r/H$

$h_1^* = h_1/H$

u_o : characteristic upper layer velocity

ΔT_o : characteristic temperature excess above ambient of upper layer

San Onofore Power plant, as an example of a submerged discharge design, has a condenser flow rate of 3.2×10^6 cf/hr. Using the theory outlined in this study, the upper layer velocity can be estimated to be approximately 0.2 ft./sec. at $r^* = 10$. The values of the heat loss coefficients are given by:

k = 150 BTU/°F-ft.^{2}-day

k_z = 10^{-4} ft^2/sec $\quad$ [Jirka and Harleman (1973)]

ρc_p = 62.5 BTU/ft^3

Substituting these numbers into eq. F.2 the dimensionless parameters in brackets can be shown to be 0.03 for the surface heat loss and 0.0001 for the interfacial mixing.

Hence heat loss effects are not important in the region of interest ($r < 10H$) treated in this study.

```
C     GENERIC APPROACH TO UNSTABLE NEAR FIELD SOLUTION,ASSUMING
C     EQUAL COUNTERFLOW
C     THE INPUTS ARE THE DENSIMETRIC FROUDE NUMBER BASED ON THE TOTAL WATER
C     DEPTH, THE INTERFACIAL AND BOTTOM FRICTION FACTOR, AND THE LENGTH OF
C     THE NEAR FIELD MIXING ZONE,MIXL
      EXTERNAL FCT,OUTP
      EXTERNAL FCR1,OUT1
      REAL MIXL
      DIMENSION PRMT(5),AUX(8)
      COMMON/NEW/DIL
      COMMON/OP/XINT
      COMMON/FC/MIXL,F1H
      READ(8,2) F1H,MIXL
    2 FORMAT(2F10.3)
      WRITE(5,4) F1H,MIXL
    4 FORMAT(2X,'F2H=',F10.3,'MIXL=',F10.3)
      CALL CRITS(F1H,C)
C     HAVING OBTAINED THE INITIAL POSITION OF THE INTERFACE AT THE CRITICAL
C     SECTION, THE RADIAL VARIATION OF THE INTERFACE IS THEN SOLVED AS AN
C     INITIAL VALUE PROBLEM
      WRITE(5,51)
   51 FORMAT(7X,'H2',10X,'R',10X,'DR/DH2')
C     GET STARTING VALUE FOR INITIAL VALUE PROBLEM, ASSUMING DILUTION
C     SINCE DERIVATIVE GOES TO INFINITY AT CRITICAL SECTION; FIRST START
C     THE NUMERICAL SOLUTION BY INVERTING THE DERIVATIVE TO OBTAIN SOME VALUES
C     (H,R) OFF THE CRITICAL SECTION; THEN CONTINUE SOLUTION BY USUAL METHOD
      PRMT(1)= 1.0 -C
      PRMT(2)= 1.0
      PRMT(3) = 0.001
      PRMT(4) = 0.0001
      Y= MIXL
      DERY= 1.0
      CALL RKGS(PRMT,Y,DERY,1,IHLF,FCT,OUTP,AUX)
      R= Y
      H2= XINT
      WRITE(5,54) H2,R
```

```
54 FORMAT(7X,'H2=',F10.3,'R=',F10.3)                                  USTB0037
   PRMT(1) = R                                                        USTB0038
   PRMT(2) = 25.0                                                     USTB0039
   PRMT(3) = 1.0                                                      USTB0040
   PRMT(4) = 0 0001                                                   USTB0041
   WRITE(5,57)                                                        USTB0042
57 FORMAT(7X,'R',11X,'H2',9X,'DH2/DR')                                USTB0043
   DERY= 1.0                                                          USTB0044
   CALL RKGS(PRMT,H2,DERY,1,IHLF,FCR1,OUT1,AUX)                       USTB0045
   CALL EXIT                                                          USTB0046
   END                                                                USTB0047
   SUBROUTINE CRITS(F1H,C)                                            USTB0048
   EXTERNAL FCT3                                                      USTB0049
   COMMON/F1/ALFA                                                     USTB0050
   ALFA= 1.0/F1H**2                                                   USTB0051
   CALL RTMI(C,F,FCT3,0.5,1.0,0.00001,200,IER)                        USTB0052
   WRITE(5,6) C,F,IER                                                 USTB0053
 6 FORMAT(4X,'INITIAL LAYER DEPTH=',F6.3,1X,'F=',F7.4,1X,'IER=',I2)   USTB0054
   RETURN                                                             USTB0055
   END                                                                USTB0056
   FUNCTION FCT3(X)                                                   USTB0057
   COMMON/F1/ALFA                                                     USTB0058
   COMMON/NEW/DIL                                                     USTB0059
   A1= (1.0-X)**3                                                     USTB0060
   A2= X**3                                                           USTB0061
   FCT3= A1+A2 - ALFA*A1*A2                                           USTB0062
   RETURN                                                             USTB0063
   END                                                                USTB0064
   SUBROUTINE FCT(X,Y,DERY)                                           USTB0065
   REAL LAMI,LAMO                                                     USTB0066
   REAL MIXL                                                          USTB0067
   COMMON/FC/MIXL,F1H                                                 USTB0068
   COMMON/NEW/DIL                                                     USTB0069
   C= 0.35                                                            USTB0070
   LAMO= C**2/8.0                                                     USTB0071
   LAMO= 0.0                                                          USTB0072
```

```
      LAMI= 0.5*LAMO                                                    USTB0073
      DUM= (F1H**2)*(MIXL/Y)**2                                         USTB0074
      F1= DUM/(1.0-X)**3                                                USTB0075
      F2= DUM/X**3                                                      USTB0076
      DUM1= (1.0-X)/X                                                   USTB0077
      DUM2= F1*(1.0+DUM1)*(1.0-DUM1)**2                                 USTB0078
      DERY= 1.0 -F1 - F2                                                USTB0079
      DERY1= F2*X/Y - F1*(1.0-X)/Y + LAMI*DUM2 + LAMO*F2                USTB0080
      DERY= DERY/DERY1                                                  USTB0081
      RETURN                                                            USTB0082
      END                                                               USTB0083
      SUBROUTINE OUTP(X,Y,DERY,IHLF,NDIM,PRMT)                          USTB0084
      REAL MIXL                                                         USTB0085
      DIMENSION PRMT(5)                                                 USTB0086
      COMMON/FC/MIXL,F1H                                                USTB0087
      COMMON/OP/X1                                                      USTB0088
      X1= X                                                             USTB0089
      R= Y/MIXL                                                         USTB0090
      WRITE(5,4) X,R,DERY,IHLF                                          USTB0091
    4 FORMAT(3(2X,F10.3),2X,I2)                                         USTB0092
      DUMX= Y - MIXL                                                    USTB0093
      IF(DUMX.GT.0.1 ) PRMT(5)= 1.0                                     USTB0094
      RETURN                                                            USTB0095
      END                                                               USTB0096
      SUBROUTINE FCR1(X,Y,DERY)                                         USTB0097
      REAL LAMI,LAMO                                                    USTB0098
      REAL MIXL                                                         USTB0099
      COMMON/FC/MIXL,F1H                                                USTB0100
      COMMON/NEW/DIL                                                    USTB0101
      C= 0.35                                                           USTB0102
      LAMO= C**2/8.0                                                    USTB0103
      LAMO= 0.0                                                         USTB0104
      LAMI= 0.5*LAMO                                                    USTB0105
      DUM= (F1H**2)*(MIXL/X)**2                                         USTB0106
      F1= DUM/(1.0-Y)**3                                                USTB0107
      F2= DUM/Y**3                                                      USTB0108
```

```
      DUM1= (1.0-Y)/Y                                                   USTB0109
      DUM2= F1*(1.0+DUM1)*(1.0-DUM1)**2                                 USTB0110
      DERY= 1.0 -F1- F2                                                 USTB0111
      DERY1= F2*Y/X -F1*(1.0-Y)/X + LAMI*DUM2 + LAMO*F2                 USTB0112
      DERY= DERY1/DERY                                                  USTB0113
      RETURN                                                            USTB0114
      END                                                               USTB0115
      SUBROUTINE OUT1(X,Y,DERY,IHLF,NDIM,PRMT)                          USTB0116
      REAL MIXL                                                         USTB0117
      DIMENSION PRMT(5)                                                 USTB0118
      COMMON/FC/MIXL,F1H                                                USTB0119
      R= X/MIXL                                                         USTB0120
      WRITE(5,4) R,Y,DERY,IHLF                                          USTB0121
    4 FORMAT(3(2X,F10.3),2X,I2)                                         USTB0122
      DUM= ABS(DERY)                                                    USTB0123
      IF(DUM.GT.2000.0) PRMT(5) = 1.0                                   USTB0124
      RETURN                                                            USTB0125
      END                                                               USTB0126
```